INFORMATION TO USERS

The most advanced technology has been used to photograph and reproduce this manuscript from the microfilm master. UMI films the text directly from the original or copy submitted. Thus, some thesis and dissertation copies are in typewriter face, while others may be from any type of computer printer.

The quality of this reproduction is dependent upon the quality of the copy submitted. Broken or indistinct print, colored or poor quality illustrations and photographs, print bleedthrough, substandard margins, and improper alignment can adversely affect reproduction.

In the unlikely event that the author did not send UMI a complete manuscript and there are missing pages, these will be noted. Also, if unauthorized copyright material had to be removed, a note will indicate the deletion.

Oversize materials (e.g., maps, drawings, charts) are reproduced by sectioning the original, beginning at the upper left-hand corner and continuing from left to right in equal sections with small overlaps. Each original is also photographed in one exposure and is included in reduced form at the back of the book.

Photographs included in the original manuscript have been reproduced xerographically in this copy. Higher quality 6" x 9" black and white photographic prints are available for any photographs or illustrations appearing in this copy for an additional charge. Contact UMI directly to order.

U·M·I

University Microfilms International
A Bell & Howell Information Company
300 North Zeeb Road, Ann Arbor, MI 48106-1346 USA
313/761-4700 800/521-0600

Order Number 9119694

Third-order optical nonlinear properties of polymers

Yang, Lina, Ph.D.

City University of New York, 1991

U·M·I
300 N. Zeeb Rd.
Ann Arbor, MI 48106

THIRD ORDER OPTICAL NONLINEAR PROPERTIES OF POLYMERS

b y

Lina Yang

A dissertation submitted to the Graduate Faculty in Engineering in partial fulfillment of the requirements for the degree of Doctor of Philosophy, The City University of New York.

1991

This manuscript has been read and accepted for the Graduate Faculty in Engineering in satisfaction of the dissertation requirement for the degree of Doctor of Philosophy.

1/22/91
Date

Chair of Examining committee
Professor Robert R. Alfano

Co-Chair of Examining committee
Professor R. Dorsinville

1/22/91
Date

Executive Officer
Dean G. Lowen

Professor S. Ahmed
Professor P. P. Ho
Professor L. Roytman
Professor N. L. Yang

Supervisory Committee

The City University of New York

Abstract

THIRD ORDER OPTICAL NONLINEAR PROPERTIES OF POLYMERS

by

Lina Yang

Advisor: Professor R. R. Alfano
Co-Advisor: Professor R. Dorsinville

The development of polymers as nonlinear optical materials coincide with a renewed interest in the field of nonlinear optics, and its applications for the future photonic devices. Large nonresonant susceptibilities, fast electronic responses, and ease of processing make polymers one of the best candidates for the applications.

This thesis describes the study of the third order optical nonlinear properties in polymers. The studies have been focused on two classes of conjugated polymers: the π-electron system and the σ-electron system. Important parameters which fully characterize the nonlinearities of materials, such as magnitude, response time, and the sign of $\chi^{(3)}$ have been measured. Various mechanisms responsible for the observed nonlinearities have also been investigated.

The thesis consists of twelve chapters. The first two chapters provide an overview of the fundamental aspects of nonlinear optics, optical properties of polymers, and the experimental techniques, apparatus which can be used to investigate the third order optical

nonlinearities of polymers, such as the degenerate four wave mixing and the single beam Z - scan technique.

The π-electron polymer systems are studied in Chapters III to VII. We have investigated the nonlinearities in polyacetylene, polydiacetylene, as well as in a relatively new material-polythiophenes. Most of the work has been concentrated on polythiophenes. For the first time, the spectrum of the nonlinear coefficient χ^3 covering the single photon transition band has been measured in polythiophene. The experimental results show that χ^3 is large($>10^{-9}$esu) and fast(<15ps) above gap. The real part of χ^3 has also been found to be negative at both 532 and 1064 nm. The single photon resonance is responsible for the negative χ^3 at 532 nm, while two photon resonant absorption is responsible for the negative χ^3 at 1064 nm. For the first time, the enhancement of $\chi^{(3)}$ was observed about photoinduced polaronic bands in polythiophene thin films. Thus, in π - electron systems, χ^3 can be enhanced through electronic contributions(π - electron delocalization) as well as through photo(doping)-induced gap state transitions.

As a class of transparent nonlinear optical materials, σ-conjugated polysilane polymers(Chapter VIII to X) have shown to posses moderate large $\chi^{(3)}(10^{-12}$esu), the upper limit of the time response has been determined to be <3ps. The sign of $\chi^{(3)}$ has been determined to be negative at 532nm and positive at 1064nm. Results implies that two photon absorption to the ultraviolet(UV) state plays an important role in nonlinear response in the visible.

The major conclusions of this thesis work are summarized in Chapter XI. Future research directions are presented in Chapter XII.

To my parents, Jieru Yang and Xigiao Liu.

ACKNOWLEDGMENTS

I would like to take this opportunity to express my sincere thanks to my parents, for their continued support and their sacrifices which persuaded me to pursue higher education.

I would like to gratefully acknowledge my thesis adviser Robert R. Alfano, Distinguished Professor of Science and Engineering of the City College of New York, for his continued support, rigorous training, numerous valuable suggestions, sharing best knowledge and patient guidance during the course of this research work. It is a great pleasure to acknowledge my co-adviser, Professor Roger Dorsinville, for his encouragement, valuable discussions and instructions, experimental and theoretical assistance during this thesis work. I am grateful to Professor P. P. Ho for his helpful instructions and most of all for his kindness to introduce me to the polymer field. I am also grateful to Professor N. L. Yang, Professor C. Taliani and Professor R. Tubino for sharing their expertise knowledge on polymer materials. Many thanks go to Mr. W. K. Zou for his work in providing polymer samples. I wish to express my sincere thanks to the faculty of the Electrical Engineering Department for their education and help, especially to Professor S. Ahmed, Professor L. Roytman and Professor P. Karmel. I would also like to thank all my fellow colleagues and friends in the Institute of Ultrafast Laser Spectroscopy and the Photonics Application Laboratory.

I would like to thank financial supports partially from NSF, CCNY Faculty Award and Hamamatsu Photonics K. K. which made this research work possible.

Finally, special thanks go to my husband, Professor Kai Shum, for his love, encouragement, understanding as well as his professional opinion in many aspects; and of course, to my son, Karlswell, for all the enjoyment he brought to us.

Table of Content

Figure Captions

LIST OF TABLES

Chapter I

Introduction

In this chapter, the basic concepts of nonlinear optics[1,2,3] will be introduced together with the possible device applications of nonlinear optics, using the third order susceptibilities. Major nonlinear materials, basically, organics and inorganics are reviewed. Their merits and demerits are listed. The advantages of polymers over other materials make them among the best candidates for nonlinear photonic applications. Both π- and σ- electron conjugated polymers are introduced. Finally, the thesis statement is presented.

1.1 Nonlinear Optics

The invention of lasers has opened the door to the field of nonlinear optics. The observation of nonlinear optical effects requires the application of intense light. To date, numerous nonlinear optical phenomena have been discovered. Each nonlinear optical process may consist of two parts. The intense light first induces a nonlinear response in a nonlinear medium, where in turn the medium modifies the optical field in a nonlinear way to generate new signal beams.

Within the framework of the semiclassical theory of radiation, the electric $\mathbf{E}(\mathbf{r},t)$ and magnetic fields $\mathbf{B}(\mathbf{r},t)$ are introduced as a classic perturbation described by Maxwell's equations(in cgs unit):

$$\nabla \mathrm{X}\, \mathbf{E} = -\frac{1}{c}\frac{\partial \mathbf{B}}{\partial t},$$

$$\nabla \mathrm{X}\, \mathbf{B} = \frac{1}{c}\frac{\partial \mathbf{E}}{\partial t} + \frac{4\pi}{c}\mathbf{J}, \qquad (1.1.1)$$

$$\nabla \cdot \mathbf{E} = 4\pi\rho ,$$

$$\nabla \cdot \mathbf{B} = 0$$

where $\mathbf{J}(\mathbf{r},t)$ and $\rho(\mathbf{r},t)$ are the current and charge densities, respectively. They are related by the charge conservation law:

$$\nabla \cdot \mathbf{J} + \frac{\partial \rho}{\partial t} = 0 . \tag{1.1.2}$$

Often, $\mathbf{J}$ and ρ can be expended into series:

$$\mathbf{J} = \mathbf{J}_0 + \frac{\partial \mathbf{P}}{\partial t} + \cdots\cdots\cdots$$
$$\rho = \rho_0 - \nabla \cdot \mathbf{P} - \cdots\cdots\cdots \tag{1.1.3}$$

Here, $\mathbf{P}$ is the electric dipole **polarization**. Normally, it is not meaningful to express $\mathbf{J}$ and ρ in terms of multipoles in the optical region, so the high order terms are neglected. Thus, the Maxwell's equations appear in the form:

$$\nabla \times \mathbf{E} = -\frac{1}{c}\frac{\partial \mathbf{B}}{\partial t} ,$$

$$\nabla \times \mathbf{B} = \frac{1}{c}\frac{\partial (\mathbf{E} + 4\pi\mathbf{P})}{\partial t} + \frac{4\pi}{c}\mathbf{J}, \tag{1.1.4}$$

$$\nabla \cdot (\mathbf{E} + 4\pi\mathbf{P}) = 0 ,$$

$$\nabla \cdot \mathbf{B} = 0.$$

From the first two equations, the wave equations that governs optical wave propagation in the medium can be obtained:

$$[\, \nabla \times (\nabla \times) + \frac{1}{c^2}\frac{\partial^2}{\partial t^2} \,]\, \mathbf{E}(\mathbf{r},t) = -\frac{4\pi}{c^2}\frac{\partial^2}{\partial t^2}\mathbf{P}(\mathbf{r},t) \tag{1.1.5}$$

where $\mathbf{P}$ is a function of $(\mathbf{r},t)$ and is now the only time-varying source term. In general , $\mathbf{P}$ is usually a complicated nonlinear function of $\mathbf{E}$ that describes fully the response of the medium to the

field. In the nonlinear case, the polarization **P** can be expanded into a power series as a function of **E**, known as the response function, in the frequency ω and **k** domains:

$$\mathbf{P}(\mathbf{k},\omega)= \mathbf{P}^{(1)}(\mathbf{k},\omega) + \mathbf{P}^{(2)}(\mathbf{k},\omega) + \mathbf{P}^{(3)}(\mathbf{k},\omega) + \cdots\cdots\cdots\cdots \qquad (1.1.6)$$

with

$$\mathbf{P}^{(1)}(\mathbf{k},\omega)=\chi^{(1)}(\mathbf{k},\omega)\cdot\mathbf{E}(\mathbf{k},\omega)$$

$$\mathbf{P}^{(2)}(\mathbf{k},\omega)=\chi^{(2)}(\mathbf{k}=\mathbf{k}_1+\mathbf{k}_2,\omega=\omega_1+\omega_2):\mathbf{E}(\mathbf{k}_1,\omega_2)\mathbf{E}(\mathbf{k}_2,\omega_2)$$

$$\mathbf{P}^{(3)}(\mathbf{k},\omega)=\chi^{(3)}(\mathbf{k}=\mathbf{k}_1+\mathbf{k}_2+\mathbf{k}_3,\omega=\omega_1+\omega_2+\omega_3):\mathbf{E}(\mathbf{k}_1,\omega_1)\mathbf{E}(\mathbf{k}_2,\omega_2)\mathbf{E}(\mathbf{k}_3,\omega_3)$$

and for the *n*th order

$$\mathbf{P}^{(n)}(\mathbf{k},\omega)=\chi^{(n)}(\mathbf{k}=\mathbf{k}_1+\mathbf{k}_2+\cdots+\mathbf{k}_n,\omega=\omega_1+\omega_2+\cdots\cdots+\omega_n):$$
$$\mathbf{E}(\mathbf{k}_1,\omega_1)\mathbf{E}(\mathbf{k}_2,\omega_2)\cdots\cdots\mathbf{E}(\mathbf{k}_n,\omega_n) \qquad (1.1.7)$$

where $\chi^{(n)}$ is the *n*th-order nonlinear susceptibility. These linear and nonlinear susceptibilities characterize the optical properties of a medium.

Both $\mathbf{E}(\mathbf{r},t)$ and $\mathbf{P}(\mathbf{r},t)$ can be decomposed into a set of infinite plane waves in terms of $\mathbf{k},\omega$ spaces:

$$\mathbf{E}(\mathbf{r},t)=\Sigma\,\mathbf{E}_i(\mathbf{k}_i,\omega_i)= \Sigma\,\mathbf{E}_{0i}e^{i(\mathbf{k}_i\cdot\mathbf{r}-\omega_i t)},$$

$$\mathbf{P}^{(1)}(\mathbf{r},t)=\Sigma\,\mathbf{P}^{(1)}(\mathbf{k}_i,\omega_i)=\Sigma\chi^{(1)}(\omega_i)\cdot\mathbf{E}_i(\mathbf{k}_i,\omega_i), \qquad (1.1.8)$$

and

$$\mathbf{P}^{NL}(\mathbf{r},t)=\Sigma\,\mathbf{P}^{(n)}(\mathbf{r},t)=\Sigma\,\mathbf{P}^{NL}(\mathbf{k}_m,\omega_m)=\Sigma\,\mathbf{P}_0{}^{NL}e^{i(\mathbf{k}_m\cdot\mathbf{r}-\omega_m t)},$$

where $\mathbf{E}_{0i}$ is time independent.

Substituting Eq(1.1.8) and $\varepsilon(\omega_i)= 1+ 4\pi\chi^{(1)}(\omega_i)$ into Eq(1.1.5) yields:

$$[\,\nabla\,X\,(\,\nabla\,X\,) - \frac{\omega^2}{c^2}\varepsilon]\,\mathbf{E}(\mathbf{k},\omega)= \frac{4\pi\omega^2}{c^2}\,\mathbf{P}^{NL}(\mathbf{k}_m,\omega_m) \qquad (1.1.9)$$

Equation (1.1.9) clearly indicates that the various waves $\mathbf{E}_i(\mathbf{k}_i,\omega_i)$ are nonlinearly coupled through the nonlinear polarization $\mathbf{P}^{NL}$, and

their propagation in the medium will be very different from the linear case where $\mathbf{P}^{NL}=0$.

The nonlinear susceptibilities $\chi^{(n)}$ are acting as the coupling coefficients. Through nonlinear coupling, energy can now be transferred back and forth between waves. The bigger $\chi^{(n)}$ is, the larger $\mathbf{P}^{NL}$ is, and the more pronounced the effect should be.

Physically, $\chi^{(n)}$ is related to the microscopic structure of the medium and its value can be properly evaluated only from quantum mechanics(density matrix formalism and perturbation theory). Simple models, such as anharmonic oscillator[2] and free electron gas[2], are also developed. Quantum mechanical calculations of second-order polarizabilities have advanced to a point where molecules can be designed to give large nonlinear effects. These calculations were confirmed by solution studies using the technique of electric field induced second harmonic generation. On the other hand, the calculation of the third order polarizabilities is still in its infancy and requires more attention

The second order nonlinearity, characterized by $\chi^{(2)}$ and third order, by $\chi^{(3)}$, are the main subjects of nonlinear optics at the moment. Second harmonic generation, sum- and diffference-frequency generation, optical parametric oscillation and amplification, and linear(Pockels) electrooptic effects belong to the second order category. Second order effects occur only in materials with asymmetric structures. The third harmonic generation, Kerr effect and intensity induced change of refractive index, four wave mixing, phase conjugation, self-focusing, two-photon absorption and Raman scattering are the typical third order nonlinear effects. Third

order nonlinear processes occur in all materials. It is the lowest order of nonlinearity in the materials with central symmetric structures. In this thesis work, only the third order nonlinearity is studied.

Nonlinear optics can have many applications. In optical computing applications, it will provide: (a)processing times potentially millions of times faster than electronics; (b)direct processing of images; and (c)neural networks for artificial intelligence. In optical communications and computing applications, nonlinear effects allow light by light switching and modulations. Nonlinear effects can also be used in the control of laser beams, such as beam combining, beam steering, correcting beam distortion and laser frequency converting. Other uses such as to protect eyes against laser damage are also considered. In the future, more applications in military and commercial areas are expected. For the fulfillment of those numerous applications, the right materials are needed. The appropriate materials should have the following characteristics: larger nonlinear susceptibilities, fast response times, low losses, and should be easy to process.

In the following section, the nonlinear optical materials are reviewed and the reasons to select polymers are discussed.

1.2 Nonlinear Materials

Scientific and commercial interest in nonlinear optical materials has increased dramatically in the past decade, in part due to a variety of anticipated applications ranging from sensor protection to optical computing. Electronics owes its success to a flexible basic

material-**silicon**, on which all devices and building blocks are based. Photonics is still searching for an analogous material to fulfill the potential of nonlinear optics.

Interest has been divided between non-centrosymmetric, $\chi^{(2)}$, and centrosymmetric, $\chi^{(3)}$, materials and between inorganic and organic materials. This thesis will focus on the third order materials. The major classes of materials competing for a role in nonlinear photonics devices are semiconductors and organic polymers .

Listed in Table 1.2.1 are the magnitude and the response time of known third order nonlinear optical susceptibility $\chi^{(3)}$, for some representative nonlinear optical materials.

As it is evident from this table, there is a fundamental tradeoff between the speed and the size of the third order susceptibilities $\chi^{(3)}$. CS_2 is listed as a reference. Inorganics materials, such as semiconductors, currently yield larger third-order nonlinear susceptibilities $\chi^{(3)}$, but the response times are generally slower. The electronic origin of $\chi^{(3)}$ for polymers makes their nonlinear optical switching time in the subpicosecond region. The moderate nonresonant $\chi^{(3)}$ for polymers are broadband from ultra-violet(UV) to the near infrared(NIR), the high semiconductor $\chi^{(3)}$ in contrast are wavelength specific, being limited to the wavelengths close to the bandgap.

Table 1.2.1 Third Order Nonlinear Optical Properties of Some Materials

Material	$\chi^{(3)}$(esu)	Speed(s)	Comments
MQW (GaAs)	10^{-3}	10^{-8}	res.(excitons)[4]
ZnS	10^{-2}	10^{-5}	thermal, single crystal
InSb	10^{-1}	10^{-7}	res. (77^0 K)[5]
PbO glass	10^{-14}	10^{-13}	Kerr effect[6]
CS_2	10^{-13}	10^{-12}	Kerr effect, liquid[7]
PTS (polymer)	10^{-11}	10^{-13}	off res.,single crystal[8]
	10^{-10}	10^{-12}	on res.[8],
trans-PA (polymer)	$>10^{-9}$	$<10^{-12}$	off res., stretched films[9]

To date, organic polymers[10,11] are considered as leading candidates also because of other additional advantages, including: synthetic and processing options that are not available with the single crystal and multiple quantum wells classes of nonlinear materials. Structurally, polymers can be made as thin or thick films,

bulk crystals, or liquid and solid solutions, and can be formed into layered film structures with molecular engineering providing different optical properties from layer to layer. Mechanically, the materials can be strong and resistant to radiation, shock, and heat. Another important attribution of polymers is that they show all the nonlinear optical properties, while MQW show third order but no optical amplification. There is no diffusion problems in polymers. Additionally, organic and polymeric materials can exhibit high optical damage thresholds, broad transparency ranges, and can be polished to high optical quality surfaces.

Recently, considerable interest has been directed to conjugated polymers. Theoretical estimations and experimental investigations have firmly established that larger electron delocalization is a prerequisite for large values of the nonlinear optical coefficients. This criteria can be met with electrons in conjugated molecules and polymers. Conjugated polymers are in general characterized by highly anisotropic optical, dielectric, conducting and mechanical properties. This is because the valence electrons are responsible for these properties. Those electrons respond more easily to perturbations along the directions where the conjugation occurs than in others. The delocalization of those electrons in the other directions is hindered by saturated bonds which keep the conjugated systems with an isolator type behavior in the directions across the conjugation direction, but semiconducting behavior along the conjugation directions. Only those semiconducting polymers will be reviewed in the following sections.

In this thesis, work was performed on two groups of conjugated polymer systems: the π electron systems, such as polyacetylenes[12-21], polydiacetylenes, polythiophenes[21-32], and σ electron systems, such as polysilane polymers[32-38].

1.2-1) π-electron Conjugated Polymers

The characteristic valence four of the C-atom is the origin of the enormous variety of these π-electron systems. Purely steric and topological considerations indicate that carbon conjugated polymeric structures can be either one- or two- dimensional since the conjugation arises from the electrons in p-orbitals which do not participate in sp-hybridization to form the skeleton of the saturated bonds. Indeed, conjugation can not be present if the four electrons are involved in four different bonding directions like in the diamond structure. Polyacetylene, such as trans-$(CH)_x$; polydiacetylene, such as poly bis(p-toulene sulfonatt) of 2,4-hexadiyne-1,6 diol(in short,PDA-PTS), 4-butoxycarbonykmethylurethane(in short, 4BCMU); and polycondensed thiophene based polymer(polythiphenes); are quasi-one dimensional π-electron semiconducting polymers based on carbon atoms.

Conjugated π electron backbone structure has been shown to be a prerequisite both for charge-transport and nonlinear optical properties. Measurements of $\chi^{(3)}$ for polymeric and macromolecular π-electron materials have permitted evaluation of some theoretical issues, including the dependence of $\chi^{(3)}$ upon electron delocalization length predicted by scaling theories, semiempirical calculations, and

ab initio calculations. The π - electron delocalization is definitely a promising mechanism for the large nonlinearity in the materials.

π electron systems, such as trans-$(CH)_X$ and polythiophene have also raised other interesting questions as to the effect of lattice charge upon nonlinear optical activity. This question has only recently started to be addressed theoretically and experimentally. Those polymers can be chemically or electrochemically doped via oxidation(removal of electrons from the polymer's π-electron system) or reduction (addition of electrons to the polymer's π-system). Those processes can also be achieved by photoexcitations. The electronic excitations of these quasi-one dimensional semiconductors are different from the electron-hole pairs found in ordinary semiconductors. It has been shown that the response of polymer chains to the added charges(either through doping or photoexcitation) is essentially nonlinear. According to Su-Schrieff-Heeger soliton model, after doping or photoexcitation, rapid lattice relaxations due to the strong electron-phonon coupling result in the formation of self-trapped excitations such as solitons, polarons and bipolarons[39,40]. The linear absorption coefficient will be dramatically affected. Bleaching of strong absorption in the visible with the accompanying appearance of infrared(IR) and near infrared(NIR) bands. The nonlinear optical activity may also change dramatically between pristine and doped forms of the polymer lattice.

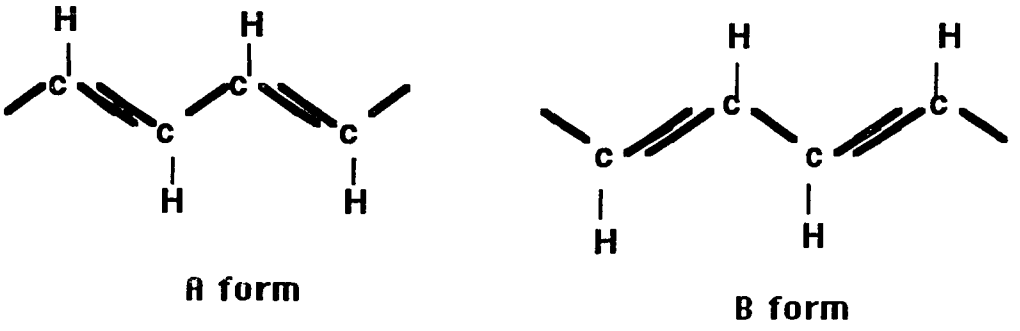

Fig. 1.2.1 Molecular Structures of Trans-$(CH)_X$

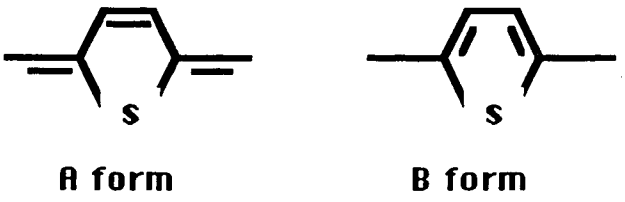

Fig. 1.2.2 Molecular Structures of Polythiophene Polymers

Two classes of polymers can be distinguished in terms of their ground state status. Polyacetylene, $(CH)_x$ (Trans-$(CH)_x$) is shown in Fig. 1.2.1. Since the two ground states of forms A and B are energetically equal, Trans-$(CH)_x$ has a degenerate ground state, solitons are proposed as the important excitations and the dominant charge carriers.

Polythiophene(PT)(see Fig. 1.2.2), is a conjugated polymer in which the ground state degeneracy is weakly lifted, energetically, form A and B are not equal, so that polarons and bipolarons are the important excitations and the dominant charge storage configurations. What is interesting about those nonlinear excitations

is the following. The generation of those nonlinear excitations with their associated electronic states inside the gap(normally in NIR and IR), will result in the redistribution of oscillator strength(produced in less than a picosecond), and this is proposed as the possible new mechanism to enhance the large nonlinear optical effects in these polymers.

The different nonlinear excitations are expected to play an important role in the nonlinear optical properties. The investigation of $\chi^{(3)}$ for corresponding doped(or photoexcited) and pristine polymer lattice is obviously an area of research activity which need to be pursued.

1.2-2)σ-electron Conjugated Polymers

The polysilane polymers represent another distinct class of conjugated polymers which are remarkably different from π electron systems. These polymers have a molecular structure: $(R_1\text{-Si-}R_2)_n$, that is, a long catenated σ - bonded silicon backbone with two sidegroups R_1 and R_2, usually carbon based, attached to each Si atom in the backbone chain. They are soluble in most hydrocarbon solvents and thin films of excellent optical quality can be fabricated with conventional spinning and coating techniques. In spite of the σ - bonded nature of the backbone, the polysilanes show extensive electronic delocalization, resulting in strong transitions for excitations polarized parallel to the backbone. They are unique in that the electron delocalization along the backbone chromophore makes the polymer transparent through the visible to the infrared in contrast to

the π electron polymers which normally absorb strongly in the visible. The measured $\chi^{(3)}$ value(10^{-12} esu) are highest ever reported for the transparent materials and can be substantially improved by adding conjugated sidechains and optimizing polymer orientation.

Polymers offer time response ranging over fifteen orders of magnitude, including the large nonresonant electronic response(fs), thermal and motional(ns), configurational and orientation(μs) and photochemical nonlinearities(s). The contribution of each of these mechanisms to the nonlinear process needs to be understood in order to design ultrafast polymers device with ultrafast response time. Nonlinear measurements then become a critical issue.

1.3 Thesis Statement

The objective of this thesis work is to study the third order optical nonlinear properties in two important class of polymers: π - and σ - electron systems. Picosecond degenerate four wave mixing, single beam Z-scan and optical Kerr gate are used to measure important parameters such as the magnitude and response time, and the sign of $\chi^{(3)}$.

1.4 Thesis Outline

First, I want to have a good understanding of the basic properties of these materials. In π - electron systems, I started with

polyacetylene which has the simplest structure. Then, I extended my work to the more complicated systems, such as polythiophene polymers. In polythiphene, the research is not restricted to the nonlinearities arising from delocalized π-electrons. I have investigated the role played by nonlinear photoexcitations, such as polarons in $\chi^{(3)}$ by comparing the response from corresponding pristine and photoexcited pristine polymer lattice. I have also studied σ-electron systems which are relative new, not fully characterized materials. These materials are very attractive since they are transparent in the visible. This thesis is outlined as follows:

In chapter II, the experimental techniques and apparatus used to investigate the third order optical nonlinearities are presented, as well as, some of the fundamental principles of those techniques.

In chapter III, measurements of the magnitude and response time of the third order nonlinear coefficient at resonance in a dilute solutions of polyacetylene are reported. The relative large and fast response compared to results in solid samples, indicates that changes in morphology and interchain order do not play a significant role in the nonlinear response.

In chapter IV, the relaxation time of the transient degenerate four wave mixing grating in 4-Butoxycarbonylmethylurethane(4BCMU) polydiacetylene in polymethylmethacrylate matrix films has been found to be laser intensity dependent. This phenomenon is attributed to a transient

reversible light-induced structure change in polydiacetylene films, involving a cooperative effect originated from side-chain intramolecular hydrogen bonding.

In chapter V, measurements of χ^3 in polythiophene and a homologous series of polycondensed thiophene based polymers above and below the absorption edge using the folded boxcar four wave mixing technique are presented. Above gap the nonlinear coefficient χ^3 was found to be one of the largest and fastest among polymers.

In chapter VI, the sign of χ^3 in polythiophene thin films are determined by the single beam Z - scan technique. Real part of χ^3 have been found to be negative at both 532 and 1064 nm. The single photon transition is the resonant mechanism for the negative χ^3 at 532 nm; while two photon absorption is responsible for the negative χ^3 at 1064 nm.

In chapter VII, the enhancement of the third order nonlinear susceptibility $\chi^{(3)}$ in polythiophene thin films was observed about photoinduced polaronic bands by a novel "pump-probe" degenerate four wave mixing technique. Enhancement of the degenerate four wave mixing signal for more than an order of magnitude was achieved with response time of less than 25 ps. Based on the fast response and the pumping fluence dependence of the enhanced signal, resonance with the fast intrachain polarons is proposed as the possible responsible mechanism for the observed enhancement.

In chapter VIII, Ultrafast relaxation kinetics of third-order nonlinear susceptibility $\chi^{(3)}$ of polysilane polymers was measured using both the picosecond Kerr gate and forward degenerate four wave mixing. The relative contributions from various nonlinear decay mechanisms were estimated from the time response. The third order nonlinear response was measured to be faster than 3ps arising from electronic mechanism. A slower component is assigned to the refractive-index grating due to light pressure.

In chapter IX, The signs of the third order optical nonlinear susceptibility $\chi^{(3)}$ of polysilane have been determined to be negative at 532nm and positive at 1064nm from single beam Z - scan measurements. Two different physical mechanisms are found to be responsible for the sign change at these two wavelengths. The small and positive $\chi^{(3)}$ at 1064nm arises from the bond-electronical process, including 'nuclear' and 'electronic' contributions. The negative $\chi^{(3)}$ at 532nm is attributed to a two photon absorption resonance transition.

In chapter X, the near infrared third order optical nonlinearity of polysilane solutions with various side groups has been studied by degenerate four wave mixing with picosecond pulse at 1064 nm. Results indicates that $\chi^{(3)}$ at 1064 nm is small($\sim 10^{-13}$esu), and fast(<25ps). It is most likely the intrinsic nonlinearity of polysilane polymers.

In chapter XI, the major conclusions drawn of this thesis are summarized.

In the final chapter XII, future research directions are proposed.

Reference

1. N. Bloembergen, ***Nonlinear Optics***, Benjamin, New York, 1965.

2. Y. R. Shen, ***The principle of Nonlinear Optics***, Join Wiley &Sons, Inc. 1984.

3. ***Quantum Electronics***, Ed. by Herbert Rabin, C. L. Tang, Vol.1, NOnlinear Optics Part A.

4. D. A. B. Miller, D. S. Chemla, D. J. Eilenberger, P. W. Smith, A. G. Gossard, W. Wiegmann, Appl. Phys. Lett. **42**, 925(1983).

5. D. A. B. Miller, C. T. Seaton, M. E. Price, S. D. Smith, Phys. Rev. Lett. **47**, 197(1981).

6. I. Thomazeau, J. Etchepare, G. Grillon and A. Migus, Opt. Lett. **10**, 223(1985).

7. S. L. Shapiro, H. P. Broida, Phys. Rev., **154**, 129 (1967).

8. G. M. Carter, Y. J. Chen, M. F. rubner, D. J. Sandman, M. K. Thakur, S. K. Tripathy, ***Nonlinear Optical Properties of Organic Molecules and Crystals***, vol. 2, Ed. by D. S. Chemla and J. Zyss(academic Press, New York, 1987).

9. S. Etemad, G. L. Baker, D. Jaye, F. Kayzar, J. Messier, Proc. SPIE, **682**, 44(1986).

10. ***Nonlinear Optical Properties of Organic Polymeric Materials,*** Ed. by D. J. Williams, American Chemical Society Symposium, Series 233(Amer. Chem. Soc., Washington D. C. 1983).

11. ***Nonlinear Optical Properties of Organic Molecules and Crystals***, vol. 2, Ed. by D. S. Chemla and J. Zyss(academic Press, New York, 1987).

12. C. V. Shank, R. Yen, R. L. Fork, J. Orenstein and G. L. Baker, Phys. Rev. Lett. **49**, 1666(1982), Phys. Rev. B **28**, 6095(1983).

13. L. Rothberg, T. M. Jedju, S. Etemad and G. L. Baker, Phys. Rev. Lett. **57**, 3229(1986), Phys. Rev. B **36**, 7524(1987).

14. F. Kajzar, S. Etemad, G. L. Baker and J. Messier, Solid State Commun.**63**, 1113(1987).

15. M. Sinclair, D. Moses, K. Akagi, and A. J. Heeger, Phys. Rev. B **38**, 10724(1988).

16. R. Dorsinville, Lina Yang, R. R. Alfano, R. Tubino, S. Destri, Solid State Commun. **68**, 875(1988).

17. D. M. Mackie, R. J. Cohen and A. J. Glick, Phys. Rev. B **39**, 3442(1989).

18. W. S. Fann, S. Benson, J. M. J. Madey, S. Etemad, G. L. Baker and F. Kajzar, Phys. Rev. Lett., **62**, 1492(1989).

19. G. B. Blanchet, C. R. Fincher, A. J. Heeger, Phys. Rev. Lett., **51**, 2132(1983).

20. A. Walser, A. Seas, R. Dorsinville, R. R. Alfano, R. Tubino, Solid State Commun., **67** 333(1988)

21. Lina Yang, R. Dorsinville, Q. Z. Wang, W. K. Zou, P. P. Ho, N. L. Yang, R. R. Alfano, R. Zamboni, R. Danieli, G. Ruani and C. Taliani, J. Opt.Soc. Am. B **6**, 753(1989).

22. R. Dorsinville, L. Yang, R. R. Alfano, R. Zamboni and C. Taliani, Opt. Lett. **14**, 1321(1989).

23. R. Worland, S. D. Phillips, W. C. Walker and A. J. Heeger, Synth. Metals **28**, D663(1989).

24. B. P. Singh, M. Samoc, H. S. Nalwa and P. N. Prasad, submitted for publication.

25. R. Zamboni, C. Taliani, G. Ruani, A. J. Pal and F. Kajzar,submitted for publication.

26. G. Harbeke, E. Meier, W. Egli, H. Kiess and E. Tosatti, Solid State Commu. **55,** 419(1985).

27. Z. Vardeny, E. Ehrenfreund, O. Brafman, M. Nowak, H. Schaffer, A. J. Heeger and F. Wudl, Phys. Rev. Lett. **56,** 671(1986).

28. K. Kaneto, F. Uesugi and K. Yoshino, J. Phys. Soc. Jpn. **56,** 3703(1987).

29. K. Kaneto, F. Uesugi and K. Yoshino, J. Phys. Soc. Jpn. **57,** 1859(1988).

30. Z. Vardeny, H. T. Grahn, A. J. Heeger and F. Wudl, Synth. Metals.**28,** C299(1989).

31. S. D. Phillips, G. Yu and A. J. Heeger, Synth. Metals, **28,** D669(1989).

32. F. Kajzar, J. Massier, C. Rosilio, J. Appl. Phys., **60,** 3040(1986).

33. J. C. Baument, G. C. Bjorklund, D. H. Jundt, M. C. Jurich, H. Looser, R. D. Miller, J. Rabolt, R. Sooriyakumaran, J. D. Swalen, R. J. Twieg, Appl. Phys. Lett., **53,** 1147(1988).

34. Lina Yang, Q. Z. Wang, P. P. Ho, R. Dorsinville, R. R. Alfano, W. K. Zou, N. L. Yang, Appl. Phys. Lett., **53,** 1245(1988).

35. Daniel J. McGraw, A. E. Siegman, G. M. Wallraff, R. D. Miller, Appl. Phys. Lett., **54,** 1713(1989).

36. F. M. Schellenberg, B. L. Byer, R. D. Miller, and R. Sooriyakumaran, *XVI International Conference on Quantum Electronics Technical Digest,* (Japan Society of Applied Physics, Tokyo, Japan, 1988),pp. 702-703.

37. F. M. Schellenberg, B. L. Byer, and R. D. Miller, Opt. Lett. **15,** 242(1990).

38. F. M. Schellenberg, R. L. Byer, and R. D. Miller, Chem. Phys. Lett. **166**, 331(1990).

39. W. P. Su and J. R. Shrieffer, Proc. Natl. Acad. USA 77, 5626(1980).

40. R. Ball, W. P. Su and J. R. Shrieffer, J. Phys.(Paris) Colloq **44**, c3(1983).

Chapter II

Experimental Techniques and Apparatus

In designing a photonic device using a nonlinear optical material, the knowledge of some important parameters, such as the magnitude, the response time and the sign of $\chi^{(3)}$ are required. Other relevant factors are the anisotropy of $\chi^{(3)}$(it is a fourth rank tensor), the dispersion of $\chi^{(3)}$, and the temperature dependence of $\chi^{(3)}$. Near a resonance, $\chi^{(3)}$ is a complex quantity. A variety of techniques have been used in this thesis research work to investigate the behavior of $\chi^{(3)}$ as it is usually very difficult to obtain complete information on $\chi^{(3)}$ by a single technique. The technique which is particularly useful in obtaining the magnitude and response time of $\chi^{(3)}$ is the time resolved degenerate four wave mixing(DFWM)[1-3]. The single beam Z-scan technique[4,5] is a simple method to determine the sign of $\chi^{(3)}$. Both techniques are used to complement each other.

The main laser source used in the experiments was the commercially available 30 picosecond(ps) Quantel Nd:YAG laser (YAG denotes yttrium-aluminum-garnet), which is both passively and actively mode locked. The laser rod which is cut at Brewsters angle, is pumped by two Xenon flash lamps. The lasing wavelength is 1.06 μm. Mode locking is achieved by both an acousto-optic crystal (active mode locking) and a saturable absorber dye (passive mode locking) placed inside the laser cavity. The acousto-optic crystal is electrically modulated by a radio frequency signal. This modulation frequency is equal to the round trip time of the laser cavity 2L/c, where L is the

cavity length and c is the speed of light. The combined action of the saturable absorber and the acousto-optic modulator allows the production of a pulse train, there are 8-12 35ps pulses within the gaussian envelope. The total energy in the train is about 7 mJ. The pulses are p-polarized. The saturable absorber has the greatest effect on decreasing the pulse duration, while the acousto-optic modulator has the greatest effect on the shot to shot stability.

The train of pulses is then directed into a Pockel's cell pulse slicer. This device essentially consist of an electro-optic crystal and polarizing optics. A laser pulse can be selected from the laser pulse train, by applying a well defined voltage pulse across the electro-optic crystal, which rotates the polarization of the selected pulse from the train such that it can pass through a cross polarizer. The pulse selected from the pulse slicer is s polarized. The selected pulse is then amplified by a double pass ring amplifier. Using a half wave plate, polarizer, and polarizing beam splitters, the single laser pulse can be amplified to 75 mJ and is p-polarized. Finally the amplified pulse passes through a type I second harmonic generator crystal (KDP). This crystal converts up to twenty percent (20%) of the incident 1.06 μm (the fundamental frequency of the laser) light to the second harmonic frequency of 0.532 μm. The pulse duration of the second harmonic laser pulse is approximately 25-30 ps and is s polarized.

2.1 Degenerate Four wave mixing

Four wave mixing refers to the nonlinear process with four interacting electromagnetic waves. In the weak interaction limit, it is a third order process and is governed by $\chi^{(3)}$. Degenerate four wave mixing is a special case in which all four beams have the same frequency.

In general, $\chi^{(3)}$ consists of 48 terms. While $\chi^{(3)}$ is governed by the symmetric properties of the materials, each term follows the selection rules on its matrix element. Near resonances(singly, doubly and triply resonance), only few terms dominate due to the resonant denominators. $\chi^{(3)}$ can be written as: $\chi^{(3)} = \chi^{(3)}_{NR} + \chi^{(3)}_{R}$.

The theory of DFWM follows closely the general theory of optical mixing. For simplicity, a cubic or isotropic medium is assumed, and only steady state case, for instance, when laser pulse is much longer than the response time of the materials, is considered. Let the input beams be: $\mathbf{E}_m = \mathbf{E}_{0m} e^{i(\mathbf{k}_i \cdot \mathbf{r} - \omega t)}$, with m=1,2,3(see Fig. 2.1.1). The output field is $\mathbf{E}_s = \mathbf{E}_{0s} e^{i(\mathbf{k}_s \cdot \mathbf{r} - \omega_s t)}$, with $\omega_s = \omega + \omega - \omega = \omega$.

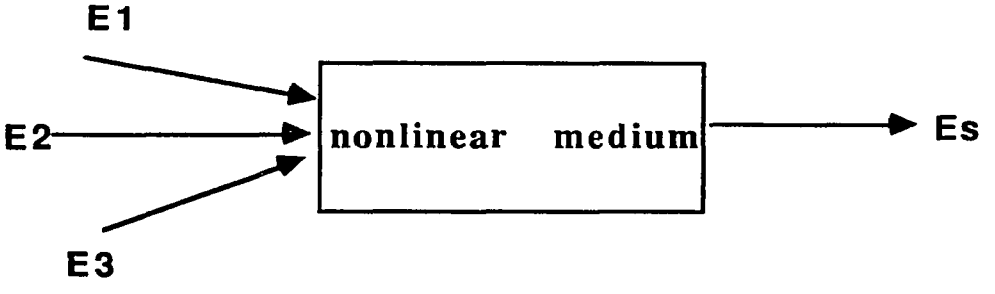

Fig. 2.1.1 Four Wave Mixing in the nonlinear medium

$\mathbf{E}_s$ is governed by the wave equation(see equation (1.1.9)):

$$[\nabla^2 + \frac{\omega^2}{c^2}\varepsilon(\omega_s)]\,\mathbf{E}_s = -\frac{4\pi\omega_s^2}{c^2}\mathbf{P}^{(3)}(\omega_s) \qquad (2.1.1)$$

where

$\mathbf{P}^{(3)}(\mathbf{k}_s,\omega_s)=\chi^{(3)}(\mathbf{k}=\mathbf{k}_1\pm\mathbf{k}_2\pm\mathbf{k}_3,\omega=\omega\pm\omega\pm\omega):\mathbf{E}(\mathbf{k}_1,\omega)\mathbf{E}^*(\mathbf{k}_2,\omega)\mathbf{E}(\mathbf{k}_3,\omega)$. Where $\mathbf{E}^*(\mathbf{k}_2,\omega)$ denotes the complex conjugate of $\mathbf{E}(\mathbf{k}_2,\omega)$. With the usual slowly varying amplitude approximation, negligible pump depletion, and simplifying boundary condition. The solution of Eq(2. 1. 1) yields:

$$E_{0si}(z)= - \frac{2\pi\omega_s^2}{(\Delta k\cdot z)k_s c^2}\chi^{(3)}_{ijkl}E_{1j}E_{2k}^*E_{3l}(1- e^{-i\Delta k\cdot z})e^{-\alpha_{si}z} \qquad (2.1.2)$$

where ijkl denote the polarization direction of the components, α_{si} is the attenuation coefficient of the waves along z. And $\Delta k= \mathbf{k}_1 \pm \mathbf{k}_2 \pm \mathbf{k}_3 \pm \mathbf{k}_4$, is the wavevector mismatch.

The phase matching($\Delta k=0$) is of prime importance here, since it greatly enhances the signal output. In four wave mixing, phase matching can be achieved in a number of ways by properly adjusting the propagation directions of three input waves. The arrangement preferred often depends on practical considerations, such as optimum beam overlapping length and better spatial discrimination against the scattering background. Different geometries, such as backward ***phase conjugation***[6,7] and ***forward folded boxcar***[8] have been used in this research. Since these methods follow the same principle, only the ***forward folded boxcar*** geometry will be discussed substantially. The other geometries and the corresponding forms of $\chi^{(3)}_{ijkl}$ will be introduced when they applied to the experiments.

The FWM apparatus using Nd:YAG laser is shown in Fig. 2.1.2. Fig. 2.1.3(a) and (b) show the schematic of the beam geometries on the surface of the sample and in the aperture plane. The three incident beams which are not collinear, are labeled 1, 2 and 3, with 4

being the output(signal) beam, which is generated by the input beams via $\chi^{(3)}$. The direction of $\mathbf{k}_4$ is determined by the other three beams such that the phase matching condition is satisfied. Given the three input beams shown in Fig. 2.1.3, and the fact that beam 4 has the same frequency as the other input beams, the fourth beam will be generated in the position shown in Fig. 2.1.3(b), where $\mathbf{k}_4 = \mathbf{k}_1 - \mathbf{k}_3 + \mathbf{k}_2$.

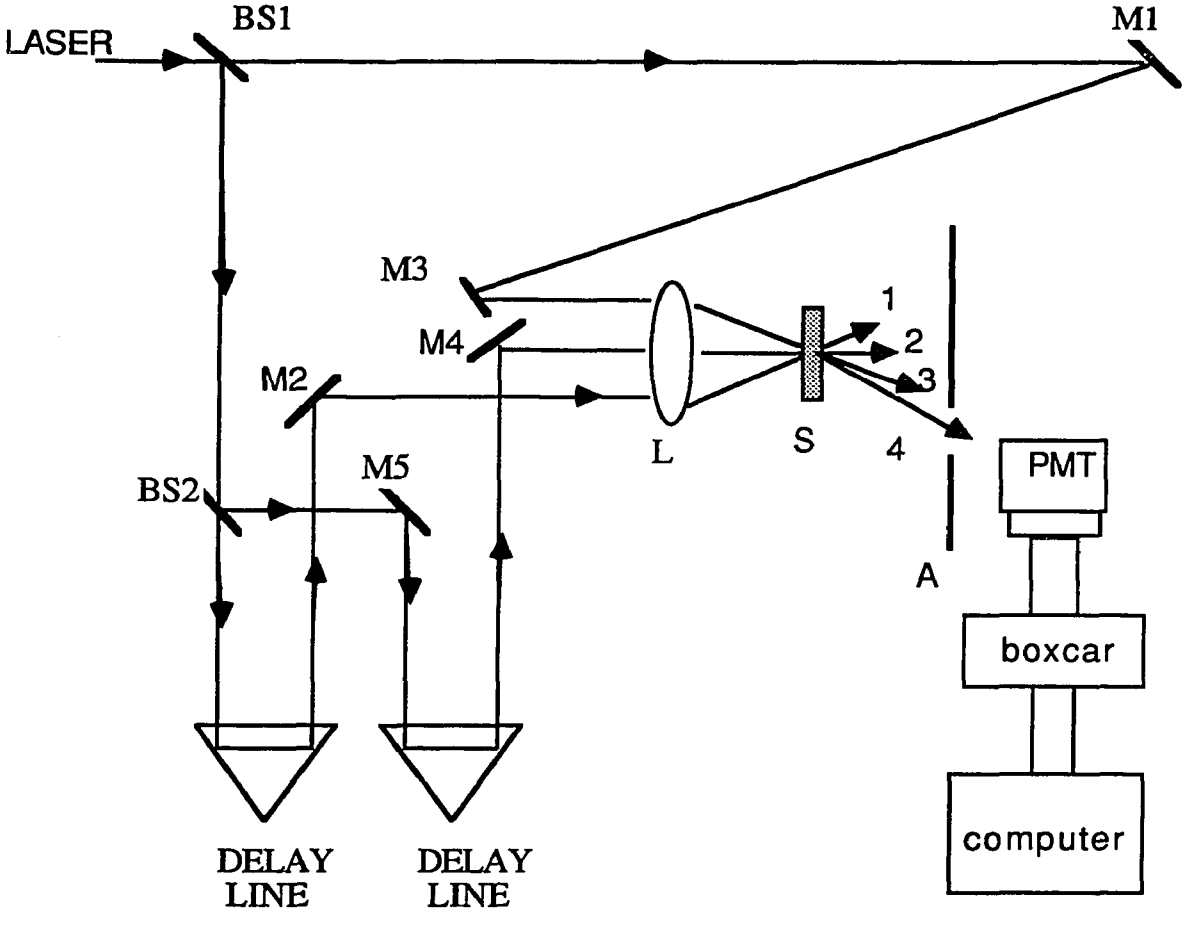

Fig.2.1.2 Experimental Set up for Four Wave Mixing

BS1-2-beam splitters, M1-5-mirrors, S-sample, L-lense, PMT-photomultiplier

The four beams in Fig 2.1.3(b) are shown after emerging from the sample, so that they are spatially separated. This ***forward folded boxcar*** geometry allows the generated signal beam 4, to be spatially separated from the more intense incident pulses. Thus this geometry increases the signal to noise ratio. This arrangement is particularly important for degenerate FWM experiments because all the beams have the same frequency.

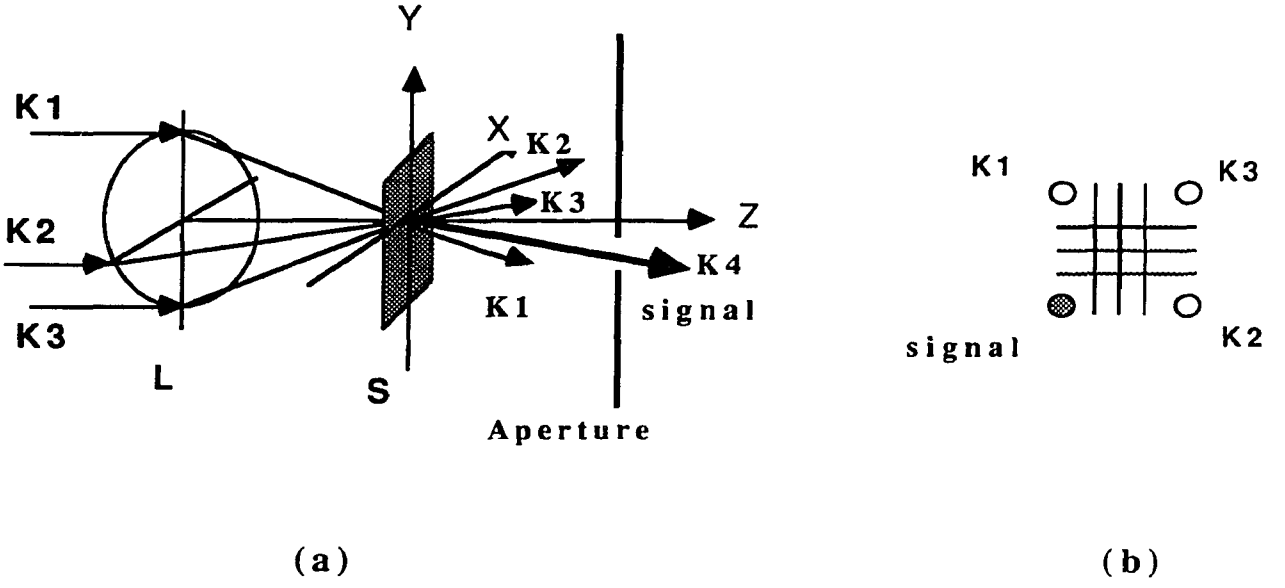

Fig. 2.1.3. (a)Schematic of the optical beam geometry in the sample; (b)beams at aperture.

In DFWM, beams 1 and 3 are coincident both in time and space to form a grating during the measurements, while beam 2 is time delayed($T_d>0$) or advanced($T_d<0$) relative to beams 1 and 3. This permits the determination of the temporal response of $\chi^{(3)}$ from the materials. Notice that when the three input beams overlap both temporally and spatially, diffractions from two gratings will contribute to the signal. Grating 1 is formed by beam 3 and 2, $k_2 - k_3$

which is presented by the dashed horizontal lines in Fig 2.1.3(b); grating 2 is formed by beam 1 and 3, $\mathbf{k}_3 - \mathbf{k}_1$ which is presented by the solid lines.

If $\mathbf{E}_m$ are gaussian beams, then $E_{0m} = A_{0m} e^{-\rho^2/\rho_0^2} e^{-t^2/a^2}$, where A_{0m} is a constant independent of the time t, ρ is the transverse (cylindrical) coordinate, ρ_0 is the beam waist, and a determines the pulse width of the beam. When the phase matching condition is satisfied, the final expression of $\chi^{(3)}$ can be deduced from equation (2.1.2)[9,10]:

$$\chi^{(3)}_{ijkl} = \frac{cn^2}{32\pi^2}\left(\frac{\lambda_0 \rho_0^2}{2aL}\right)\left[\left(\frac{45}{8}\right)\frac{E_{si}}{E_{1j}E_{2k}E_{3l}}\right]^{1/2} e^{-\alpha L}, \qquad (2.1.3)$$

where L is the sample length. Phase matching is achieved by setting $\Delta k = 0$.

Note that when equation (2.1.3) is used to determine $\chi^{(3)}$, accurate knowledge of the temporal and spatial dependence of the optical fields is required. Normally, CS_2 is used as a reference with a known $\chi^{(3)}_{xxxx}$ value of 8.0 x 10^{-13}esu. If $\chi^{(3)}$ of the sample and CS_2 are measured under the same excitation conditions, then:

$$\chi^{(3)}_{S\,xxxx} = \chi^{(3)}_{CS_2 xxxx}\left(\frac{n_S}{n_{CS_2}}\right)^2\left(\frac{L_{CS_2}}{L_S}\right)\left[\frac{E_{si}}{E_{CS_2}}\right]^{1/2}\frac{e^{-\alpha_S L_S}}{e^{-\alpha_{CS_2} L_{CS_2}}}. \qquad (2.1.4)$$

This formula is going to be used frequently in our measurements.

When two-level(ground and excited states) system is assumed for the material, the time information of the fourth beam can be obtained from the following equation:

$$E_4(t)=K[E_3(t)\int_{-\infty}^{t}dt'E_2(t'+T_d)E_1(t')f(t,t')$$

$$+E_2(t+T_d)\int_{-\infty}^{t}dt'E_3(t')E_1(t')f(t,t')] \qquad (2.1.5)$$

where $f(t,t')=e^{(t'-t)/T_1}$, T_1 is the lifetime of the excited state, K is a time independent complex constant, and T_d is the time delay set by beam 2 relative to beams 1 and 3. For the experiments described here the fourth beam is detected with a photomultiplier(PMT) that has a response time much greater than either the laser pulse duration or T_1. Thus we can approximate the signal $S_4(T_d)$ from the PMT as the integral of $|E_4|^2$ over all time.

When the temporal response is studied, two cases are going to be considered. The first case is when the material response time T_1 is slower than the laser pulse. The output signal S_4 is asymmetric with respect to $T_d=0$ point, with the fast rise edge on the $T_d<0$ side. T_1 can be obtained by the best fitting of the experimental data using equation (2.1.5).

In the second case, T_1 is much faster than the laser pulse. Letting T_1 approach zero , f(t',t) becomes a delta function,

$$f(t',t)=\begin{cases}1, & t'=t\ ;\\ 0, & \text{otherwise.}\end{cases}$$

In this case, S_4 is symmetric with respect to T_d, giving the pulse duration.

2.2 Single beam Z - scan technique

The Z-scan technique, shown in Fig. 2.2.1, is a new single beam technique to give the sign and the size of $\chi^{(3)}$. It is based on the transformation of phase distortion to amplitude distortion during Gaussian beam propagation. The principle of this technique can be qualitatively explained as follows.

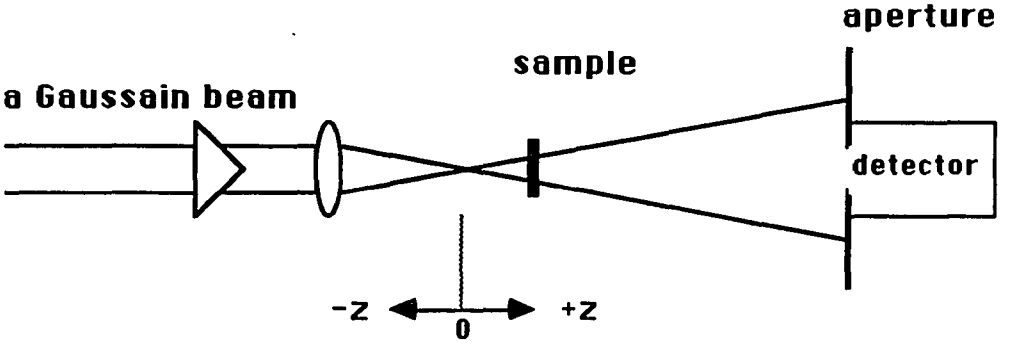

Fig. 2.2.1 Single Beam Z-scan Set-up

The transmittance through a finite aperture placed in the far field of a tight focused Gaussian laser beam can be measured as a function of the nonlinear sample position(z) with respect to the focal plane. The focal plane is defined as z=0 plane. Assuming the sample having a negative $\chi^{(3)}$, with the sample on the -z side of the focal plane, the negative lens effect of the sample will tend to collimate the beam, thus increasing the transmittance; the same effect will result in the reduction of the transmittance when the sample is on the +z side. If sample has a positive nonlinearity, the opposite effect,

i.e., lowered transmittance for the sample at -z and enhanced transmittance for the sample at +z, will be expected.

In order to formulate and analyze the z-scan technique, we start from the index of refraction n. For a fast cubic nonlinearity, n is expressed in terms of nonlinear indices n_2 through:

$$n = n_0 + \frac{n_2}{2} | E |^2 = n_0 + \Delta n, \qquad (2.2.1)$$

where n_0 is the linear index of refraction and E is the electric field, which is a Gaussian beam:

$$| E(r,z,t) | = | E_0(t) | \frac{\omega_0}{\omega(z)} e^{- r^2/\omega^2(z)} , \qquad (2.2.2)$$

where $\omega^2(z) = \omega_0^2(1 + z^2/z_0^2)$ is the beam radius at z, $z_0 = k\,\omega_0^2/2$ is the diffraction length of the beam, $k = 2\pi/\lambda$ is the wave vector, λ is the laser wavelength, and E_0 denotes the field at focus.

And n_2 is related to $\chi^{(3)}$ by:

$$n_2 = \frac{12\pi}{n_0} \chi^{(3)} . \qquad (2.2.3)$$

Notice that any change in the index of refraction Δn will result in a change of the phase of the field $\Delta\phi$: $\frac{d\Delta\phi}{dz} = 2\pi/\lambda\, \Delta n$. The phase shift $\Delta\phi$ at the exit surface of the sample for a given sample position z is:

$$\Delta\phi(r,z,t) = \frac{\Delta\Phi_0}{1 + z^2/ z_0^2} e^{- 2r^2/\omega^2(z)} , \qquad (2.2.4)$$

with

$$\Delta\Phi_0(t) = \frac{2\pi}{\lambda} \Delta n_0(t) \frac{1 - e^{-\alpha L}}{\alpha} , \qquad (2.2.5)$$

where L is the sample length and $\Delta n_0(t)$ is the instantaneous on axis index change at the focus(z=0). The electric field at the exit surface of the sample at z_1 now contains the nonlinear phase distortion,

$$E'(r, z_1, t) = E(r,z_1,t) e^{-\alpha L/2} e^{i\Delta\phi(r,z_1,t)} . \qquad (2.2.6)$$

The far field pattern of the beam at the aperture plane E_a can be obtained through the zeroth-order Hankel transformation of E'. The normalized instantaneous Z-scan power transmittance is

$$T(z,t) = \frac{\int_0^{ra} | E_a(\Delta\Phi_0,r,z,t) |^2 \, r \, dr}{S \int_0^{\infty} | E_a(0,r,z,t) |^2 \, r \, dr}, \qquad (2.2.7)$$

where r_a is the aperture radius and S is the aperture transmittance in the linear regime.

Assuming a constant input field, Fig. 2.2.2 shows a computer simulations of T(z) from equation (2.2.7) with (a) a positive $\Delta\Phi=0.5$, and (b) a negative $\Delta\Phi=-0.5$. The other parameters are chosen as: $\lambda=1.06\mu m$, $\omega_0=25\mu m$, and $r_a=0.7mm$; if our Nd:YAG is used. Thus, a valley followed by a peak transmittance indicates a positive nonlinearity, that is, n_2(or $\chi^{(3)}$)>0, and a reversed order of peak and a valley shows a negative nonlinearity. The sign of the nonlinearity is readily determined.

From the difference between the normalized peak and valley transmittance, defined as $\Delta T_{p-v}= T_p- T_v$, one can estimate the value of n_2 (or $\chi^{(3)}$) without performing a detailed fit to the experimental data. Within a 0.5% accuracy, for small aperture($S\approx 0$) and for phase distortions $|\Delta \Phi_0| = |k \Delta n \frac{1-e^{-\alpha l}}{\alpha}| \leq \pi$, the relationship of the difference between the normalized peak and valley transmittance ΔT_{p-v} and n_2 is given by:

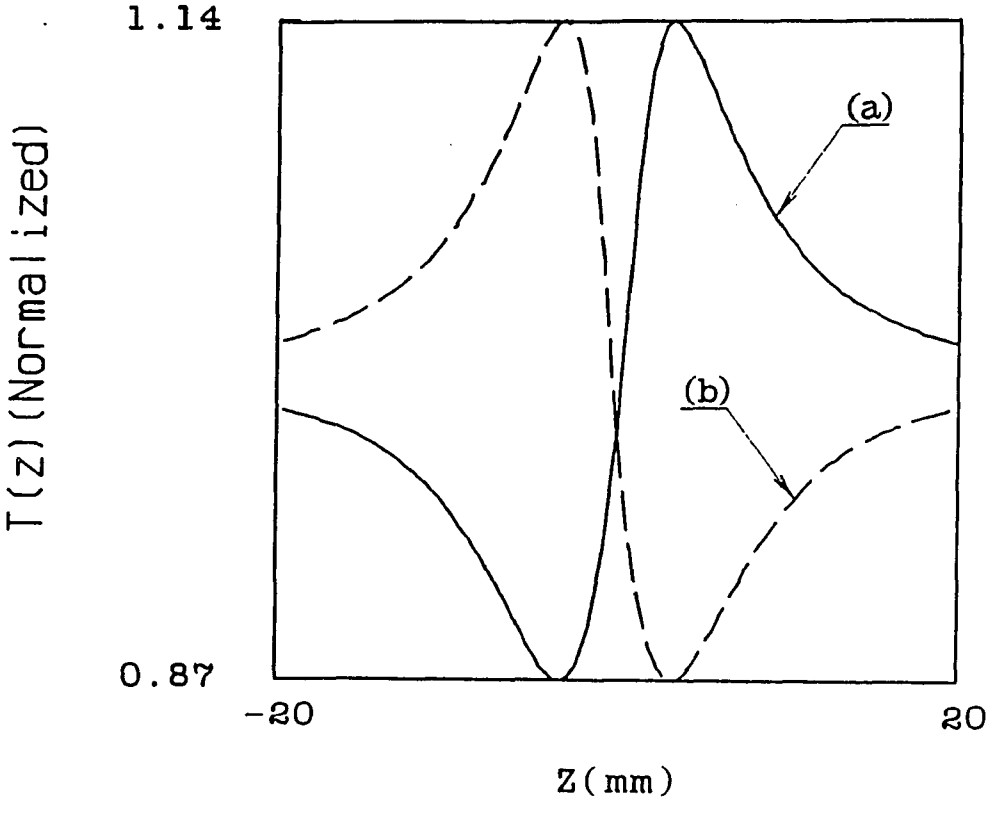

Fig.2.2.2 Calculated T(z) from equation (2.2.7) with (a) a positive $\Delta\Phi$=0.5, and (b) a negative $\Delta\Phi$=-0.5.

$$\Delta T_{p-v} \approx A\,|\Delta \Phi_0| \approx A\,\left|\frac{\pi n_2}{\lambda}|E|^2\frac{(1-e^{-\alpha l})}{\alpha}\right|, \qquad (2.2.8)$$

where l is sample length, α is the absorption coefficient and A is a constant which may depend on the aperture size.

When CS_2 is used as a reference under the same excitation conditions, the value of $\chi^{(3)}$ from the sample can be obtained from:

$$\chi^{(3)}{}_s = \chi^{(3)}{}_{CS_2}\frac{(\Delta T_{p-v}\, n_0)_p}{(\Delta T_{p-v}\, n_0)_{CS2}}. \qquad (2.2.9)$$

where, ΔT should be obtained from the normalized transmittances for both CS_2 and the sample.

Furthermore, the distance between the peak and the valley, defined as Δz_{p-v}, is found to be equal to $1.7z_0$ for the third order nonlinearity.

Reference

1. Y. R. Shen, ***The principle of Nonlinear Optics***, (Join Wiley &Sons, Inc. 1984), Chap.14, P242.

2. H. J. Eichler, P. Gunter, and D. W. Pohl, ***Laser Induced Dynamic Gratings***, (Springer-Verlag, Berlin Heidelberg, 1986).

A. Yariv, Quatum Electronics, 2nd ed. (Wiely, New York, 1975).

3.***Ultrashort Laser Pulses***, Ed. by W. Kaiser,(Springer-Verlag, Berlin Heidelberg, 1988), Chap.3, p60.

4. M. Sheik-bahae, A. A. Said, and E. W. Van Stryland, Opt. Lett. **14**, 955(1990).

5. M. Sheik-bahae, A. A. Said, and E. W. Van Stryland, IEEE J. Quan. Elec. **26**, 760(1990).

6. Robert A. Fisher, ***Optical Phase Conjugation***, Academic Press, 1983.

7. ***Laser Hand Book***, vol.4 Ed. by M. L. Stitch and M. Bass, (Elsevier Science Publishers, B. V.,1985), Chap. 4, p333

8. J. A. Shirley, R. J. Hall, and A. C. Eckbreth, Opt. Lett. **5**, 380(1980).

9. G. M. Carter, M. K. Thakur, Y. J. Chen, and J. V. Hryniewicz, Appl. Phys. Lett. **47**, 457(1985).

10. G. M. Carter, J. Opt. Soc. Am. B **6**, 1018(1987).

Chapter III

Phase Conjugation measurements in Soluble Polyacetylene

3.1 Introduction

Polyacetylene (PA)(see Fig. 1.2.1) is one of the simplest conjugated polymer, consisting of chains of CH units forming a pseudo-1-D lattice. Because of its simple molecular structure, PA electronic properties can be described using relatively simple theoretical models. This makes PA the ideal system to obtain a better understanding of the nonlinear properties of conjugated polymers. The **soluble** polyacetylene gives the possibility to study relatively isolated polyenic chains in which the contribution to the nonlinear optical response arising from interchain effects could be possibly separated from the intrachain effects.[1]

Most recently, the nonlinear optical response χ^3 inside the semiconducting bandgap was determined from third harmonic measurements in polyacetylene films.[2] The measured magnitude of χ^3 was larger than 10^{-9} esu. But, third harmonic generation is due to the fast (electronic) response of the material. Temporal information about nonlinear mechanisms cannot be resolved using this technique. In this chapter, measurements of the third order nonlinear optical coefficient in **soluble** polyacetylene using a time resolved phase conjugation method[3] are reported. The time resolved phase conjugation method with picosecond pulses give a measure of the time response of the nonlinearity.[4] From such measurements the

relative contributions of various mechanisms can be separated in time and estimated.[5]

3.2 Experimental set-up

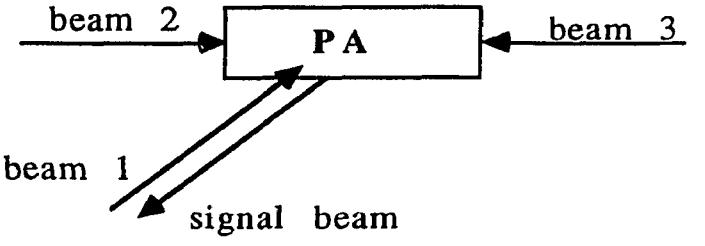

Fig.3.2.1 Phase Conjugation beam geometry

The beam geometry of phase conjugation set-up is shown in Fig. 3.2.1. The Nd:YAG laser system and second harmonic crystal generates 25 ps single laser pulses at 530 nm which are subsequently split into three beams with beam splitters and directed, through variable delay lines, toward the sample. One beam is used as a probe (beam #1) , the other as one of the counterpropagating pump beams (beam #2). The angle between pump and probe was about ~ 6^0. All three beams were focused into the sample cell with 25-30 cm lenses . The signal beam, phase conjugate to the probe beam, was directed by a wedge glass plate toward the entrance slit of a spectrometer and recorded and analyzed using a photomultiplier and a boxcar interfaced to a microcomputer. The pump (beam #2) was delayed relative to the two other beams and the intensities of the phase conjugate and

probe beams was measured for different delays. This geometry allows the study of the nonlinear response due to transient grating effects. All three beams were vertically polarized. The soluble PA was placed in a 1 mm glass cell.

The samples were prepared using the Shirakawa catalyst and growing polyene chains into activated sites of polybutadiene, which acts as a soluble carrier in conventional aromatic solvents. The solution concentration was about 1 X 10^{-5} M/l in toluene. At this concentration absorption was found to be less than 20% at 530 nm. The soluble PA conjugated length was determined from spontaneous Raman spectra and found to be about 20 -25 double bonds.[6] TEM of cast films obtained from a similar solution at a much larger concentration (8 X 10^{-3} M/l) have shown a substantial difference in morphology between our sample and Shirakawa solid films[6]. No fibrillar morphology was observed and although some aggregation was detected the size of the microdomains ($\approx$ 100 Å) was considerably lower than in the films. At the solution concentration used in this work aggregation is not expected to be a problem and with an average distance between chains of about $\approx$ 350 Å, interchain interactions should be negligible.

3.3 Results and discussion

The time resolved phase conjugation signal from soluble trans-PA is shown in Fig. 3.3.1. The third order nonlinear coefficient was determined from measurements of the phase conjugate reflection coefficient, R_{pc}. The phase conjugate reflection coefficient was

measured from the intensities of the phase conjugate and probe beams $R_{pc}= I_{signal}/I_{probe.}$ No signal could be detected from a cell containing the solvent (toluene) alone. Under identical conditions (same geometry , same pump power) the reflectivity of a 1 mm cell containing CS_2 was also measured .

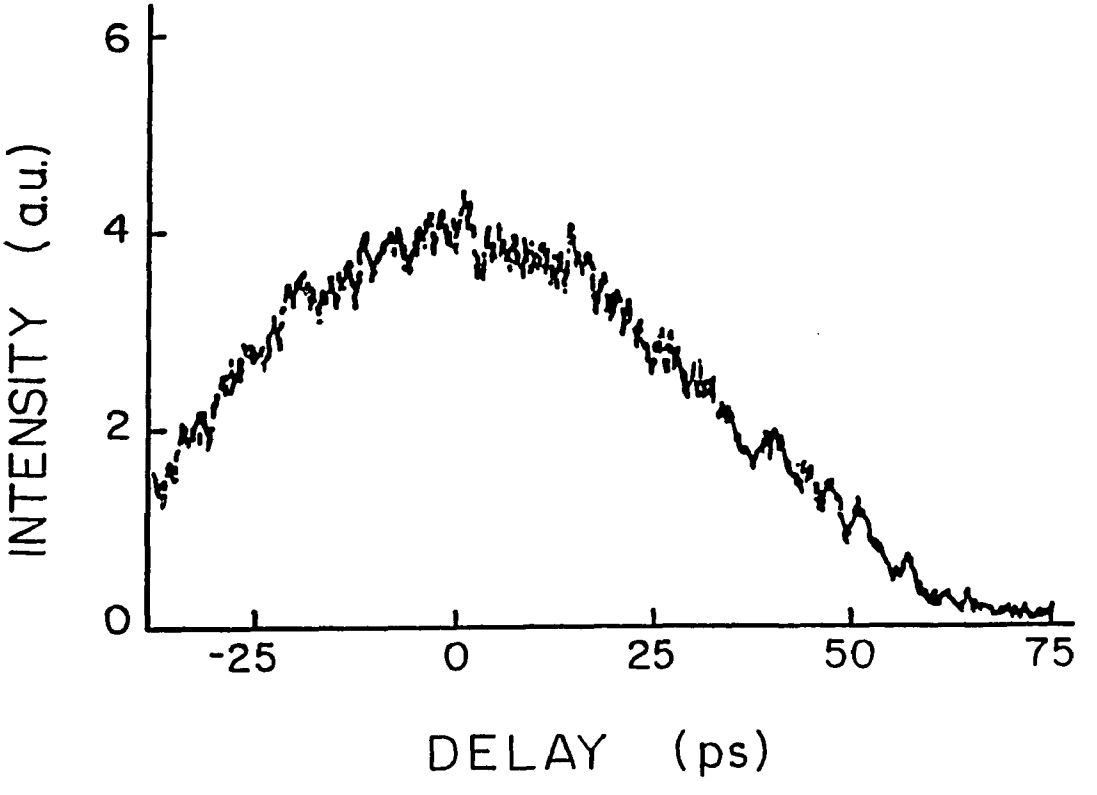

Figure 3.3.1. Soluble trans-PA time resolved phase conjugate signal.

The reflected signal is expected to be a combination of the bound electron and free carrier responses. In a resonant medium, such as PA at 530 nm, the free carrier response is expected to dominate. Under conditions far from absorption saturation, the nonlinear coefficient of the PA solution is proportional to the absorption coefficient. The third order nonlinear coefficient of the PA solution is given by [7]:

$$\chi^3_{sol}=\frac{4c^2n^2\varepsilon_o a\sqrt{R_{pc}}}{3I_pT(1-T)}\ , \qquad (3.3.1)$$

where a the absorption coefficient, T the transmission coefficient, I_p is the pump intensity, R_{pc} the reflection coefficient, n is the solvent (toluene) refractive index, and ω the laser frequency. Using equation (3.3.1) χ^3_{sol} was calculated and found to be equal to:

$$\chi^3_{sol} = 1 \pm 0.2 \text{ X } 10^{-14} \text{ e.s.u..} \qquad (3.3.2)$$

The third order nonlinearity was also determined by comparing the phase conjugate signals for CS_2 and the PA solution. In this case, the third order nonlinearity was calculated using the equation:

$$\chi^3_{sol} = \chi^3_{CS_2}\gamma\left(\frac{I_{sPA}}{I_{sCS_2}}\right)^{1/2} \qquad (3.3.3)$$

where $\gamma = \frac{\alpha n^2 L}{n_c T(1-T)}$, I_s the phase conjugate signal intensity, n_c is the index of refraction of CS_2. In this case $\chi^3_{sol} = (1.4 \pm 0.2) \text{ X } 10^{-14}$ e.s.u., in agreement with the value given above (equation 3.3.2).

In all cases, the calculation used the average intensity of each beam both in time, over the 25 psec duration of the pulse, and in

space over the 1 mm spot size at the sample site. This value of the third order nonlinear coefficient corresponds to a PA density in solution of $N_{sol} = 5.9 \times 10^{-6}$ g/cm^3. PA films prepared using the Shirakawa method have a density $N \approx 0.4$ g/cm^3. An extrapolation of the value of χ^3_{sol} to a PA solid film gives:

$$\chi^3_{PA} \approx \frac{N}{N_{sol}} \chi^3_{sol} = 0.9 \times 10^{-9} \text{ e.s.u.} \qquad (3.3.4)$$

in good agreement with solid samples results.[2] Since the environment experienced by the PA chains in solution is quite different than in the insoluble Shirakawa films these results seem to indicate that interchain interactions do not contribute substantially to the nonlinear response.

The response time of the third order nonlinear coefficient was investigated. In these experiments, the pump beam #2 was delayed so the lifetime of the transient grating formed by the probe beam #1 and beam #3 was measured. This lifetime is expected to be a combination of the bound electron and free carrier responses. The intensity of the phase conjugate signal as a function of delay time is shown in figure 3. 3. 1. The curve is symmetrical with no apparent tail. The rise and decay was identical to those measured with CS_2. This indicates that the grating lifetime was shorter than the time resolution of the experimental set-up: less than 20 ps. These results are in agreement with earlier steady state and time resolved emission studies of soluble[1] and solid[8] PA. The steady state data have shown that the emission spectrum in soluble PA is dominated by a strong multiphonon Raman activity and lack a distinctive band-edge recombination luminescence peak. Time resolved spectra

consist of a sharp peak with a fast decay (<<20 ps) followed by a slower but much weaker background emission. These results were interpreted as indicative of a fast non-radiative recombination into a mid-gap state due to an intrinsic instability of the photogenerated electron-hole pair. Recent optically induced absorption measurements by Rothberg et al.[9] have shown that the mid-gap state lifetime was less than 1 psec. Furthermore, following Su et al.[10] the velocity of the excited species is about 10^6 cm/sec which implies that with a chain length of about 20-25 double bonds and assuming a double bond spacing of 4Å the excited state will come into contact with the chain end within less than a picosecond. Our results would then indicate that slower (>50 ps) interchain charge transfer mechanisms[11] can be ruled out as expected in a dilute solution.

3.4 Conclusion

In conclusion, we have measured the magnitude and response time of the third order nonlinear coefficient at resonance in a dilute solution of polyacetylene and found that χ^3_{PA} in PA was large ($\approx$ 10^{-9}e.s.u.) and fast (<20 ps) implying that interchain interactions do not play a significant role in the nonlinear response. Furthermore, these results were obtained with chains of relatively short conjugation length (20-25 double bonds) indicating that PA can potentially provide even larger nonlinear susceptibilities.

Reference

1. R. Tubino, R. Dorsinville, W. Lam, R. R. Alfano, J. B. Birman, A. Bolognesi, S. Destri, M. Castellani, W. Porzio, Phys. Rev. B, **30**, 6601 (1984).

2. S. Etemad, G. L. Baker, D. Jaye, F. Kajzar, J. Messier, SPIE Proc., **682**, 44 (1986).

3. Robert A. Fisher, "Optical Phase Conjugation," Academic Press, 1983.

4. B. S. Wherrett, A. L. Smirl, T. F. Borggess, IEEE J. of Quant. Elec., QE-**19**, 680 (1983).

5. H.J. Eichler, P. Gunter, D.W. Pohl, "Laser Induced Dynamic Gratings," Springer-Verlag (1986). B. Ya. Zeldovich, N.F. Pilipetsky, V.V. Shkunov, " Principles of Phase Conjugation," Springer-Verlag (1985).

6. R. Dorsinville, R. Tubino, S. Krimchansky, R. R. Alfano, J. L. Birman, A. Bolognesi, S. Destri, M. Castellani, W. Porzio, Phys. Rev. B, **32**, 3377 (1985).

7. C. Maloney, W. Blau, K. H. Drexhage, Optics Letters, **11**, 434 (1986)

8. C. Shank, R. Yen, J. Orenstein, G. L. Baker, Phys. Rev., **B28**, 6095 (1983)

9. L. Rothberg, T. M. Jedju, S. Etemad, G. L. Baker, IEEE Journal of Quantum Electronics, **24**, 311 (1988)

10.W. P. Su, J. R. Shrieffer, Procceedings of the National Academy of Science, USA, **77**, 5626 (1980)

11. J. Orenstein, Z. Vardeny, G. L. Baker, G. Eagle and S. Etemad, Phys. Rev., **B30**, 786 (1984)

Chapter IV

Intensity Dependence of Picosecond Nonlinear Response Time of Polydiacetylene

4.1. Introduction

Polydiacetylenes (PDAs) are a class of π - electron organic polymers that have been of interest as nonlinear optical materials after the discovery that they possess a very large nonresonant $\chi^{(3)}$[1]. The large nonlinear coefficient has been attributed to the delocalization of the π electrons along the carbon backbone(see the expression below) on polymerization. The basic repeat unit and the bonding scheme of the polymer are shown in expression. Each carbon chain can be viewed as a quasi-one-dimensional unit, and these chains are linked by the side groups, R and R', which are large molecular groups that determine the structural properties of the polymer. Depending on the side groups, these polymers may exist in crystalline, liquid crystalline, monolayer, multilayer, and solution states. The sample introduced here is the red form of 4-Butoxycarbonylmethylurethane polydiacetylene, with R=R', being an urethane substituent groups, in polymethylmethacrylate (4BCMU-PDA in PMMA) thin films,

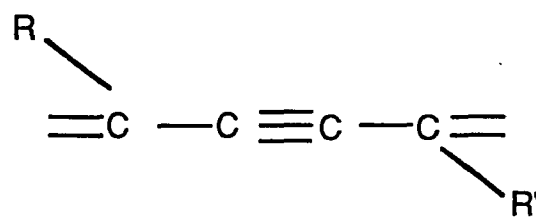

where, R=R'= $-(CH_2)_m\overset{O}{\overset{\|}{C}}-NH-X$.

Using optical pulses, the fast response time of PDAs was determined to be under 2ps for the resonance pumping while below 100fs for the nonresonance pumping[2-6]. The fast relaxation time was attributed to the electronic response. Recently, photo-induced irreversible structure change was observed in the blue PDA-(12,8) films[7-9]. The photochromic behavior in these blue PDA films was ascribed to the irreversible change in the bond structure in conjugated polymer backbone chains. In this chapter, time resolved forward degenerate four wave mixing (DFWM) experiments have been done in red form of 4-Butoxycarbonylmethylurethane polydiacetylene in polymethylmethacrylate(4BCMU-PDA in PMMA) thin films using picosecond laser excitations. The decay time of the DFWM signal is monitored as a function of the intensity.

4.2 Sample and experimental set-up

Red color films of 4BCMU-PDA in PMMA matrices were prepared from polymer solutions[5]. After filtration of monomer solution and crystallization, the monomer crystal was irradiated for 24 hours using a Ce^{137} source to obtain metallic color poly 4BCMU. Methylene chloride (MC) was used to dissolve the poly 4BCMU. After 24 hours, a proper amount of PMMA was added to the PDA-MC solution. Polymer solutions were deposited to glass slides with minimum exposure to ambient atmosphere and the solidification

took place in about an hour. Film samples were then sealed for laser experiments.

The sample absorption was 80% at 530nm. To avoid damaging the sample, single shot laser pulses were used. The time between two successive shots was > 2 minutes. The excitation source was a mode-locked YAG laser system producing 30ps pulses of 60MW peak power at 530nm. A forward co-plane DFWM geometry was used for the experiment which is displayed in the inset of Fig. 4.3.1. In this configuration, the measurement provides the information on transient grating response times. The laser pulse was split into three beams with parallel polarization. The relative time of arrival of the three incident pulses was adjustable by using two stepper-driven optical delay lines. Two pump beams (B1 and B2) separated by an angle $\theta<5^0$ were focused upon a spot about 0.5mm diameter on the sample such that they were both spatial and temporal coincident creating a transient grating in the medium. The grating decay was monitored by measuring the first order diffracted light from the probe beam(B3) as a function of the delay between pump beams and the probe beam. The incident energy intensity was varied using neutral density filters.

4.3 Results and discussion

The diffracted fourth signal beam(B4) as a function of the arrival time of the probe(B3) beam relative to the other two pump beams(B1,B2) for different energy intensities is displayed in Fig. 4.3.1. Negative time means that the probe beam arrives before the

pump beams. The asymmetric profile of the signal with respect to time delay is clearly displayed in Fig.4.3.1. The signal profile consists of a fast and a slow components. The slow component is found to be intensity dependent.

After choosing the proper parameters, all the measured intensity decay profiles have been fitted by a double exponential equation given by:

$$I(t) \propto c(e^{-t/\tau_{df}} + r\, e^{-t/\tau_{ds}}), \qquad (t>0) \qquad (4.3.1)$$

where τ_{df} and τ_{ds} are the fast and slow component of the decay time, respectively. The data displayed in Fig.4.3.1 can be fitted by equation(4. 3. 1) as shown by the solid lines. The rise time and the fast component of the decay slope are consistently found to be 20ps and intensity independent.

The relationship between the slow decay time τ_{ds} and the incident intensity I is plotted in Fig.4.3.2. The salient feature of Fig.4.3.2 is the nonlinear dependence of τ_{ds} upon light intensity. When the incident intensity is less than 0.50mJ/cm^2, no obvious slow component was observed. At low intensities(0.5 ~ 5.0mJ/cm^2), the slow component is not sensitive to increasing incident intensities. While at higher intensities, τ_{ds} increases very fast. The solid line in Fig. 4.3.2 is the calculated curve for τ_{ds} from the following equation:

$$\tau = \tau_0 + a\,(\frac{I}{I_0} - 1\,)^n\,, \qquad (4.3.2)$$

where τ_0 =280ps, a=0.5ps, I_0 =1.0mJ/cm^2, and n satisfies n=2 or 3. The fitting started from I>1.0mJ/cm^2. A theoretical model for the intensity dependence of τ_{ds}(I) and the form of equation (4.3.2) needs to be developed.

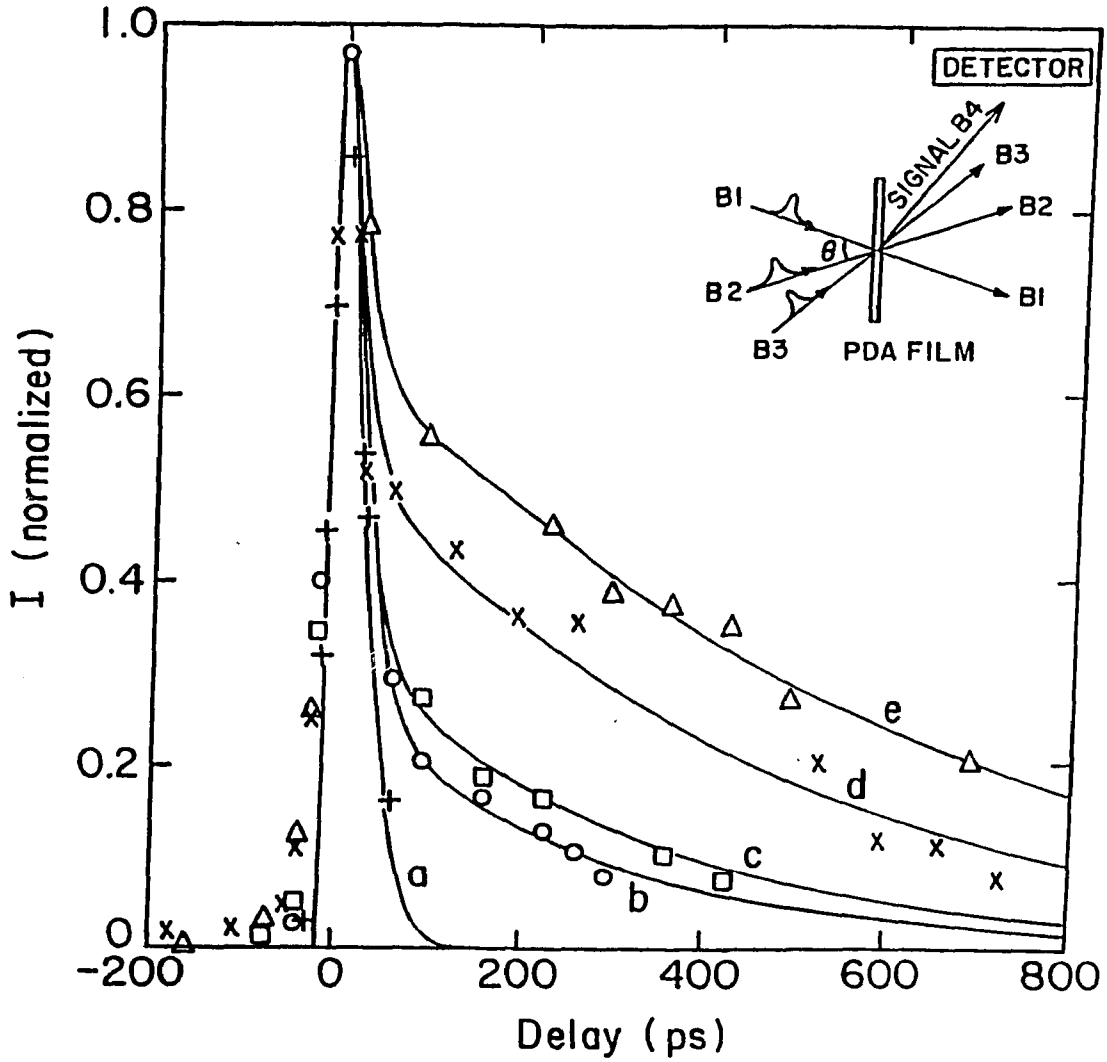

Fig. 4.3.1 Normalized DFWM signal as a function of the arrival time of B3 relative to B1 and B2 at different intensities(I).

(a)I< 0.50mJ/cm^2, t_{ds} =0;

(b)I=0.92mJ/cm^2, t_{ds} =280ps;

(c)I=5.11mJ/cm^2, t_{ds}=320ps;

(d)I=7.56mJ/cm^2, t_{ds} =440ps,

(e)I=9.90mJ/cm^2, t_{ds} =600ps.

The inset indicates the geometry of DFWM measurements.

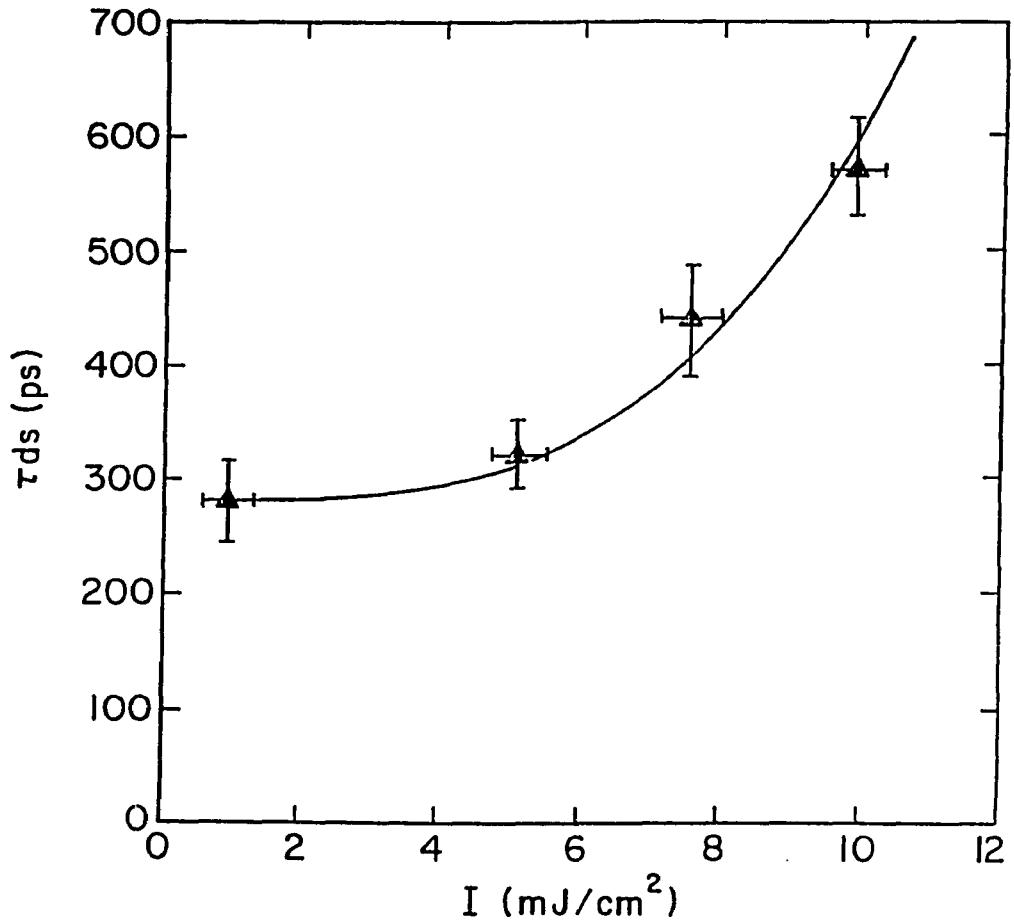

Fig. 4.3.2 The slow component of decay time t_{ds}(ps) is a function of the incident intensity I(mJ/cm^2). The solid line is a curve calculated from equation (4.3.2),
where t_0=280ps, a=0.5ps, I_0 =1.0mJ/cm^2, and n=3.

The fast decay component is unresolved and most likely due to the electronic contributions associated with the coherent artifact[2-5]. The slow component could arise from the population grating. From Photoluminescence decay measurements[5,6], the population grating lifetime is expected to be around 12ps. Based on our experimental results, the mechanism responsible for the slower and intensity dependent component is probably due to photo-induced structure changes in the thin films by light irradiation. This proposed model will be discussed next.

The conjugated conformation of PDA molecular structure in the 4BCMU-PDA(in PMMA) films is stabilized by intramolecular hydrogen bondings between urethane functionalities on adjacent sides chains. The conjugated length, which controls the polymer optical properties, is maintained through the cooperative effect of the array of hydrogen bondings. The reduction of conjugation length requires the simultaneous breakage of neighboring hydrogen bonds. When molecules are optically excited by the intense laser irradiation, the excess vibrational energy is dissipated internally via the strong electron-lattice interaction, leading to the breaking of H-bonds. After the passage of the excitation, the structure returns to it's initial state. The breakage of H-bonds blocks the "pathways" for the process, therefore the slower recovery will be associated with the larger number of the broken H-bonds. The number of affected H-bonds and the induced structure change are expected to depend on the laser excitation intensity due to the cooperative nature of the processes. The nonlinear rise of τ_{ds} upon the incident intensity implies that the number of broken H-bonds and the recovery are not promoted by

independent photoexcitations but through a certain cooperative multiple excitation process.

The question now is whether the light induced change could be caused by heating due to high laser intensity. The expression for the laser-induced temperature rise ΔT for a semi-infinite isotropic solid, uniformly illuminated by an optical pulse of duration t_p at the surface has been given by[10]:

$$\Delta T = (1-R)\frac{\alpha E_0}{\rho c}, \qquad (4.3.3)$$

in the limit $t_p << t_0$, where, R is the reflectivity of the surface(0.1), α is the absorption coefficient(2 X 10^3/cm), ρ is the density of PMMA(1.17g/cm^3),[11] c is the specific heat of PMMA(1.464J/g°C, at 23° C)[11], and E_0 is the energy per unit area of the radiation incident on the sample(the maximum in the experiments is 10mJ /cm^2). Substitution of the appropriate parameters into Eq(4.3.3) yields ΔT(23° C) = 10°C , for a single 30ps optical pulse. The thermal response time t_0 is defined as:

$$t_0 = \frac{4\rho c}{\pi \alpha^2 K} , \qquad (4.3.4)$$

where K is the thermal conductivity of PMMA (2.51 x 10^{-3}W/cm°C). Physically, t_0 gives an order of magnitude estimate of the time for the heat to diffuse one absorption depth ($1/\alpha$). In our case, t_0 = 0.22ms. Therefore, compared to the conformational transition due to simple heating the film from room temperature to 110°C[4], the laser-induced temperature rise can not affect the equilibrium of the two forms. Besides, the time response t_0 from the heating effect is 0.22ms which is 6 orders of magnitude slower than t_{ds} and 6 orders faster

than the repetition time of the pulses. These results suggest that the heating effect is unlikely to play a significant role in this experiment.

To verify the above proposed model, the following experiments were carried out.

Time resolved DFWM measurement in the yellow form films was carried out. The yellow films were obtained through exposing red films to the vapor of trifluoracetic acid(TFA), a hydrogen bonding breaking agent[12]. The yellow films could be converted back to the original red films by evacuation under vacuum clearly indicating that the only difference between the two forms is the extent of side group hydrogen-bonding. Experimental results in the yellow form did not show the intensity dependent slow component as observed in the red form of 4BCMU-PDA films.

Furthermore, the optical absorption spectra of the red film were measured before and after the intense laser pulse excitation. No difference was observed between two spectra indicating the structure change in the PDA thin films is reversible. A theoretical model needs to be developed to explain the intensity dependence of τ_{ds}.

4.4 Conclusion

In conclusion, the slow relaxation component of 4BCMU-PDA red films in time resolved DFWM measurements was found to be intensity dependent. The cause is unknown. However, under intense light irradiation, the 4BCMU-PDA red films most likely experienced a

transient reversible structural change due to the breaking of the side-chain intramolecular hydrogen bonding.

References

1. G. M. Carter, M. K. Thakur, Y. J. Chen and J. V. Hryniewicz, Appl. Phys. Lett. **47**, 457(1985).

2. G. M. Carter, J. V. Hrynuewicz, M. K. Thakur, Y. J. Chen and S. E. Meyler, Appl. Phys. Lett. **49** 998(1986).

3. B. I. Green, J. Orenstein, R. R. Millard and L. R. Williams "Nonlinear Optical Response of One-Dimensional Excitons in Polydiacetylene" in Ultrafast Phenomena V , Ed. by G. Fleming and A. Siegment, 472-474, (Springer-Verlag, New York, 1986).

4. D. Narayana Rao, Pratibha Chopra, Suniti K.Ghoshal, Jacek Swiatkienwicz and Paras N. Prasad, J. Chem. Phys. **84** 7049(1986).

5. P. P. Ho, R. Dorsinville, N. L. Yang, G. Odian, G. Eichmamn and R. R. Alfano, "Molecular and Polymeric Optoelectronic Materials", G. Khanarian,ed.,Proc. Soc. Photo-Opt. Instrum. Eng. 682, 36(1986).

6. P. P. Ho, N. L. Yang, T. Jimbo, Q. Z. Wang and R. R. Alfano, J. Opt. Soc. Am.B **4** 1025(1987).

7. T. Kanetake, Y. Tokura and T. Koda, Solid State Commun. **56**, 803(1985).

8. E. Hanamura and N. Nagaosa, Solid State Commun. **62**,5(1987).

9. Y. Tokura, K. Ishikawa, T. Kanetake and T. Koda, Phys. Rev. B **36** 2913(1987).

10. F. Bartoli, M. Kruer, L. Esterowitz and R. Allen, J. App. Phys. **44**, 3713 (1973).

11. Edward A. Collins, Jan Bares, and Fred W. Billmeyer,Jr., **Experiments in Polymer Science,** by: Edward A. Collins, Jan Bares and Fred W. Billmeyer,Jr. (New York John Wiley & Sons, Inc., 1973).

12. G. N. Patel, R. R. Chance and J. D. Witt, J. Chem. Phys. **79** 4387(1979).

Chapter V

Nonlinear Optical Response in Polythiophene films

5.1 Introduction

Comprehensive studies of the third order optical nonlinear properties accomplished in π-electron systems, such as polyacetylene[1-3] and polydiacetylene[4-6] have shown that the π electron backbone structure is a prerequisite for nonlinear optical properties. In this chapter and the following one, we will focus our attention to another π - electron system, polythiophene, whose third order nonlinearity has not been studied before. χ^3 will be measured in a homologous series of thiophene based conjugated polymers : polythiophene (pT) as well as two new polycondensed thiophene based polymers, polythieno (3,2-b)thiophene (pTT) and polydithieno(3,2-b;2'.3'-d)thiophene (pDTT), which have in common the thiophene ring as the building blocks[7-9].

For a thorough understanding of the mechanisms responsible for the nonlinearity, a comparison between the nonresonant nonlinear response for pumping well below the absorption edge and the resonant response for pumping directly into the principal absorption band is needed. The dispersion of χ^3 in the absorption band, at the edge of the absorption band and off the absorption band was obtained from DFWM measurements.

5.2 Sample

The molecular structures for PT, PTT, PDTT are shown in Fig. 5.2.1. The conjugation backbone is stabilized by the sulfur atoms.

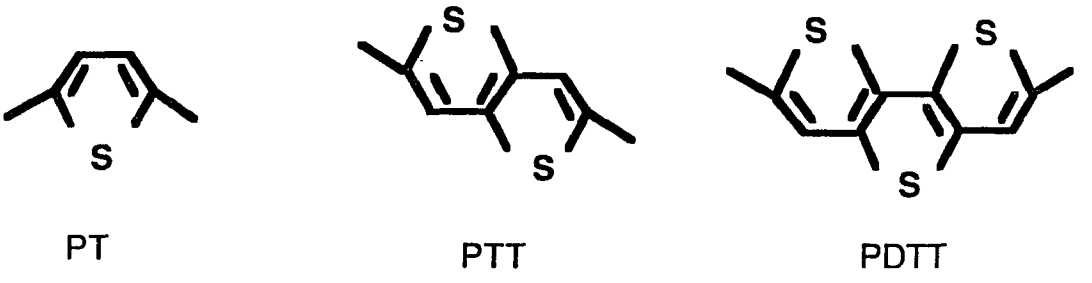

5.2.1 Molecular structures of PT, PTT and PDTT

Polymer thin films were obtained by electrochemical polymerization of the monomers in a two compartment cell at room temperature with Indium tin oxide (ITO) electrodes in suitable solvents and electrolyte. Detailed description of the preparation of pTT and pDTT are reported in refs. 8 and 9, respectively. The polymer film which grows at the anode in the doped conducting form is subsequently undoped by short-circuiting the electrodes. Film thickness was controlled by varying the current density (typically 0.1 mA/cm^2) and the time of deposition and was measured by means of a surface profiler (Tencor Alpha-Step 200). Typical thickness was in the order of 0.5 - 2 μm. Completeness of the undoping process was established by monitoring the disappearance of the two bipolaron bands in the near IR.

Although the three polymers have a conjugated π electron backbone structure, which is a prerequisite both for charge transport and non-linear optical properties, they have a different optical

contribution of the alternating single and double bonds. Consequently, the electronic structure will be different in the three polymers as shown by quantum chemical calculations.

The single photon absorption and photoluminescence spectra are shown in Figure 5.2.2. The spectra are broad and structureless with a smooth low energy slope. Despite the different electronic structures the overall spectral features of the three polymers are very similar to each other.

The absorption and emission maxima are reported in table 5.2.1 together with the estimated optical band gap. These data show that strong electronic resonance enhancement of the optical nonlinearity should be expected for wavelengths shorter than 605 nm.

Table 5.2.1. Optical properties of pT, pTT, pDTT.

Polymer	Absorption maximum (eV)	Fluorescence maximum (eV)	Optical band gap (eV)
pT	2.7	1.93	2.0
pTT	2.83	1.95	1.97
PDTT	2.67	1.92	1.9

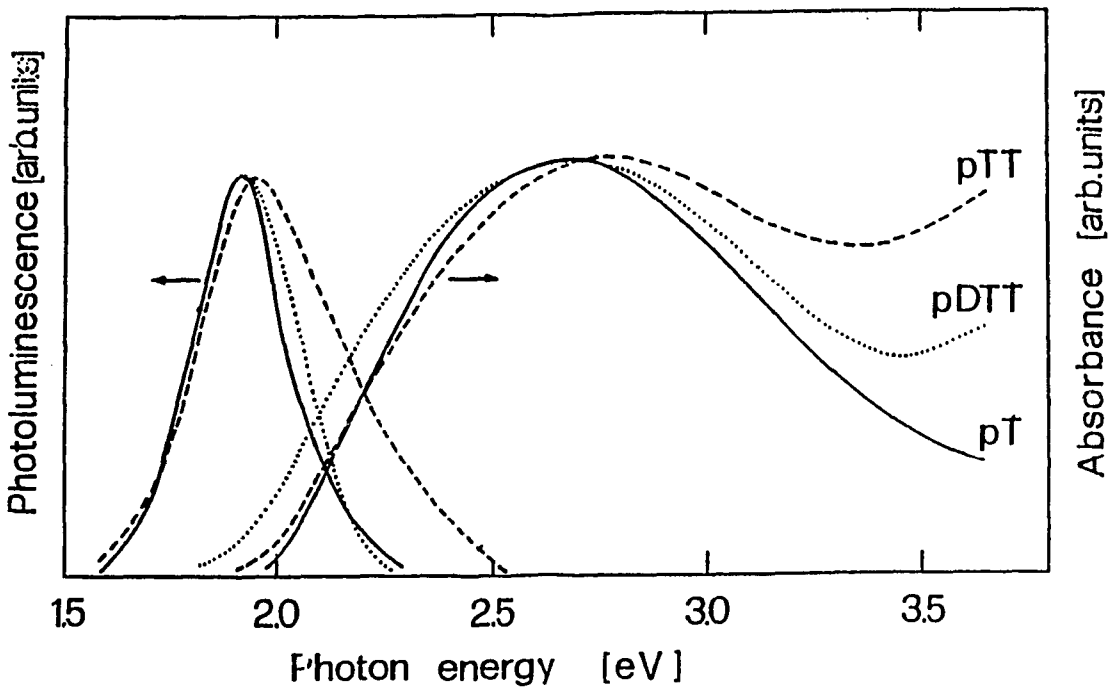

Fig.5.2.2 Absorption and emission spectra of polycondensed thiophene polymers

All three polymers in the doped form show the characteristic IR doping induced bands (DIB) which are identified as signatures of charged species in the polymer chains. Absorption measurements at different doping levels in pTT and pDTT show the strong activity at two DIB in the near IR which are symmetric with respect to the energy-gap. Both findings confirm that the two new polymers , pTT and pDTT, support charged species in the polymer backbone in the form of (bi)polarons in analogy with polythiophene(PT). The broad electronic absorption which is very similar in the three polymers, together with the narrow emission suggests that the absorption is characterized by inhomogeneous broadening due to a wide distribution of conjugation lengths. The similar optical band-gap suggests that even though the electronic structure of the different polymer backbones is different, as derived from band structure calculations, the π electron delocalization is similar.

5.3 DFWM Experimental results

A forward folded boxcar degenerate transient grating technique was used for the measurements. The details of the experimental set-up are given in chapter II. A Quantel PTL10 picosecond tunable dye laser pumped by the Nd:YAG laser was used to provide a tuning range from 585 to 605nm,. The output pulse duration of this dye laser is 15ps. The pulse duration of the different laser sources used in these experiments was measured with a 2 ps streak camera. The stimulated Raman line generated from ethanol pumped by a 532nm laser pulse produced 629nm pulses. Thus, the

third order optical nonlinear coefficient was determined at 1064 nm, 629 nm, between 585 and 605 nm and at 532 nm.

The degenerate four wave mixing signal as a function of delay time was measured for the different samples. As an example, typical FWM signal profile from PT at 585nm is shown in Fig.5.3.2. The curve were symmetrical with respect to time delay indicating a response time limited by the pulse duration of the laser. In each sample the time resolved four wave mixing signal was identical to the expected cross-correlation signal. The central sharp peak is the coherent spike.

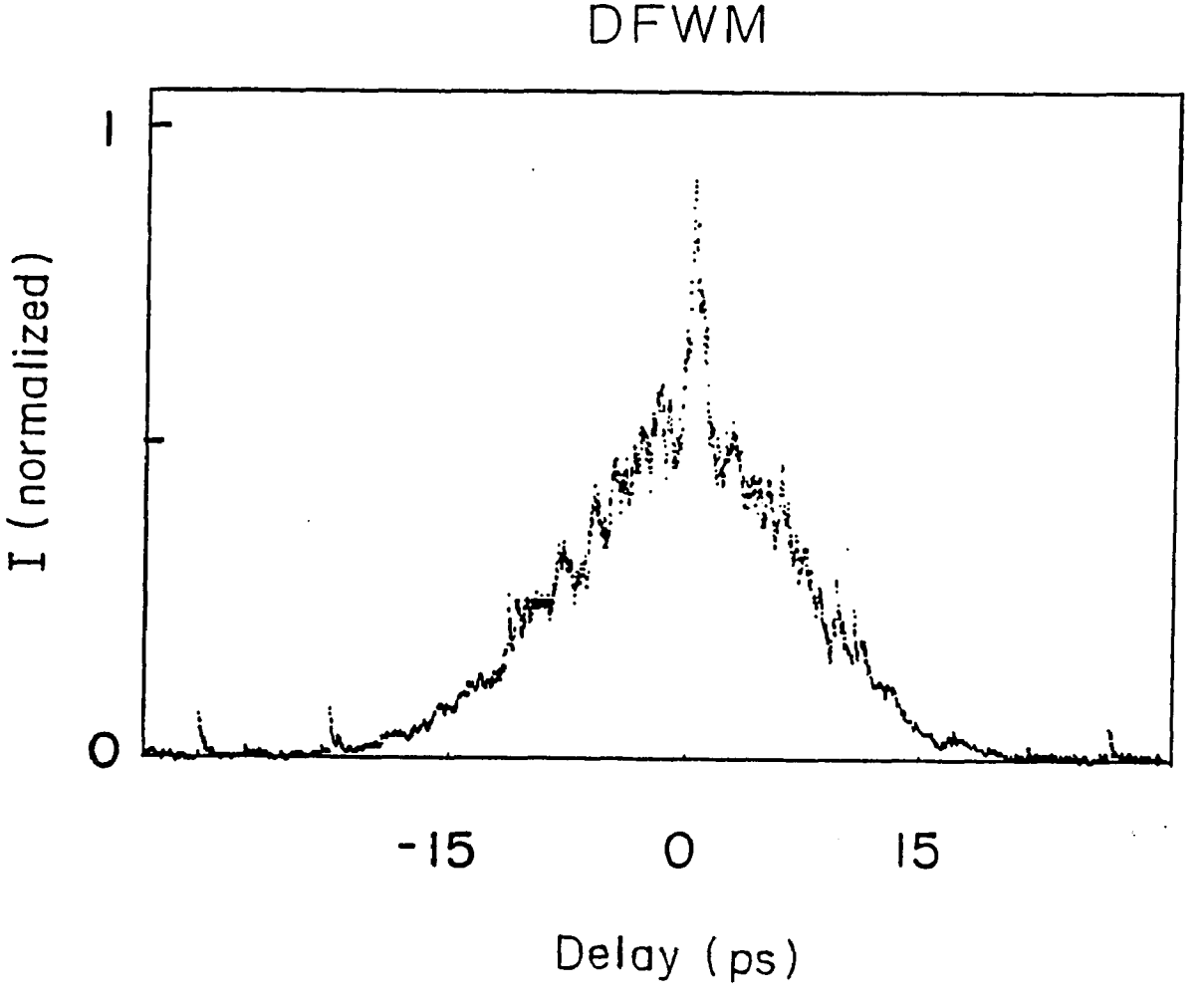

Fig.5.3.2 DFWM signal from polythiophene films at 585nm.

The third order nonlinearity in an absorbing medium is obtained from measurements of the four wave mixing signal by using the formula in chapter II, equation (2.1.3):

$$\chi^{(3)}_{ijkl} = \frac{cn^2}{32\pi^2}\left(\frac{\lambda_0\rho_0^2}{2aL}\right)\left[\left(\frac{45}{8}\right)\frac{E_{si}}{E_{1j}E_{2k}E_{3l}}\right]^{1/2} e^{-\alpha L}, \qquad (5.3.1)$$

where α is the absorption coefficient of the investigated sample, n is the index of refraction of the sample, E_{si} the energy of the four wave mixing signal, E_{1j}, E_{2k}, E_{3l} are the energies of the three interacting beams. In this work, the third order nonlinear coefficient was determined by comparing the signals for CS_2 and the polythiophene films using the equation:

$$\chi^{(3)}_{S\ xxxx} = \chi^{(3)}_{CS_2xxxx}\left(\frac{n_S}{n_{CS_2}}\right)^2\left(\frac{L_{CS_2}}{L_S}\right)\left[\frac{E_{si}}{E_{CS_2}}\right]^{1/2}\frac{e^{-\alpha_S L_S}}{e^{-\alpha_{CS_2}L_{CS_2}}} \qquad (5.3.2)$$

Where, n_{cs_2} and L_{cs_2} are the index of refraction and the thickness of CS_2, respectively, and $\chi^3_{CS_2} = 8.8 \times 10^{-13}$ e. s. u..[10] In all cases, the calculation used the average intensity of each beam both in time, over the 15 psec duration of the pulse, and in space over the 1 mm spot size at the sample site. The indices of refraction of the different thin film samples were determined by measuring the Brewster angle at different wavelengths. The values of n varied from 1.9 to 2.1.

The third order nonlinear optical coefficient χ^3 was measured for all three polymer samples at different wavelengths: at 532 nm, where the absorption loss of the samples was about 40 %, at 1064 nm, where the absorption was negligible and between 585nm (about 20%) and 605 nm (less than 3%). At these wavelengths the values of the absorption coefficient varied from about 5 - 8 10^4 cm^{-1} at 532 nm to less than 0.5 10^4 cm^{-1} at 630 nm, close to the band edge and negligible below gap at 1064 nm. For all the measurements all the interacting beams had parallel polarizations and no significant change in the value of the four wave mixing signal was observed when the samples were rotated, indicating that the films were quite isotropic. Under these conditions the observed four-wave mixing signal was generated by the χ^3_{1111} component of the optical nonlinear susceptibility. The values of χ^3 as a function of wavelength are given in table 5.3.1.

There are three important findings in the results shown in table 5.3.1. First, above gap the values of $\chi 3$ are larger than 10^{-9} esu for all three samples; second there is a large increase in the value of $\chi 3$ (up to 10^{-8} esu for pDTT at 532 nm) from pT to pDTT for all the frequencies above gap; and finally below gap at 1064 nm all three samples have about the same value of $\chi 3 \sim 10^{-11}$ esu. This latter value is about one order larger than in CS_2.

According to table 5.3.1, the maximum measured value of χ^3 = 11 X 10^{-9} e.s.u. for pDTT at 532 nm. This value is comparable to measured values (at resonance) of the third order nonlinear optical coefficient in polydiacetylenes polymers.[11]

Table 5.3.1. Nonlinear coefficient χ^3 vs. wavelength.

Wavelength (nm)	pT χ^3(X 10^{-9} e.s.u.)	pTT χ^3(X 10^{-9} e.s.u.)	pDTT χ^3(X 10^{-9} e.s.u.)
532	6.6±1	5.9±1	11.3±2
585	5±1	4.4±1	7.7±1
590	3.±1	3.0±1	5.8±1
595	3.8±1	3.6±1	6.1±1
600	3.2±1	2.9±2	4.5±1
605	3.0±1	3.0±1	5.5±1
630	0.7±0.5	0.7±0.5	1.3±0
1064	0.03±0.02	0.03±0.02	0.03±0.02

At longer wavelength, at photon energy 1.96 eV (629 nm), where the sample absorption loss was below 3%, the nonlinear optical coefficient was larger than 10^{-10} e.s.u. for all three samples. The optical nonlinearity at resonance is usually the result of a combination of bound electron and free carrier responses. In an absorbing material the contribution of the spatially varying density of excited molecules or population grating can be relatively large. This contribution can be estimated by plotting the measured nonlinear optical coefficient as a function of the absorption

coefficient. The nonlinear response due to the population grating is proportional to the absorption coefficient $(\chi^3 \sim \alpha)$.[12]

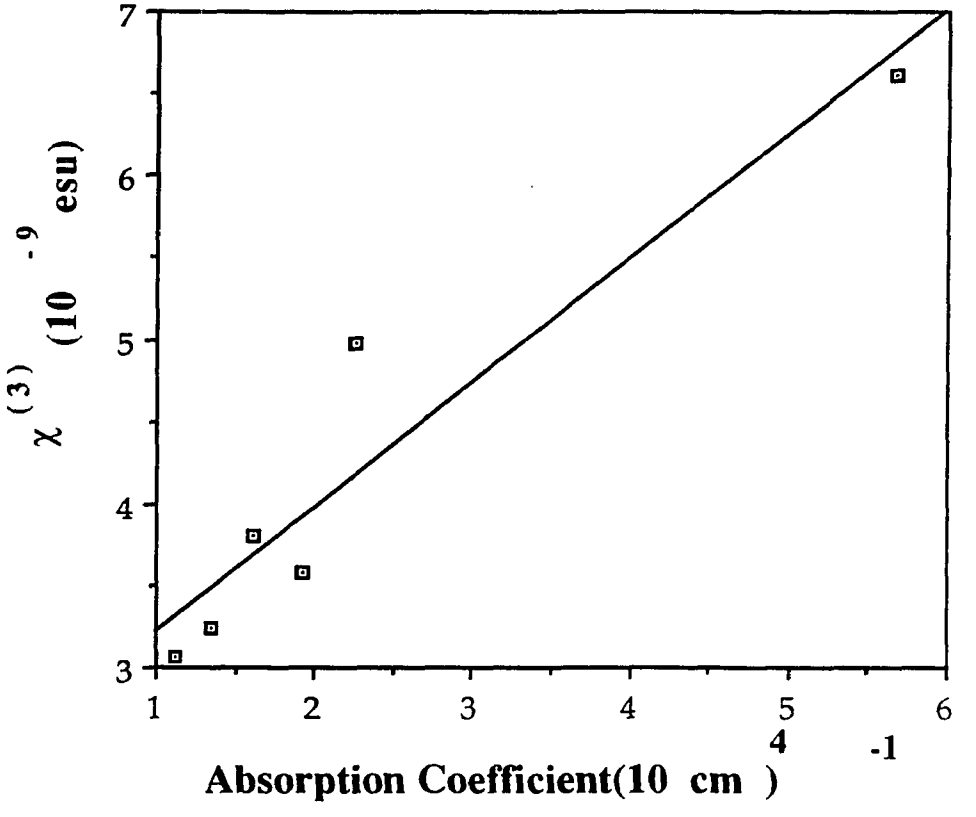

Figure 5.3.2. Third order nonlinear optical coefficient versus absorption coefficient for pT. Solid line is the theoretical fit for $\chi^3 \sim \alpha$.

Figure 5.3.2 shows a plot of the nonlinear coefficient versus the absorption coefficient for polythiophene. Similar results were obtained for pTT and pDTT. The solid line is a theoretical fit assuming $\chi^3 \sim \alpha$. The plot is compatible with the experimental curve. This agreement suggests that the optical nonlinear response above gap is mostly due to the population grating. The fact that pDTT has both the largest χ^3 above gap and the largest value of the absorption coefficient seems to confirm this suggestion. In the case of a population grating, the response time of the nonlinearity should then be a measure of the free carrier lifetime. The four wave mixing measurements suggest a carrier lifetime of less than < 15 ps. Direct photoluminescence measurements [13] in polythiophene using a streak camera have given an upper limit of $t < 9$ ps for the lifetime of the luminescence, in agreement with the four wave mixing results. Similar results were obtained on our samples.

Below gap, at 1064 nm the value of χ^3 was greater than 3×10^{-11} esu for all three polymers. Although 1064 nm correspond to the peak of an induced polaronic band in pT, the magnitude of the nonlinear optical coefficient at 1064 nm is about two order of magnitude smaller than the values at resonance.

5.4 Conclusion

Using DFWM technique, we have measured the magnitude and response time of the third order optical nonlinear coefficient near the absorption edge in three thiophene based polymers and found that above gap χ^3 was large ($>10^{-9}$e.s.u.) with a time response limited by

the pulse duration of the laser (<15 ps). Those values are similar to polydiacetylenes which indicates that the nonlinearity is entirely associated with the nonlinear polarizability of the π - electrons in the conjugated polymer backbone. Below gap, χ^3 was about 2 order of magnitude smaller ($\geq 10^{-11}$ e.s.u.) but greater than CS_2 by one order of magnitude.

Reference

1. F. Kajzar, S. Etemad, G. L. Baker and J. Messier, Solid State Commun. **63**, 113(1987).

2. M. Sinclair, D. Moses, K. Akagi, and A. J. Heeger, Phys. Rev. B, **38**, 10724(1988).

3.W. S. Fann, S. Benson, J. M. J. Madey, S. Etemad, G. L. Baker and F. Kajzer, Phys. Rev. Lett., **62**, 1492(1989).

4. G. M. Carter, M. K. Thakur, Y. J. Chen and J. V. Hryniewicz, Appl. Phys. Lett. **47**, 457(1985).

5. G. M. Carter, J. V. Hrynuewicz, M. K. Thakur, Y. J. Chen and S. E. Meyler, Appl. Phys. Lett. 49 998(1986).

6. B. I. Green, J. Orenstein, R. R. Millard and L. R. Williams "Nonlinear Optical Response of One-Dimensional Excitons in Polydiacetylene" in Ultrafast Phenomena V , Ed. by G. Fleming and A. Siegment, 472-474, (Springer-Verlag, New York, 1986).

7. C. Taliani, R. Danieli, Z. Zamboni, P. Ostoja, W. Porzio. Synth. Met., **18**, 177 (1987).

8. R. Danieli, C. Taliani, R. Zamboni, G. Giro, M. Biserni, M. Mastragostino and A. Testoni, Synth. Met., **14**, 325 (1986).

9. P. Di Marco, M. Mastragostino,and C. Taliani, Molec. Cryst. and Liq. Cryst., **118**, 241 (1985).

10. S. L. Shapiro, H. P. Broida, Phys. Rev., **154**, 129 (1967).

11. F. Kajzar and J. Messier. Thin Solid Films, **132**, 10 (1986).

12. B. Ya Zeldovich, N. F. Pilipetsky, V. V. Shkunov, "Principles of Phase Conjugation," Springer-Verlag, 1985.

13. K. S. Wong, W. Hayes, T. Hattori, R. A. Taylor, J. F. Ryan, K. Kaneto, Y. Yoshino and D. Bloor. J. Phys. C: Solid State Physics, **18**, L843 (1985).

Chapter VI

Sign Determination of in Polythiophene Thin Films

6.1 Introduction

In the previous chapter, the magnitude and the response time of $\chi^{(3)}$ were determined by DFWM measurements. Since DFWM is only sensitive to the square of $\chi^{(3)}$, information such as the sign can not be obtained from DFWM measurements. In this section, the sign of $\chi^{(3)}$ has been determined using the single beam Z -scan technique[1,2] at both 532 and 1064 nm.

6.2 Single beam Z - scan measurements

The single beam Z - scan technique has been introduced in Chapter II, section 2. In the Z-scan approach, a single Gaussian beam is tightly focused into a thin nonlinear medium. The transmittance through a small aperture in the far field is measured. A negative lens effect arising from nonlinear materials having negative n_2 will result in a peak followed by a valley in the transmittance curve, while positive n_2 will give a curve with a valley-peak sequence as the sample is translated from -z side to +z side. Thus, the sign of the nonlinearity can be readily determined. Moreover, the size of n_2 can be determined from the difference in peak and valley in transmittance.

A mode-locked Quantel YAG laser with a frequency doubler provided the laser pulses with 30ps duration at 532 and 1064 nm at a 10Hz repetition rate. In the experiment, the laser beam was tightly focused to a spot size ω_0 of 20μm. A 1mm diameter aperture was placed at a distance of more than 1.5 m away from the focus point. The light transmission through the aperture was detected, recorded, and analyzed by a photomultiplier (PMT) and a boxcar averager interfaced with a microcomputer. Each point was an average over 30 shots. Narrow Band Filters (either NB532 or NB1064) were used in front of the PMT. Z-scans from a 1mm cell containing CS_2 was also measured and used for standards and references. Measurements have been performed in polythiophene(PT) as well as in PTT and PDTT.

6.3 Results

The normalized transmittance through the far field aperture as a function of z from PT and CS_2 at 532 nm are shown Fig. 6.3.1(a) and (b), respectively. The excitation energy was 0.3μJ for those measurements. The peak-valley configuration in Fig.6.3.1(a) indicates PT has a negative nonlinearity(n_2 or $\chi^{(3)} < 0$). The reversed valley-peak configuration obtained from CS_2 shows CS_2 has a positive nonlinearity at 532 nm.

Fig.6.3.2 displays the normalized transmittance from PT at 1064nm. The excitation energy was 10μJ. The peak valley sequence in Fig.6.3.2 shows a negative nonlinearity at 1064nm. Thus, $\chi^{(3)}$ of PT has the same negative sign at 532nm and 1064 nm.

The Z - scan transmittances were measured for all three polymer samples at both 532 nm and 1064 nm, they show the same sign behavior. Fig. 6. 3. 1. and 6. 3. 2 only display the transmittances for PT.

From the maximum and minimum transmittance, one can estimate the value of n_2 (or $\chi^{(3)}$) without performing a detailed fit to the experimental data. Within a 0.5% accuracy, for phase distortions $|\Delta \Phi_0| = |k \Delta n L_{eff}| \leq \pi$, the relationship of the difference between the normalized peak and valley transmittance ΔT_{p-v} and n_2 is given by[1,2]:

$$\Delta T_{p-v} \approx A |\Delta \Phi_0| \approx A \left| \frac{\pi n_2}{\lambda} |E|^2 L_{eff} \right|, \qquad (6.3.1)$$

where $L_{eff} = \frac{1 - e^{-\alpha l}}{\alpha}$ is the effective sample length, and A is a constant which may depend on the aperture size.

When CS_2 is used as a reference with the assumption that the measurements for CS_2 have been performed under the same condition as for PT, the value of $\chi^{(3)}_{pT}$ is obtained from:

$$\chi^{(3)}_{pT} = \chi^{(3)}_{CS_2} \frac{(\Delta T_{p-v} n_0)_{PT} \quad (L_{eff} E_{exci})_{CS_2}}{(\Delta T_{p-v} n_0)_{CS_2} \quad (L_{eff} E_{exci})_{PT}}, \qquad (6.3.2)$$

where L_{eff} for CS_2 is equal to the cell length L since CS_2 dose not absorb at both 532 nm and 1064 nm, and E_{exci} is the excitation energy .

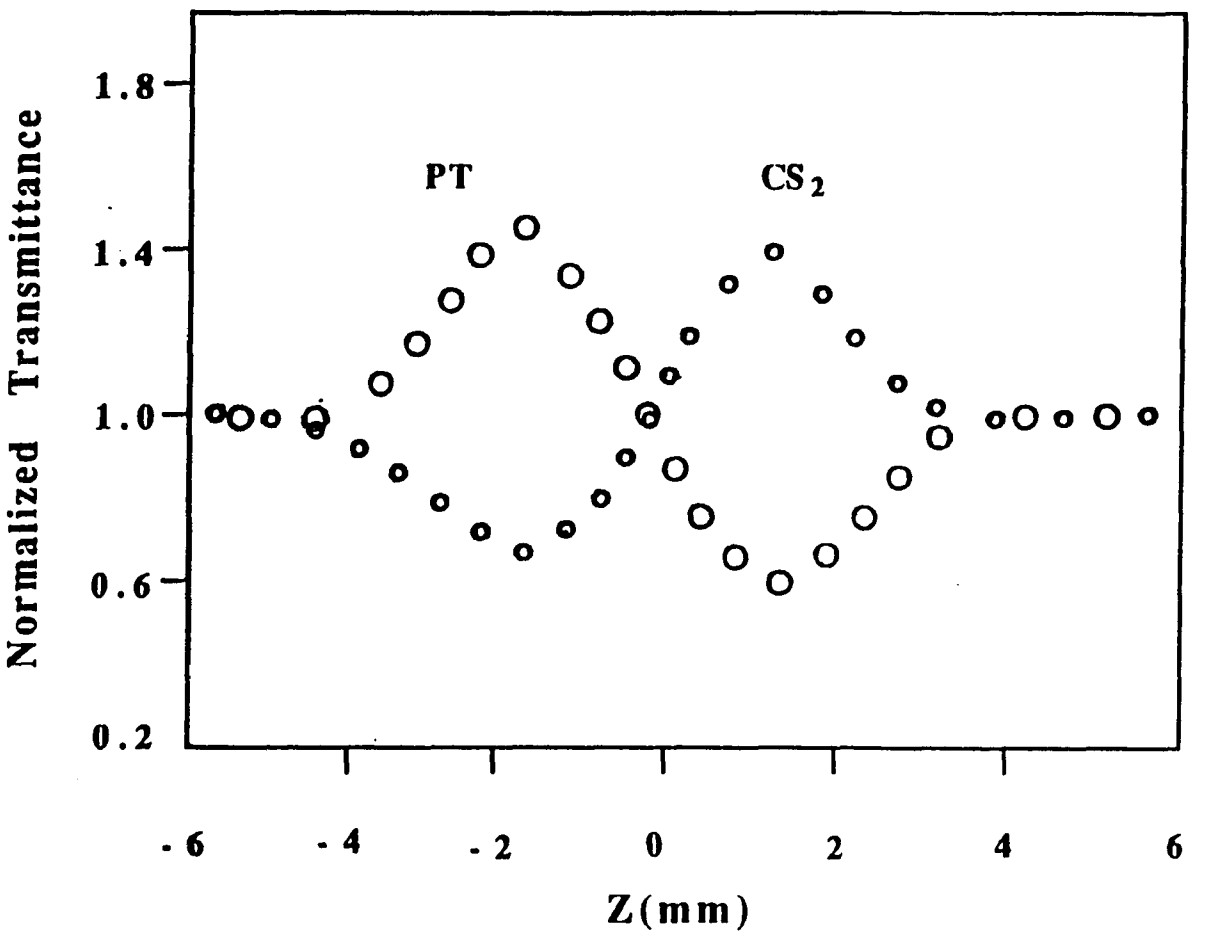

Fig.6.3.1 Normalized transmittance of Z - scan measurements from PT and a 1mm CS_2 at 532nm, the excitation energy is 0.3μJ.

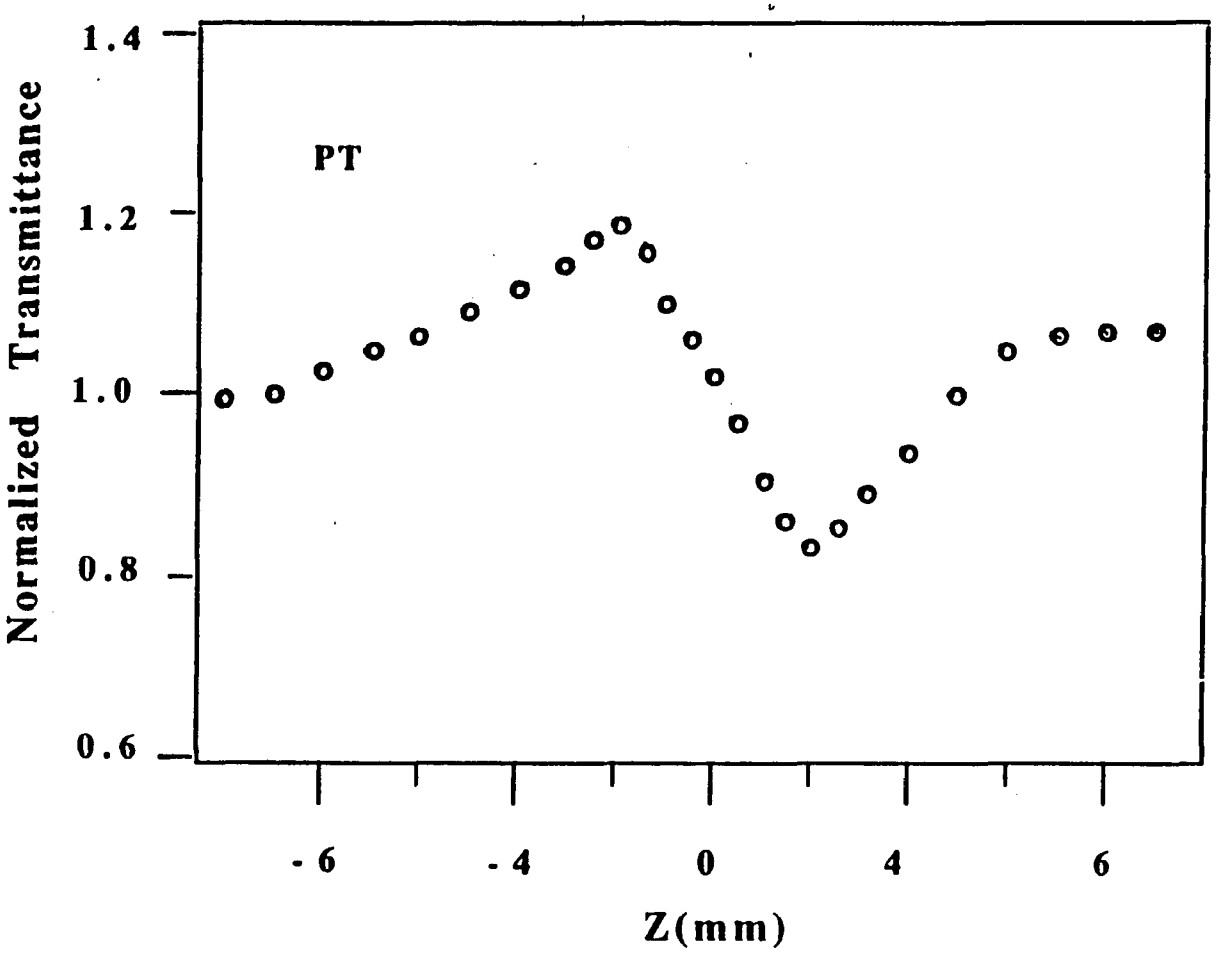

Fig.6.3.2 Normalized transmittance of Z - scan measurements from PT at 1064 nm, the excitation energy is 10μJ.

The transmittance for CS_2 at 1064 nm is also measured. The valley-peak sequence indicates that the nonlinearity for CS_2 at 1064 nm is still positive. For CS_2, it has been well known that the positive nonlinearity is due to a Kerr type nonlinear response. And n_2 has the same magnitude (1.2 X 10^{-11} esu) at both wavelengths. The transmittance for CS_2 at 1064 nm is not shown in Fig. 6.3.2, since the excitation energy needed to produce the same ΔT_{p-v} value as that for PT shown in Fig. 6.3.2, was 3.75μJ. When CS_2 is used as a reference to obtain the nonlinearity of PT at 1064 nm, the difference in the excitation energies has to be taken into account.

Using equation(6.3.2) and the data obtained from transmittance curves, the calculated values of $\chi^{(3)}$ for all three samples are listed in table 6.3.1. The values of $\chi^{(3)}$ at 532 nm are comparable to the values obtained from DFWM measurements(see table 5.3.1), while the values at 1064 nm are somehow larger than DFWM values.

Table 6.3.1 Measurements of $\chi^{(3)}$ vs wavelength from Z - scan

Wavelength (nm)	$\chi^{(3)}$ (10^{-9}esu)		
	PT	PTT	PDTT
532 nm	-4.50	-2.24	-4.60
1064 nm	-0.797	-0.663	-0.900

6.4. Discussion

The single photon absorption spectra of polythiophene polymers(see Fig. 5. 2. 2) have shown that there is a strong absorption(corresponding to the main π - π^* transitions) at 532 nm for all three samples, thus optical nonlinearities at 532 nm are resonantly enhanced. This resonance has been pointed out in the last section where it was shown that $\chi^{(3)}$ has a linear dependence on the absorption coefficient α.

Generally, $\chi^{(3)}$ consists of resonant and nonresonant parts. The resonant part of $\chi^{(3)}$ can be separated from the nonresonant part through resonant dispersion. At resonant frequencies, the resonant terms of $\chi^{(3)}$ are enhanced through the resonant denominators. These resonant terms of $\chi^{(3)}$ are complex quantities since the damping coefficients in the denominators are no longer negligible. For the present case, if a simple two level model is assumed, $\chi^{(3)}_R(\omega,\omega,-\omega,\omega)$ is dominated by four triply resonant terms[3]:

$$\chi^{(3)}_R=-\frac{e^4N}{h^3}\sum_{gi}\rho_{(g)}\Omega_{gi}\Omega_{ig}\Omega_{gi}\Omega_{ig}\; i(T_{lg}+T_{li})$$

$$\times\left[\frac{1}{(\omega_{gi}-\omega+i\Gamma_{gi})^2}-\frac{1}{(\omega_{gi}-\omega)^2+\Gamma_{gi}^2}\right] \qquad (6.4.1)$$

where: g denotes the ground state(valence band), i denotes the excited state(conduction band), Ω_{gi} is the dipole matrix element for the transitions between the valence and the conduction band. Γ_{gi} is the phenomenological damping factor. $T_{li(g)} = 1/\Gamma_{ii(gg)}$ is the longitudinal relaxation time for state i(or j), and N is the number of excited electrons or holes per unit volume.

We are only interested in the relative values of $\chi^{(3)}$ around resonance, and will neglect the unknown factors in equation (6.4.1). Equation (6.4.1) can be further simplified as:

$$\chi_R^{(3)} \propto -i\left[\frac{1}{(\omega_{gi} - \omega + i\Gamma_{gi})^2} - \frac{1}{(\omega_{gi}-\omega)^2 + \Gamma_{gi}^2}\right]. \qquad (6.4.2)$$

Fig. 6.4.1 shows the theoretical calculations of real and imaginary part of $\chi^{(3)}$ using last equation with: ω_{gi}=2.253eV and Γ_{gi}=0.3eV, they correspond to the maximum single photon absorption frequency and the half-bandwidth of g to i single photon transitions.

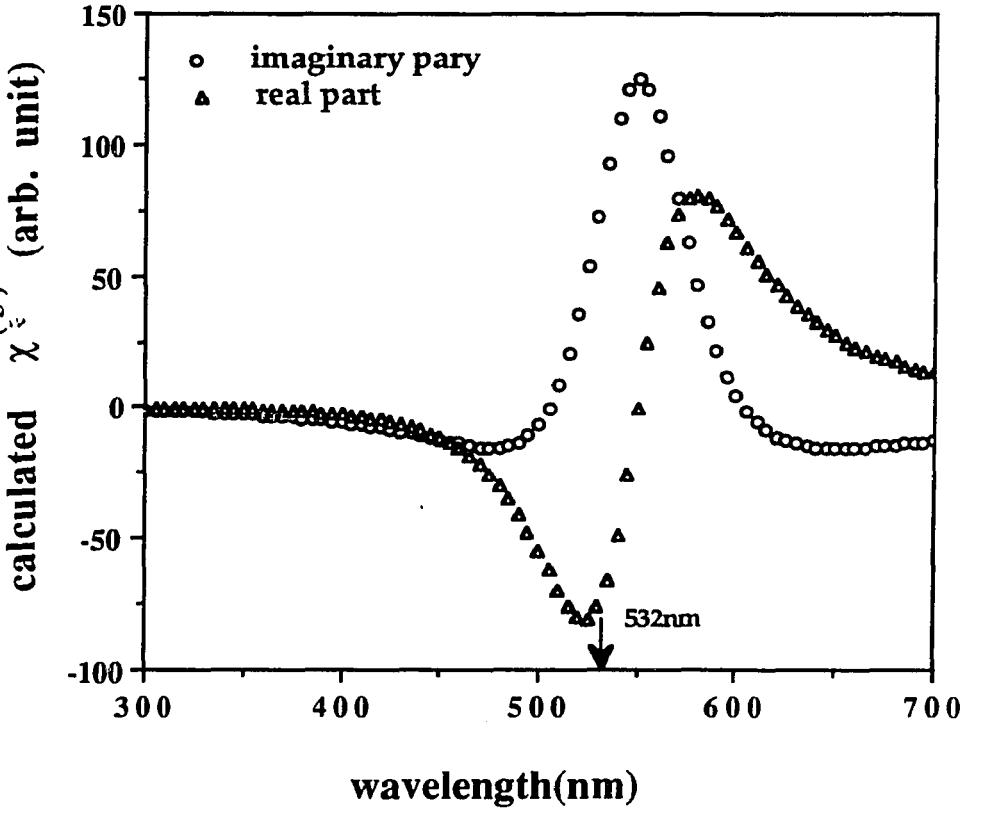

Fig. 6.4.1 The calculated real and the imaginary part of χ^3, in resonant with the single photon transition, as a function of the excitation photon frequency. The parameters are: ω_{gi}=2.253eV, Γ=0.3eV.

532 nm is indicated by the arrow in Fig. 6.4.1. The calculations predicted that the real part of $\chi^{(3)}$ at 532 nm is negative which is in agreement with our Z - scan experimental observations. Note that Fig. 6.4.1 also predicts the sign change from negative to positive at longer wavelength(for low energy side).

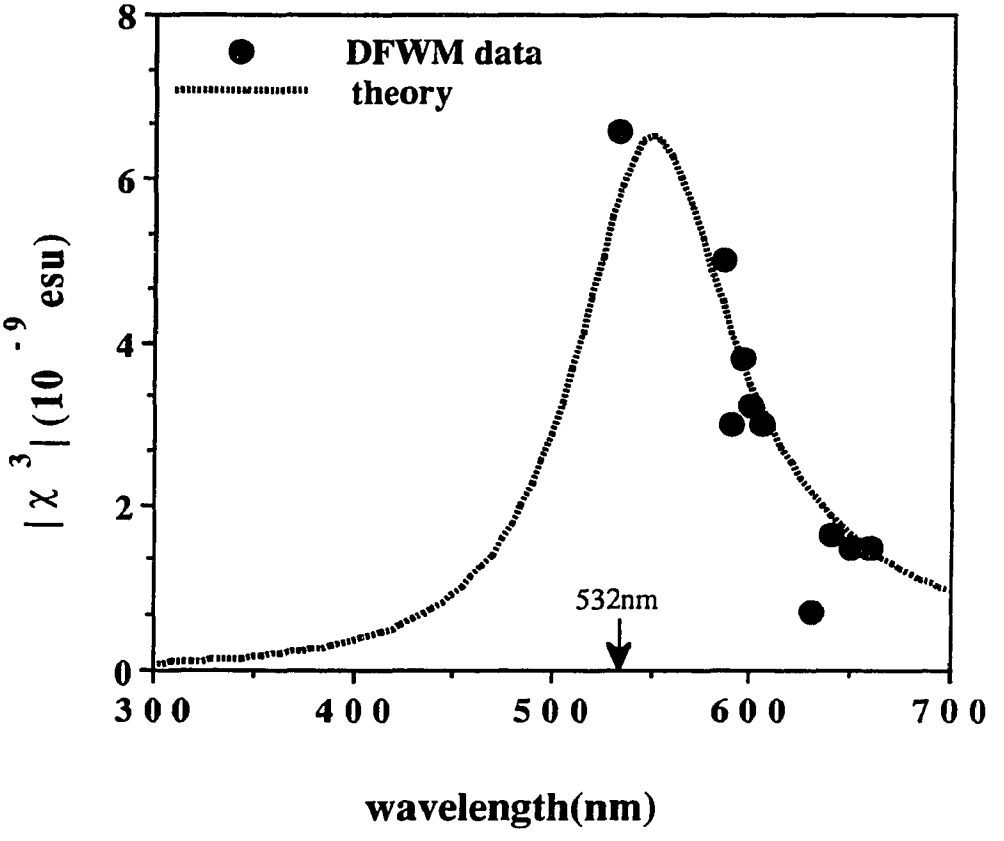

Fig. 6. 4. 2 The calculated $|\chi^{(3)}|$ values from equation (6.4.2) with ω_{gi}=2.253eV, Γ=0.3eV. The solid dots are data of $|\chi^{(3)}|$ obtained from DFWM measurements.

Notice that the values obtained from DFWM are the square root of χ^3, i.e. the absolute values of χ^3. The absolute values of χ^3 are also calculated from equation (6.4.2) with the same parameters used for Fig. 6.4.1. In order to compare with the data obtained from DFWM, the calculated values are normalized by a factor which gives the best fitting. The result is shown in Fig. 6.4.2. The theoretical calculation agrees well with the DFWM data.

The single photon absorption spectra do not show any absorption at 1064 nm for all three samples. Recent third harmonic generation studies in polythiophene polymers[17] have successfully determined the presence of two photon absorption states, by using the four - level model. These two photon absorption states(i and j) are located on each side of the first one photon allowed transition(state g to state f). i is about 0.1239eV(Δ) below, j is about 0.6197eV(Δ') above. The schematic energy diagram is shown in Fig.6.4.3.

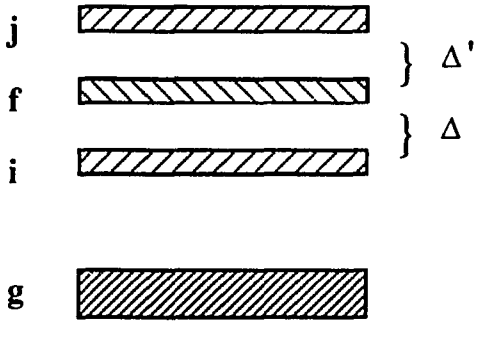

Fig.6.4.3 Schematic energy diagram for a four-level model of polythiophene polymers

Since two photon absorption at 1064 nm can reach the first two photon state i, thus in our Z - scan measurements, the nonlinearity at 1064 nm could be in resonance with the two-photon transition g to i. In a 4 - level approximation(see Fig.6.4.3), with $\omega_1=\omega_2=\omega$ and $\omega_3=-\omega$, the TPA resonant part of $\chi^{(3)}_R$ can be obtained using the same principle as for the single photon resonant transition[16]:

$$\chi^{(3)}_R \propto \frac{A}{(\omega_{fg} - \omega)(\omega_{ig} - \omega - \omega - i\Gamma)(\omega_{fg} - \omega)}, \qquad (6.4.3)$$

where ω_{ij} are the energy difference between states j and i (in h units), Γ is the band width of the excited state f, and ω is the photon energy (in h units). States i have the same parity as the ground state g(two photon absorption transition allowed), whereas f has the opposite parity(single photon transition allowed). A is a factor related to the transition dipole moments.

Fig. 6.4.4 shows the theoretical calculation using equation (6.4.3). The parameters are chosen as following: ω_{fg}=2.253eV, ω_{ig}=2.129eV, and Γ=0.3eV.

From Fig. 6.4.4, the sign of the real part of two photon transition resonant $\chi(3)$ at 1064 nm is predicted to be negative, this is in agreement with the Z -scan measurement.

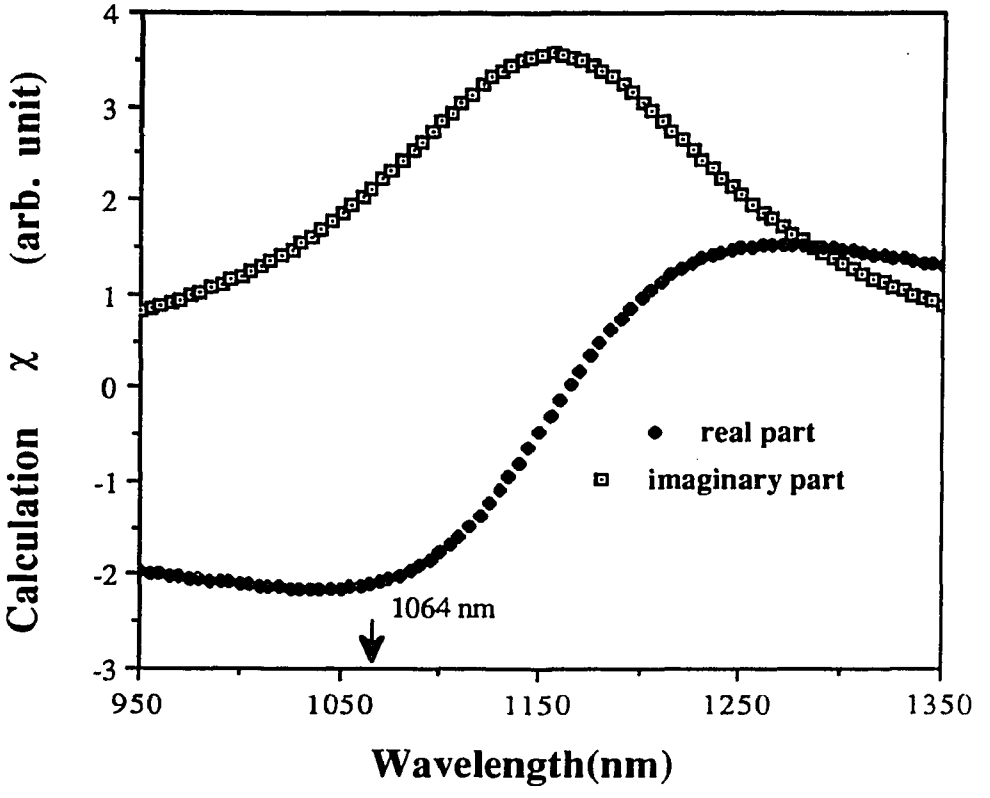

Fig. 6.4.4 The calculated real and the imaginary part of two photon absorption resonant χ^3 as a function of the excitation photon frequency. The parameters are: ω_{fg}=2.253eV, ω_{ig}=2.129eV, and Γ=0.3eV.

6.5 Conclusion

From the single beam Z -scan measurements, the sign for the real part of χ^3 has been determined to be negative at both 532 nm and 1064 nm. The negative nonlinearity at 532 nm is in resonance with the one photon absorption transition; while negative nonlinearity at 1064 nm may be due to the resonance with the two photon absorption transition.

The discrepancy between obtained values of the real part of χ^3 at 1064 nm from DFWM and Z - scan measurements is probably due to the higher excitation intensity in Z - scan measurements. Two photon absorption dose not play an important role at low intensities.

A simple two level model is used to explain the observed nonlinearity around π - π^* transition band, the theoretical calculation shows a good agreement with the experimental observations of the sign and the magnitude of χ^3 .

Reference

1.. M. Sheik-bahae, A. A. Said, and E. W. Van Stryland, Opt. Lett. **14**, 955(1990).

2. M. Sheik-bahae, A. A. Said, and E. W. Van Stryland, IEEE J. Quan. Elec. **26**, 760(1990).

3. Y. R. Shen, ***The principle of Nonlinear Optics***, (Join Wiley &Sons, Inc. 1984), Chap.14, or see the **Appendix** of this thesis, p146.

4. W. E. Torruellas, D. Neher, R. Zanoni, G. I. Stegeman, F. Kajzar and M. Leclerc, *"Dispersion measurements of the third order nonlinear susceptibility of polythiophene thin films"*, to be published in Chem. Phys. Lett.

Chapter VII

Enhanced Third-Order Optical Nonlinear Response about Photoinduced Polaronic Bands in Polythiophene Films

7.1 Introduction

Considerable interest has been directed to π electron systems, such as polyacetylene [1-6] and polythiophene [7-11], both form model systems of quasi-one dimensional semiconductors. The electronic excitations of these materials are different from the electron-hole pairs found in ordinary semiconductors. After doping or photoexcitation, rapid lattice relaxations due to the strong electron-phonon coupling result in the formation of self-trapped excitations such as solitons, polarons and bipolarons with their associated electronic states inside the gap. Consequently, the redistribution of oscillator strength, produced in less than a picosecond, is the possible reason for the large nonlinear optical response in these polymers. These nonlinear excitations are expected to play an important role in the nonlinear optical properties and charge transport in polymers.

In nondegenerate ground state systems such as polythiophene(PT), polarons and bipolarons are predicted [12,13] as the dominant charge carriers after doping or photoexcitation. Upon doping, spectroscopic evidence for polarons in PT compounds has been reported only in the case of very lightly doped samples[14].

Spinless bipolarons are more favorable than two polarons when polaron density is high enough to interact with each other upon heavy doping. In the case of photoexcitaton, Vardeny *et al.*[15] reported that the dominant photocarriers with excitation above the energy gap are charged spinless metastable bipolarons since their steady state photoinduced absorption signal was related to the small photoinduced electron spin resonance(ESR) signal. Kaneto *et al.*[16] , on the other hand, claimed that polarons are the dominant photocarriers by comparing the photoinduced absorption (steady state) spectra with those dopant-induced absorption spectra at dilute doping levels. These results were confirmed by their photoinduced ESR measurements later on[17]. Ultrafast pulsed-laser time-resolved interband bleaching experiments[18] which monitor the ground-state recovery have been performed to investigate the origin of the observed bipolarons. These results are difficult to interpret in terms of bipolarons generation and decay because of the existence of other excitations. Thus, the nature and formation mechanism of these lattice deformations still remain unknown. Recently, fast photoconductivity[19] and fast and large $\chi^{(3)}$[7-11] associated with fast shift of oscillator strengths have been measured in polythiophene. The question of (bi)polarons on the short time scale and their role in nondegenerate ground state systems still remains an open question.

In the previous chapter, the third order nonlinearity in PT and polycondensed thiophene based polymers was measured using a degenerate four wave mixing technique[7,8]. The dispersion spectra of $\chi^{(3)}$ was obtained about the absorption region. The value of $\chi^{(3)}$ was also found to be linearly proportional to the absorption coefficient α

which strongly suggested that a population grating dominates for above gap radiations. Below gap measurement gave a $\chi^{(3)}_{1064nm}$ value of 10^{-11} esu. A special attention has been paid to $\chi^{(3)}_{1064nm}$ since 1064nm was found to be near one of the photoinduced absorption peaks(polaronic bands) in previous steady-state photoinduced absorption measurements[15,16] .

In this chapter, $\chi^{(3)}$ is measured at 1064 nm when the PT sample is photoexcited with an above gap light at 532 nm. The purpose of this work is two fold. Firstly, experimental studies to date have only studied $\chi^{(3)}$, either in resonance with the interband π - π^* transition.[7,8,10,11] or due to two and three photon resonances[3,4,6] . In view of this, we have measured $\chi^{(3)}$ directly inside the polaronic bands to seek experimental evidence of the role played by polarons (P) or bipolarons (BP) in the third order optical nonlinearities. Secondly, the dynamics of polarons and bipolarons have not been time resolved in polythiophene. The present novel pump-probe degenerate four wave mixing(DFWM) technique provides a tool to determine the picosecond dynamics of photogenerated carriers and the notion of dominant photocarriers on the short time scale. Direct enhancement with a fast rise and decay time of $\chi^{(3)}_{1064nm}$ about photoinduced polaronic bands is reported in this chapter.

7.2 Experiment

The polythiophene thin films(1000 - 2500 Å) are electrochemically polymerized on tin oxide glass substrates. The

detailed information about the polythiophene polymer samples were given in Chapter V or can be found in ref. 20,21.

A 10-Hz mode-locked Quantel Nd:YAG laser system with a second-harmonic generator was used to generate 25 ps pulses at 1064 and 532 nm. A new pump-probe DFWM technique is introduced and schematically shown in Fig. 7.2.1. The fundamental output at 1064 nm is divided into three beams and used in a degenerate four wave mixing(DFWM) geometry. This part of the setup was described in detail in chapter II. A fourth beam at 532 nm is added to the DFWM setup and acts as a pump beam. The 532 nm beam has the same polarization direction as the 1064nm beams. In this configuration, the 532 nm beam photoexcites PT sample. The DFWM beams at 1064 nm probe the excited system at different times subsequent to the 532 nm excitation. The experiments have been performed at room temperature.

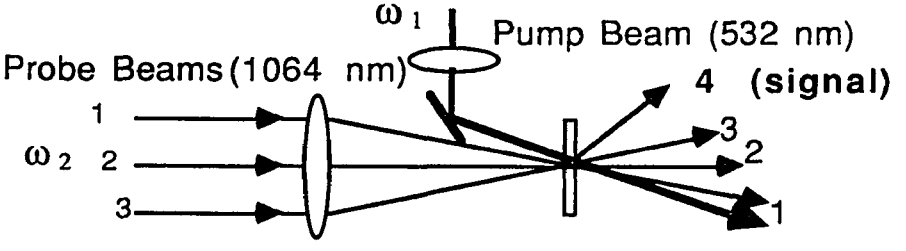

Fig. 7.2.1 Beam geometry for pump-probe DFWM

7.3 Results

Fig. 7.3.1 illustrates the ***increased*** DFWM signal at 1064 nm as the function of delay between 532 and 1064nm beams. The signal was detected in the phase matching direction $\hat{K}_4 = \hat{K}_1 + \hat{K}_2 - \hat{K}_3$ [7] (see Fig.2.1.3(b)). The data were obtained with 3 DFWM beams fixed at "0" delay(that is, spatially and temporally overlapping). The 532 nm beam is delayed(shown as the inset of Fig. 7.3.1). It is apparent that when 532nm overlaps with three 1064 nm beams, a maximum enhancement is achieved. When the 532 nm beam arrives too early, or too late relative to the 1064 nm laser pulses, there is no enhancement. The enhancement follows the laser pulse at 532 nm which tells us that the enhancement is truly photoinduced by 532 nm beam. Notice, when three 1064 nm beams overlap, a nonresonant signal, which is about 10 times less than the enhanced signal, is present even without 532 nm beam. For simplicity, this nonenhanced signal has been taken as the "0" background for Fig. 7.3.1. The Y axis represents the ***increased*** DFWM signal.

In order to determine the response time of the enhanced DFWM signal, one of the probe beam at 1064 nm for the DFWM is delayed and the other two 1064 nm and 532 nm beams are fixed at "0" delay (see inset of Fig. 7.3.2). The time resolved enhanced DFWM signal (includes the nonresonant part) is obtained and displayed in Fig. 7.3.2. This result clearly shows that the response time is still limited by the laser pulse resolution(<25 ps) which indicates that the enhanced DFWM signal at 1064 nm is ultrafast.

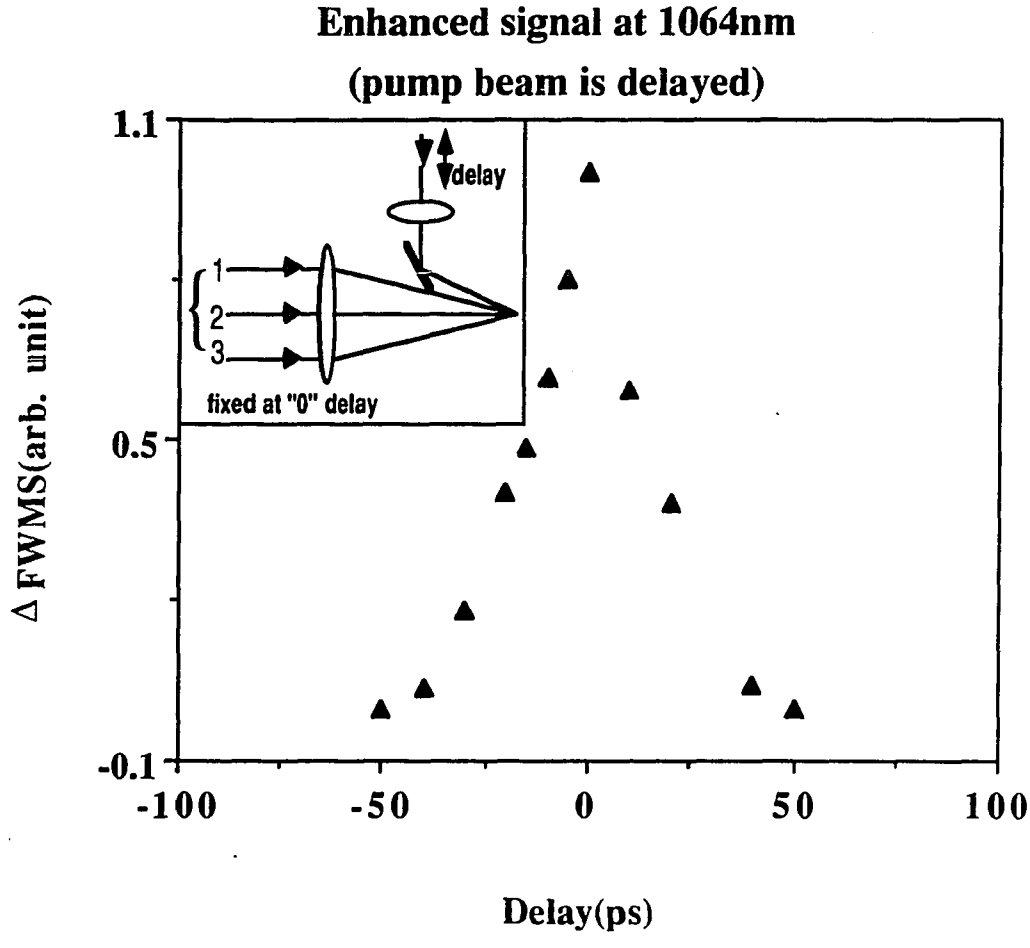

Fig. 7.3.1 The increased DFWM signal (ΔFWMS) at 1064 nm of PT as a function of delay between 532 and DFWM 1064 nm beams. The inset shows the experimental arrangement used to obtain the data: the 1064 nm beams are fixed at "0" delay and 532 nm beam is delayed.

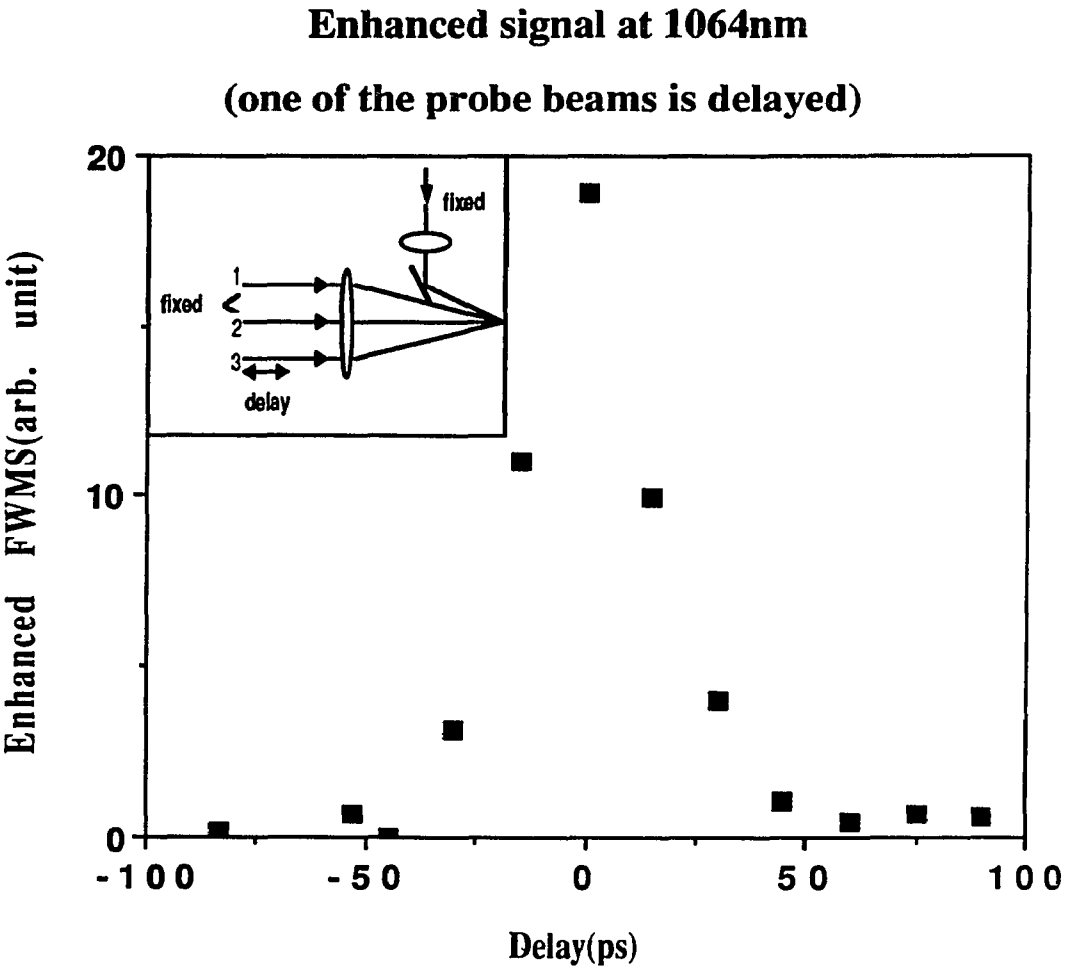

Fig. 7.3.2 Time resolved enhanced DFWM signal at 1064 nm when 532nm beam is fixed at 0 delay and one of 1064 nm beams is delayed (the inset shows this experimental arrangement).

7.4 Discussion

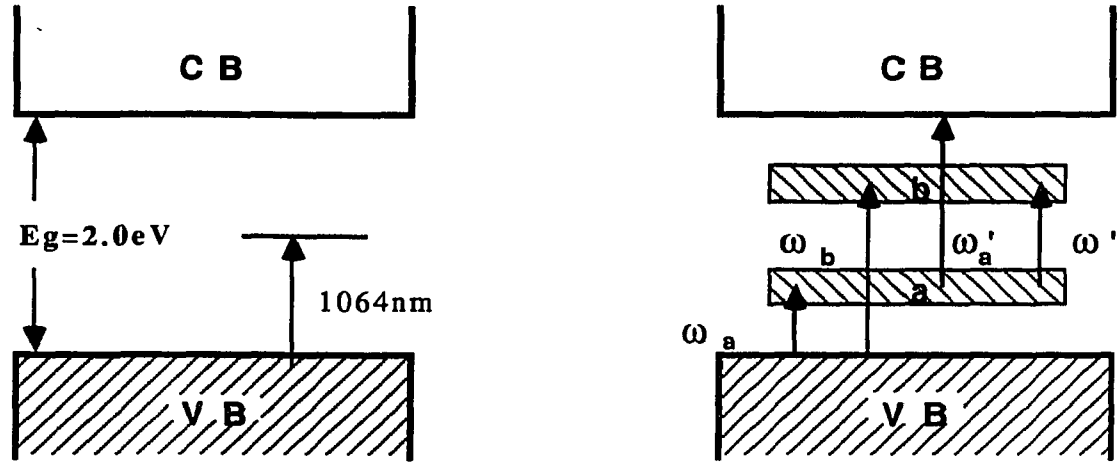

(a) (b)

Fig. 7.4.1(a)The schematic band diagram for polythiophene polymers. (b)The schematic band diagram for the photon excited polythiophene.

The schematic band diagram of polythiophene polymers before photon excitation is shown in Fig.7.4.1(a). The band gap is about 2.0eV. Only the band gap transitions are the real transitions(except two photon absorption at 1064nm).

The schematic band diagram of polythiophene after photon excited above gap is displayed in Fig. 7.4.1(b). The two midgap states (bonding-antibonding states a and b), along with the possible transitions for polarons and bipolarons is also displayed in Fig. 7.4.1(b). ω_a , from the valence band to the lower midgap state, and ω_b , from the valence band to the top midgap state, are allowed for a positively charged bipolaron, BP^+ (or from midgap states to the conduction band for BP^-). Two extra transitions: ω' between the two

midgap states(subgap transition) and ω_a' from the lower midgap state to the conduction band are allowed for a positively charged polaron, P^+ (or from the valence band to the top midgap state for P^-). Usually, the transition probability of ω_a' is smaller compared to the others, and $\omega_a' \approx \omega_b$, if midgap states are assumed symmetric about the gap center. Transitions for the positively charged species are only shown in Fig. 7.4.1(b) for simplicity.

We have observed an enhancement of the DFWM signal at 1064nm using the novel pump-probe DFWM technique. This result is rather interesting and surprising. In the absence of ω_1(532 nm beam), the energies of the stationary excited states in PT are much higher than the photons at ω_2(1064 nm) since the lowest excited state is at E > 2eV(see Fig.7.4.1(a)). The excitation intensities can be kept so low such that the two photon absorption at 1064 nm dose not play an important role. Thus, without the excitation beam at 532 nm, the DFWM measurements at 1064 nm give $\chi^{(3)}{}_{\omega 2} = \chi^{(3)}{}_{NR}$, which has been obtained in our previous DFWM experiments[7,8]. Two midgap states are formed inside the gap after photoexcitation at 532nm(see Fig. 7.4.1(b)). The salient point is that the probe beams at 1064 nm now could be in resonance with the two newly available optical transitions: ω_b (for both BP and P) and ω' (for P only). Now $\chi^{(3)}$ has two triply resonant terms [22] :

$$\chi_R^{(3)} \propto -i\, N\, A_{ij}^4 \left[\frac{1}{(\omega_{ij} - \omega_2 - i\Gamma_{ij})^2} - \frac{1}{(\omega_{ij} - \omega_2)^2 + \Gamma_{ij}^2}\right]\left(\frac{1}{\Gamma_{ii}} + \frac{1}{\Gamma_{jj}}\right) \qquad (7.4.1)$$

where, ij = vb (ac or ab), A_{ij} includes the dipole matrix element for the transitions between valence(conduction) and the polaronic band b (a) or between polaronic bands a and b. Γ_{ij} is the phenomenological damping factor. $T_{1i(j)} = 1/\Gamma_{ii(jj)}$ is the longitudinal relaxation time for state i(or j), and N is the number of polarons or bipolarons per unit volume. The full expression of $\chi^{(3)}$ is simply:

$$\chi^{(3)}_{total} = \chi^{(3)}_{NR} + \chi^{(3)}_{R} . \qquad (7.4.2)$$

If the creation of the photoexcited midgap states is faster than our temporal resolution and the dipole matrix elements in the second part give a sizable contribution, we would expect an enhancement of $\chi^{(3)}_{total}$. That is, the enhancement of DFWM signal at 1064 nm is expected when the system is photoexcited by 532 nm because of the resonance of $\chi^{(3)}$ about the photoinduced polaronic bands in PT.

It is necessary to discuss the dynamics of the primary photogenerated species since much longer decay time was expected according to the previous experiments[15,16]. Considering that after electron-hole photoinjection, chain distortions will quickly form around these single charges, leading to the formation of polarons. The possible relaxation processes of photogenerated polarons are modeled in Fig. 7.4.2. The intrachain and interchain excitations have been taken into account.

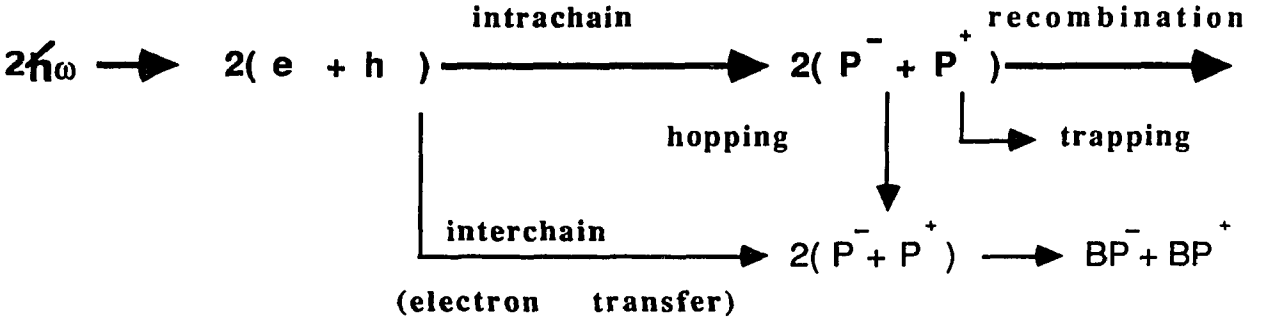

Fig.7.4.2 Decay processes of photogenerated polarons

Most of polaron pairs formed on the same chain will quickly recombine through the geminate recombination (intrachain process). Thus, those intrachain polarons have a very short lifetime. In general, this pathway dominates, only rare polarons can escape the geminate recombination. Then the polarons will move(drift) along the chain until they are trapped by defects(for example, until they hit the end of the chain). They also can hop to the neighboring chains. Because of the finite transverse bandwidth due to interchain coupling, the polarons can also be photogenerated by electrons and holes formed on different chains(interchain electron transfer processes). The polarons with the same sign, generated by interchain excitation or transferred from the neighboring chains can combine to form bipolarons. A single charged bipolaron should be metastable since recombination could occur only when two electrons(or two holes) hop together from one chain to another. The long lived (bi)polarons are responsible for the steady-state photoinduced absorption signals[15,16].

The fast intrachain process has been probably observed in our measurements. The rise slope of the signal is limited by our laser resolution which indicates that the formation time of intrachain polaron pairs is very fast in agreement with the theoretical predictions[12,13]. The lifetime of intrachain polarons is < 25 ps as deduced from the fast decay slope. The resonance contribution to $\chi^{(3)}$ due to long lived (bi)polarons was not observed in our measurements. We believe this slow component is small in the picosecond time region partly because our measurements have been done at room temperature(the photoinduced absorption signal was hardly observed at room temperature[15,16]). Our observation is also consistent with the recent photoinduced absorption studies of polythiophene[19] , where it was estimated that only 0.02 of the initial excitations survive and are mobile beyond 25ps.

The hypothesis of intrachain polarons recombination can be tested by investigating the pumping fluence(F) dependence of the photoinduced enhancement of the DFWM signal. Assuming that $\chi^{(3)}_R$ depends on the polaron oscillator strength, its value will linearly depend on the number of the photogenerated polarons per unit volume N_p. The number of polarons per unit volume N_p would yield a steady-state density that grows as F without saturation when bimolecular recombination term is omitted from the rate equation for the photogeneration of polarons.

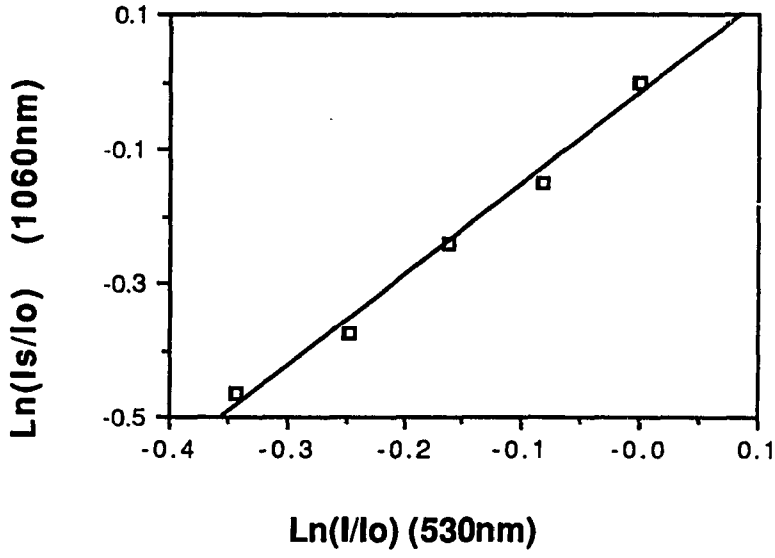

Fig.7.4.3 The enhanced DFWM signal at 1064 nm as a function of 532 nm pump fluence.

The curve in Fig. 7.4.3 is a plot of the photoenhanced DFWM signal as a function of pump fluence at 532nm within a limited fluence range $\sim 10^{16}$ photons/cm^2. It is apparent that the enhanced signal is increasing as the fluence of 532nm beam increases. The slope is found to be about 1.38 giving sublinear dependence of $\chi^{(3)}$ on F. Due to the sensitivity of our detection system at lower fluence and the damage to the sample with larger fluence(532 nm is strongly absorbed in PT), the dynamic range of the fluence is limited to the order of 10^{16} photons/cm^2. At this fluence level, we believe that we are operating near the saturation regime which normally has a reduced slope. Similar saturation of a simple volume(or phase-space) filling of the lattice by photogenerated solitons has been observed in Trans-$(CH)_x$[2]. The enhanced signal shown in Fig. 7.4.3 includes the nonresonant part which could also reduce the observed slope to less

than 2. Typically, one order of magnitude enhancement of the signal is observed within our fluence range.

7.5 Conclusion

Photoinduced enhancement of $\chi^{(3)}$ about polaronic bands in polythiophene on picosecond time scale was observed for the first time by a novel "pump-probe" DFWM technique. Intrachain polarons are most likely responsible for the enhancement at times less than 25 ps. In addition, our results have shown that dominant photocarriers are most likely fast polarons on the short time scale.

Reference

1. C. V. Shank, R. Yen, R. L. Fork, J. Orenstein and G. L. Baker, Phys. Rev. Lett. **49**, 1666(1982), Phys. Rev. B 28, 6095(1983).

(2)L. Rothberg, T. M. Jedju, S. Etemad and G. L. Baker, Phys. Rev. Lett. 57, 3229(1986), Phys. Rev. B **36**, 7524(1987).

3. F. Kajzar, S. Etemad, G. L. Baker and J. Messier, Solid State Commun. **63**, 1113(1987).

4. M. Sinclair, D. Moses, K. Akagi, and A. J. Heeger, Phys. Rev. B **38**, 10724(1988).

5. D. M. Mackie, R. J. Cohen and A. J. Glick, Phys. Rev. B **39**, 3442(1989).

6. W. S. Fann, S. Benson, J. M. J. Madey, S. Etemad, G. L. Baker and F. Kajzar,Phys. Rev. Lett. **62**, 1492(1989).

7. L. Yang, R. Dorsinville, Q. Z. Wang, W. K. Zou, P. P. Ho, N. L. Yang, R. R. Alfano, R. Zamboni, R. Danieli, G. Ruani and C. Taliani,J. Opt.Soc. Am. B **6**, 753(1989).

8. R. Dorsinville, L. Yang, R. R. Alfano, R. Zamboni and C. Taliani, Opt.Lett. **14**, 1321(1989).

9. R. Worland, S. D. Phillips, W. C. Walker and A. J. Heeger, Synth. Metals **28**, D663(1989).

10. B. P. Singh, M. Samoc, H. S. Nalwa and P. N. Prasad, submitted for publication.

11. R. Zamboni, C. Taliani, G. Ruani, A. J. Pal and F. Kajzar,submitted for publication.

12. W. P. Su and J. R. Shrieffer, Proc. Natl. Acad. USA **77**, 5626(1980).

13. R. Ball, W. P. Su and J. R. Shrieffer, J. Phys.(Paris) Colloq **44**, c3(1983).

14. G. Harbeke, E. Meier, W. Egli, H. Kiess and E. Tosatti, Solid State Commun. **55**, 419(1985).

15. Z. Vardeny, E. Ehrenfreund, O. Brafman, M. Nowak, H. Schaffer, A. J. Heeger and F. Wudl, Phys. Rev. Lett. **56**, 671(1986).

16. K. Kaneto, F. Uesugi and K. Yoshino, J. Phys. Soc. Jpn. **56**, 3703(1987).

17. K. Kaneto, F. Uesugi and K. Yoshino, J. Phys. Soc. Jpn. **57**, 1859(1988).

18. Z. Vardeny, H. T. Grahn, A. J. Heeger and F. Wudl, Synth. Metals.**28**, C299(1989).

19. S. D. Phillips, G. Yu and A. J. Heeger, Synth. Metals. **28**, D669(1989)

20. C. Taliani, R. Danieli, R. Zamboni, P. Ostoja and W. Porzio, Synth. Metals. **18**, 177(1987).

21. C. Taliani, R. Zamboni, R. Danieli, P. Ostoja, W. Porzio, R. Lazzaroni and J. L. Bredas, Physica Scripta **40**, 781(1989).

22. Y. R. Shen, ***The Principles of Nonlinear Optics*** (Join Wiley & Sons,Inc. 1984) Chap. 14.

Chapter VIII

Ultrafast Time Response of Optical Nonlinearity in Polysilane Polymers

8.1 Introduction

The third-order nonlinear susceptibility $\chi^{(3)}$ of polysilane was measured to be comparable to that of polydiacetylenes in the nonresonance regime. Polysilane polymers are transparent in the visible region where polydiacetylenes are highly absorbing. These characteristics, together with the facility of producing good quality thin-films, make polysilane a new interesting nonlinear material[1,2]. In the past, $\chi^{(3)}$ of polysilane thin films was obtained primarily by third harmonic generation measurements and four wave mixing with nanosecond laser pulses without any time resolution. In this chapter, we report on the temporal behavior of $\chi^{(3)}$ of polysilane in thin films and solutions using both the picosecond time resolution optical Kerr gate and four wave mixing. The relative contributions from various nonlinear mechanisms were separated by the time resolved measurements. In the next chapter, we will discuss the sign of $\chi^{(3)}$ in the transparent region.

8.2 Sample

The molecular structure of polysilane polymer:$[\phi\text{-Si-}(CH_3)]_n$ is shown in Fig. 8.2.1. The polymer was synthesized by the method described in Reference 3. The film casting of polyphenylmethylsilane was prepared on a large crystallization dish with controlled vapor pressure of organic solvents(toluene, tetrahydrofuran (THF)). In these polymers, each monomer unit is composed of a central Si bonded to a methyl group ((CH_3)) and a large "side group"  . All monomers are σ bonded to each other through the silicon atoms to form the polymer chain. This type of bonding results in Si-Si σ-electron delocalization[4].

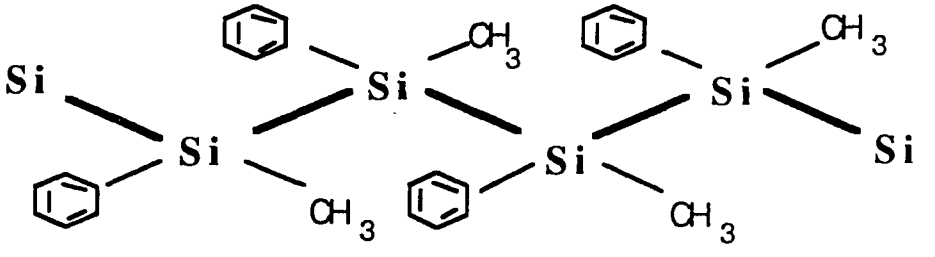

Fig. 8.2.1 Molecular structure of polysilane polymers

A typical optical absorption spectrum of polysilane is displayed in Fig. 8.2.2. The spectrum shows that there is no apparent absorption from 360nm to 1060nm. No single photon resonance should occur in that region.

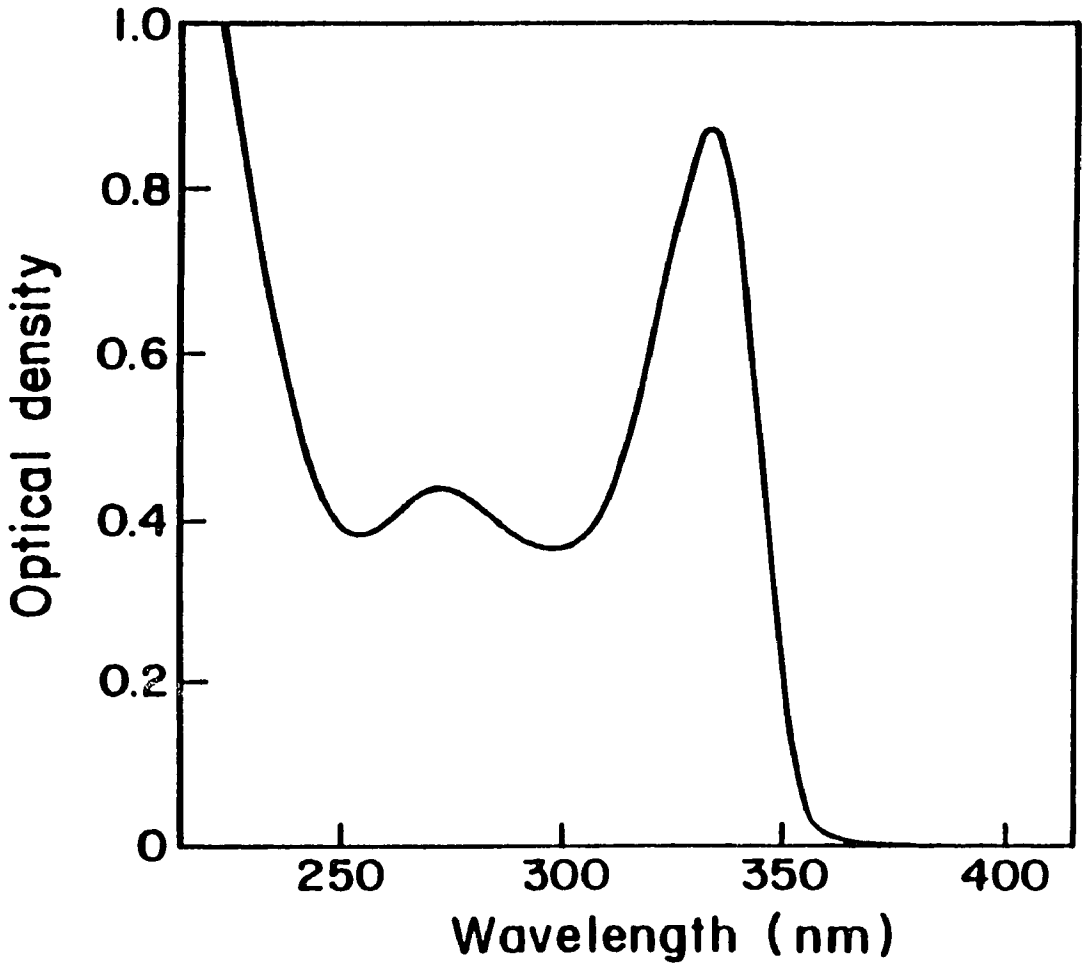

Fig. 8.2.2 Optical absorption spectrum of polysilane solution with concentration of 6.7 $x10^{-5}$g/ml.

8.3 Experimental Techniques

Picosecond Optical-Kerr gate(OKG) was used to determine the nonlinear optical kinetics of polysilane thin films and solutions. The single optical pulses with ~ 8ps (full width at half maximum) duration were generated from a mode-locked Nd:glass laser with a single-pulse selector, an amplifier and a second harmonic generator. The pump and probe wavelengths were at 1060nm and 530nm, respectively. The detail geometry of OKG is shown in Fig.8.3.1.

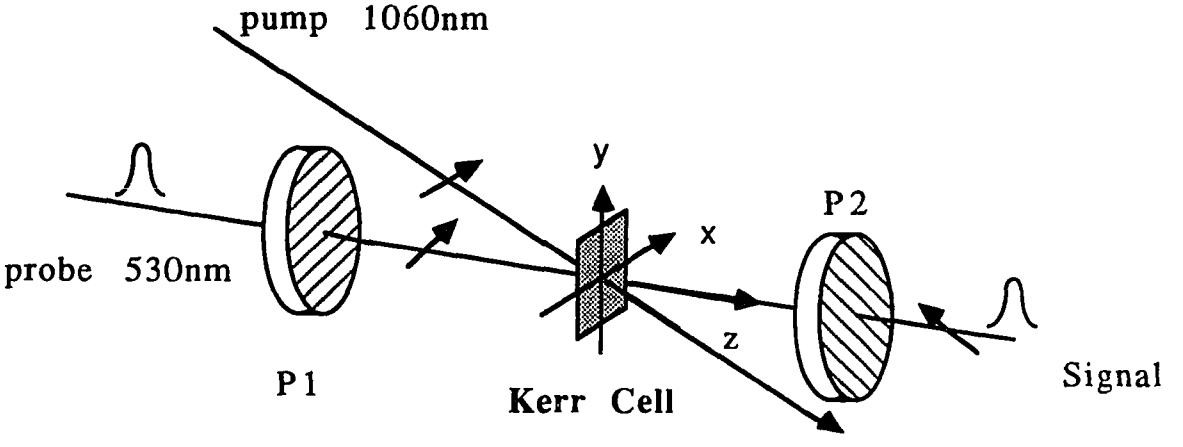

Fig.8.3.1 Schematic diagram of optical Kerr gate. P1, P2 are a pair of crossed polarizers.

In the optical Kerr effect, an intense linearly polarized light(pump beam) generates a nonlinear polarization in the medium resulting in an induced optical birefringence. When a linearly polarized weak beam(probe beam) is interacting with the medium, the output light polarization is rotated due to pump induced

birefringence. The Kerr medium is placed between a pair of crossed polarizers such that there is no light coming through the polarizers when the pump is absent. This "gate" is only open when the pump arrives. The polarization direction of the pump beam is at 45° to the probe beam. In order to get the time information, a delay line is introduced in the probe beam. The time resolution for this OKG was determined to be about 3ps from the rise and decay time slopes of the Kerr signal profile of CS_2.

8.4 Results and Discussion

The normalized transmitted signal I (τ_D) through a (10 ±1.0) μm polysilane thin film Kerr gate as a function of the time delay τ_D between the pump and probe pulses is displayed in Fig. 8.4.1. The slopes of the rise and decay of Kerr signal profile are 3ps. Therefore, the relaxation time of $\chi^{(3)}$ process of polysilane thin films was unresolved(<3ps). The Kerr signal profile for solutions is identical to Fig. 8.4.1.

The transmitted Kerr signal through a Kerr medium as a function of delay time τ_D between the probe and pump pulses is given by:

$$I(\tau_D) = \int_{-\infty}^{\infty} < E_{probe}{}^2{}_{(t-\tau_D)} > \sin^2 [\frac{\delta\phi_{(t)}}{2}] \, dt \, . \qquad (8.4.1)$$

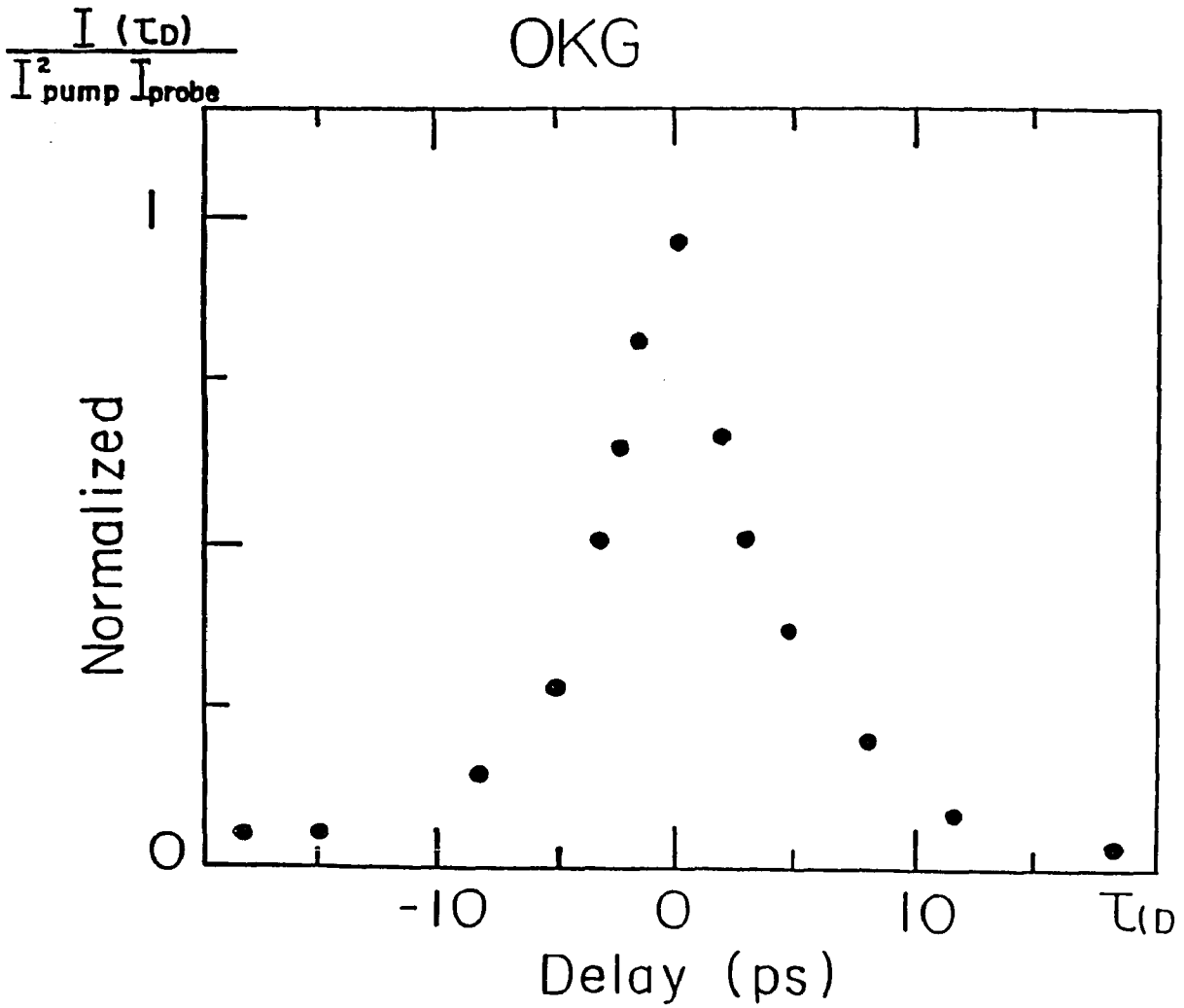

Fig. 8.4.1 Normalized time-resolved Kerr transmitted signal from polysilane thin films using 8ps laser pulses.

Both rise and decay slopes are 3ps.

In general, the total induced phase retardation[5] at the peak value (τ_D =0) is obtained through integration over the sample length L :

$$\delta\phi_{(0)} = \frac{2\pi}{\lambda_2} \frac{n_2 I_1}{\alpha_1} (1 - e^{-\alpha_1 L}) \quad , \qquad (8.4.2)$$

for a Kerr medium with the relaxation time faster than the laser pulses duration and with absorption coefficients α_1, α_2 at pump and probe wavelengths, respectively. When $\delta\phi << 1$, the peak value of the transmitted Kerr signal is approximately given by:

$$I_{(0)} \sim (\frac{2\pi}{\lambda_2 \alpha_1})^2 n_2^2 [1 - e^{-\alpha_1 L}]^2 e^{-\alpha_2 L} I_1^2 I_2, \qquad (8.4.3)$$

where λ_2 is the probe wavelength.

Equation (8.4.3) can be simplified to:

$$I_{(0)} \sim (\frac{2\pi}{\lambda_2})^2 n_2^2 L^2 I_1^2 I_2, \qquad (8.4.4)$$

since the sample absorption at pump and probe wavelengths is negligible.

The nonlinear index of refraction n_2 is related to $\chi^{(3)}$ by:

$$n_2 = \frac{12\pi}{n_0} \chi^{(3)}_{1212} \quad . \qquad (8.4.5)$$

The value of the third-order nonlinear susceptibility $\chi^{(3)}$ was measured to be on the order of $2.0 \pm 0.6 \times 10^{-12}$esu from the peak value of the OKG.

The relaxation kinetics of $\chi^{(3)}$ of polysilane solutions was also determined by the forward degenerated four-wave mixing(DFWM) technique in the phase-matched three-dimensional folded boxcar configuration(see Chap.II, Fig2.1.3(a)). In this case, the excitation source was a 10 Hz mode-locked Quantel YAG laser pulses with 30ps duration at 530nm. The temporal evolution of the generated fourth

beam $\mathbf{K}_4$ was measured by varying the arrival time (delay time) of one incident beam $\mathbf{K}_2$(probe beam) relative to the other two beams $\mathbf{K}_1$, $\mathbf{K}_3$(pump beams) via a stepper-driven optical delay line. In these measurements, all three beams are polarized parallel to the Y axis. The signal from the solvent(THF) was below the detection threshold.

The intensity I of the fourth beam $\mathbf{K}_4$(signal) as a function of the delay time was measured and displayed in Fig. 8.4.2. The signal profile consists of a fast and a weak slow component. The fast component is clearly unresolved(<20ps) in agreement with the OKG data. It took a certain time (on the order of > 0.1s, several successive pulses) to build up the grating responsible for the weak slow component in the solution. Once the grating was formed, the signal was independent of the delay time up to 1ns which is the maximum delay time of our delay line. The origin of the weak slow component will be discussed after estimating $\chi^{(3)}$.

By integrating the equation for the power in the the fourth beam generated per unit length in the sample and neglecting absorption at 530nm, $\chi^{(3)}$ can be evaluated by equation 8.4.4.

The calculated $\chi^{(3)}$ of the fast component is estimated to be on the order of $1.6 \pm 0.2 \times 10^{-12}$esu. This value is in good agreement with the value obtained from OKG experiment.

The observed large value of cubic susceptibility of polysilane most likely arises from the electrons delocalized in the polymer backbone and from the transition dipole moments parallel to the molecular axes. The fast decay (<3ps) which is unresolved by our measurements points to an electronic contribution[1,2].

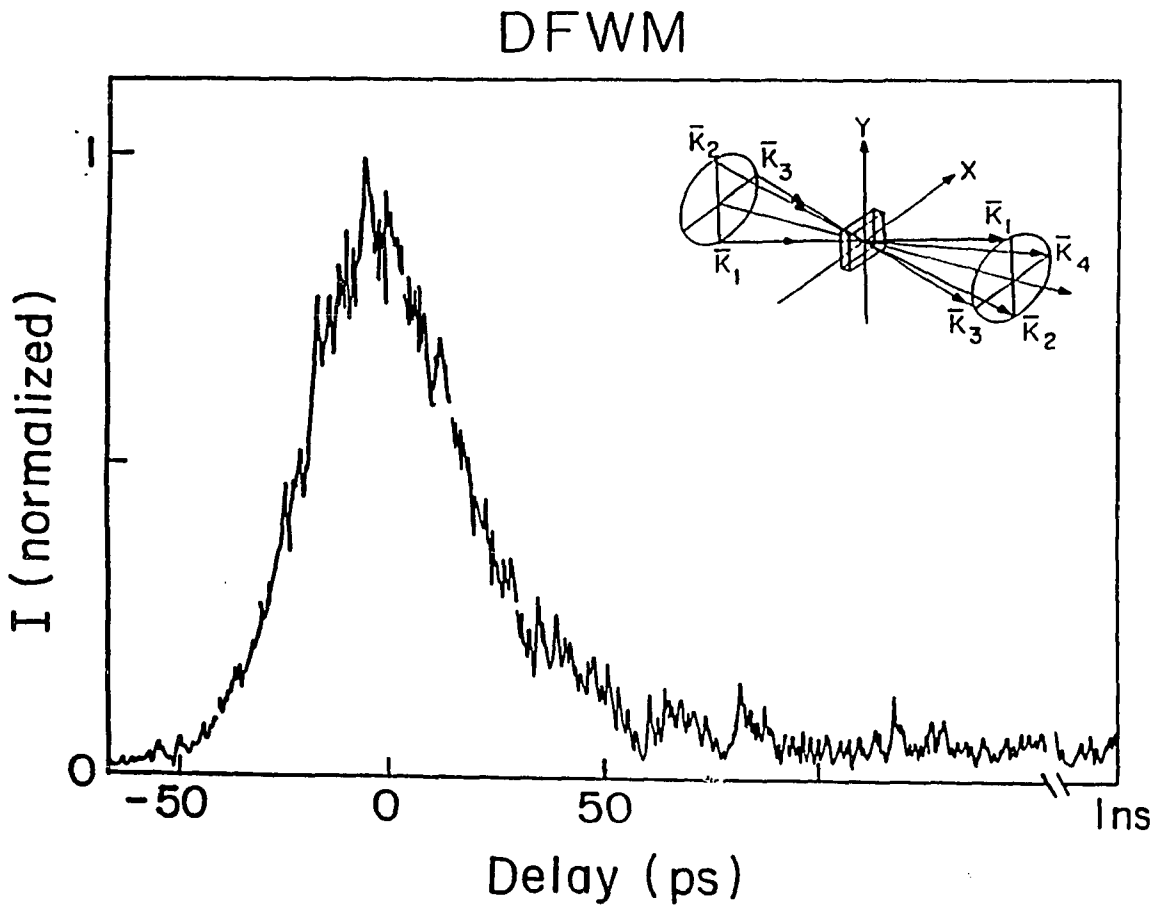

Fig. 8.4.2 Normalized intensity of DFWM signal from polysilane solution as a function of the delay time between probe and pump pulses.

The excitation wavelength is at 530nm.

The inset indicates the wave vector diagram of DFWM configuration.

The slow component(>0.1s) could arise from a thermal grating formed by two-photon absorption in the solution or the spatial motion of polysilane molecules caused by diffusion in the optical field gradient.

The decay of the thermal grating is related to the thermal parameters of the solvent THF by[7]:

$$\tau = \frac{\rho C_p \Lambda^2}{4\pi^2 K}, \qquad (8.4.7)$$

where ρ=density, C_p=heat capacity, K=thermal conductivity,and Λ=grating space. The grating space is obtained from: $\Lambda = \frac{\lambda}{2n}\sin(\theta/2)$, where θ is the angle between the pump beams. Substituting these parameters into equation (8.4.7), τ is obtained on the order of 10^{-5}s which is much faster than the experimental observations.

An alternative model to explain the slow component arises from the radiation pressure. The polysilane molecules in the optical field **E** acquires an induced polarization $\mathbf{P} = \alpha$ E. The radiation pressure from the laser light produces a force[8] $\sim \alpha \nabla \mathbf{E}^2$ acting on the polysilane molecules which causes the molecules to move into the high light intensity regions since $n_{polysilane} > n_{THF}$. The increasing density of the molecules in the high-field regions increases the average refractive index, thus creating a refractive-index grating in the material. The thermal Brownian diffusion of the molecules opposed the motion from light force, which will tend to wash out the optically formed grating. The grating decay time which is approximately the time for the molecules to diffuse one quarter of the grating space Λ is given by[8] :

$$\tau = \frac{3\pi r \eta \Lambda^2}{16\ k\ T}, \qquad (8.4.8)$$

where η is the viscosity of the solvent THF(0.438 centi-poises), k is the Boltzmann's constant and T is the absolute temperature, and r is the radius of polysilane molecules. The polysilane molecule has been shown to have an unusually high characteristic ratio, C_∞[9], and is considered here as an extended coil, having a hydrodynamic radius of 600 Å. The calculation from equation (8.4.8) gives τ = 0.4s. The formation time(>0.1s) for the grating is roughly on the same order of magnitude as the observed decay time under our experimental condition[8]. The absence of a slower component from polysilane solution in OKG measurement is consistent with the radiation pressure model since OKG measurements were performed with single laser shots at greater than 2 minutes intervals.

8.5 Conclusion

In conclusion, the electronic part of $\chi^{(3)}$ in polysilane is measured to be ~1.6 x 10^{-12} esu at 532nm in good agreement with previous observations[1,2]. The response time of the nonlinear optical process associated with the electronic mechanism is found to be faster than 3ps. The slower component in polysilane solution is assigned to the refractive-index grating arising from the radiation pressure.

References

1. F. Kajzar, J. Messier and C. Rosilio, J. Appl. Phys. **60** 3040(1986).

2. D. J. Mcgraw, C. E. Barker, R. Trebino, A. E. Siegman, M. Thakur, G. M. Wallraff and R. D. Miller, a report in **The Third International Laser Society Conference**, American Physical Society, Atlantic City,
Vol.32 No.8, p.162 (1987).

3. P. Trefonas III, P. I. Djurovich, X. H. Zhang, R. West, R. D. Miller and D. Hofer, J. Polym. Sci. Polym. Lett. Ed. **21** 819(1983).

4. Michael J. S. Dewar, J. Am. Chem. Soc. **106**, 669(1984).

5. P. P. Ho, N. L. Yang, T. Jimbo, Q. Z. Wang and R. R. Alfano, J. Opt. Soc. Am. B **34**, 1025(1987).

6. G. M. Carter, M. K. Thakur, Y. J. Chen and J. V. Hryniewicz, Appl. Phys. Lett. **47**, 457(1985).

7. H. J. Eichler, G. Salje and H. Stahl, J. Appl. Phys. **44**, 5383(1973).

8. P. W. Smith, A. Ashkin and W. J. Tomlinson, Opt. Lett. **6**, 284(1981).

9. P. M. Cotts, R. D. Miller, P. T. Trefonas III, R. West and G. N. Ficks, Macromolecules, **20**, 1046(1987).

Chapter IX

Sign of $\chi^{(3)}$ in Polysilane Polymers

9.1 Introduction

In previous measurements[1-7], the value of the third order optical nonlinear coefficient $\chi^{(3)}$ was determined to vary between 10^{-12} - 10^{-10} esu, depending on the wavelengths and mechanisms. The time response of $\chi^{(3)}$ at 532 nm was determined to be < 3ps in our previous optical Kerr gate and degenerate four wave mixing(DFWM) measurements in phenylmethyl polysilanes[3]. However, the sign of $\chi^{(3)}$ has not yet been reported. The sign is an important parameter for many nonlinear optical applications, such as self-focusing. In this chapter, we report on the determination of the sign of $\chi^{(3)}$ in phenylmethyl polysilane using the single beam Z-scan technique[8,9] with picosecond pulses at both 532 nm and1064 nm.

9.2 Experimental Techniques

The molecular structure and linear absorption spectrum of poly(phenylmethyl)silane was reported in chapter VIII, Fig.8.2.1. Poly(phenylmethyl)silane is transparent from 360 nm to the infrared. The sample used here was a solution in the solvent tetrahydrofuran (THF) .

In the Z-scan approach[8,9], as shown in Chapter II, a single Gaussian beam is tightly focused into a thin nonlinear medium. The

transmittance through a small aperture in the far field is measured. A negative lens effect arising from nonlinear materials having negative n_2 will result in a peak followed by a valley in the transmittance curve, while positive n_2 will give a curve with a valley-peak sequence as the sample is translated from -z side to +z side. Thus, the sign of the nonlinearity can be readily determined. Moreover, the size of n_2 can be determined from the difference in peak and valley in transmittance. A mode-locked Quantel YAG laser with a frequency doubler provided the laser pulses with 30ps duration at 532 and 1064 nm at a 10Hz repetition rate. In the experiment, the laser beam was tightly focused to a spot size ω_0 of 20mm. The polysilane solution was contained in a 1mm cuvette. A 1mm diameter aperture was placed at a distance of more than 1.5 m away from the focus point. The light transmission through the aperture was detected, recorded, and analyzed by a photomultiplier (PMT) and a boxcar averager interfaced with a microcomputer. Each point was an average over 30 shots. Narrow Band Filters (either NB532 or NB1064) were used in front of the PMT. Z-scans from a 1mm cell containing CS_2 or THF solvents were also measured and used for standards and references.

9.3 Results and Discussion

The transmittances through the aperture as a function of sample position z from the Z-scan measurements of a polysilane solution with a concentration of 0.5M and CS_2 at 532 nm are shown in Fig. 9.3.1(a) and (b), respectively. The excitation energy is 0.9 μJ.

There is no detectable signal from the solvent (THF) at this excitation energy.

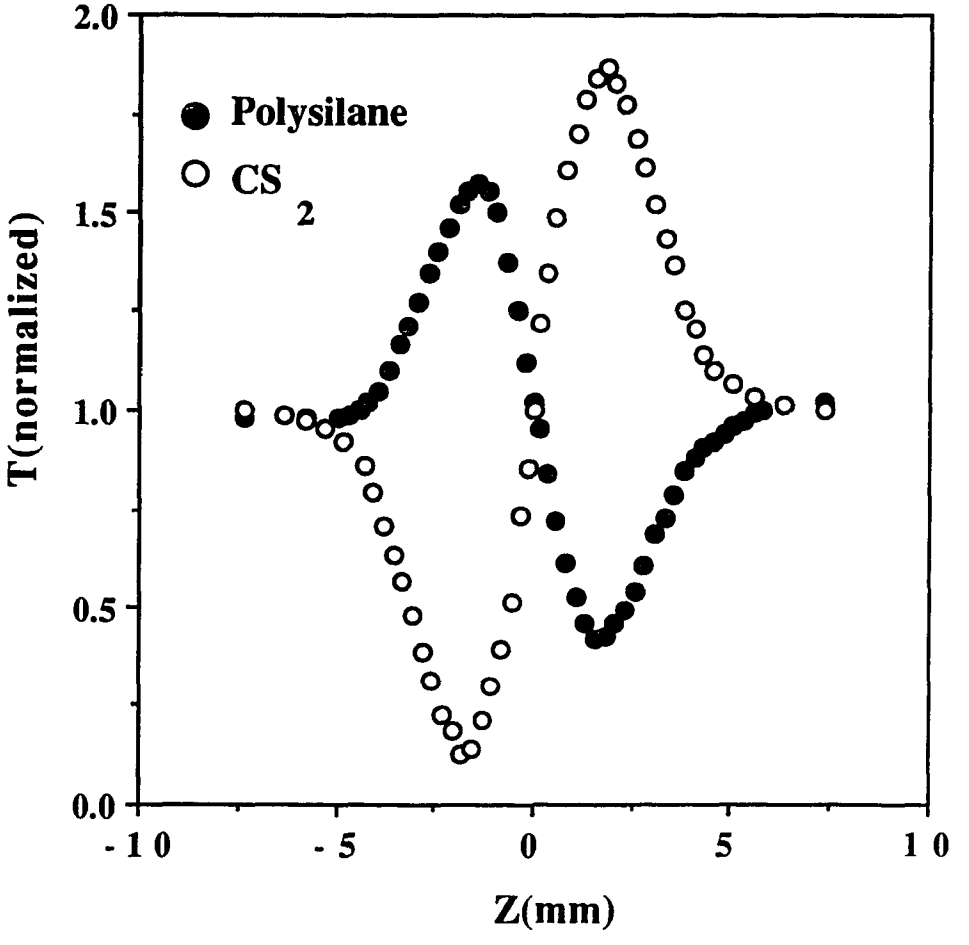

Fig. 9.3.1 (a)Normalized transmittance of the Z- scan measurements from a 1 mm polysilane solution with 0.5M concentration, the excitation is at λ=532 nm, with 0.9μJ. (b)Normalized transmittance from a 1mm CS_2 at the same excitation energy as in (a).

The symmetric peak-valley configuration as the sample is moved from -z to +z in Fig.9.3.1 (a) indicates polysilane has a negative nonlinearity ($n_2 < 0$) at 532 nm. Care must be taken to avoid any cumulative thermal induced contributions which normally result in a negative sign. To reduce thermal effect, a mechanical shutter was used to select single shots, and the time between shots was at least 1 minute.

A different Z-scan profile was observed when the excitation wavelength was changed from 532 nm to 1064 nm. The transmittance through the aperture from polysilane solution at 1064 nm is shown in Fig. 9.3.2. The energy for this measurement is 20μJ.

The reversed symmetric valley - peak configuration clearly shows that n_2 of polysilane at 1064 nm is positive. When the energy is increased from 20 μJ to 2mJ, the signal remains positive. A positive $n_2 = 1.2 \times 10^{-11}$ esu value is obtained for CS_2 at both 532 nm and 1064 nm wavelengths.[9] The signal from the solvent (THF) alone at 1064 nm with 20mJ excitation energy is also positive and the signal is about 80% of that from the polysilane solution. The signal from the pure solvent was then subtracted from the signal of the polysilane solution in THF. Within a 0.5% accuracy, for phase distortions $|\Delta\Phi| = |k\Delta n L_{eff}| \leq \pi$, the relationship of the difference between the normalized peak and valley transmittance ΔT_{p-v} and n_2 is given by[9]:

$$\Delta T_{p-v} \approx A\,|\Delta\Phi_0| \approx A\,\left|\frac{\pi n_2}{\lambda}\right| |E|^2 L_{eff}|, \qquad (9.3.1)$$

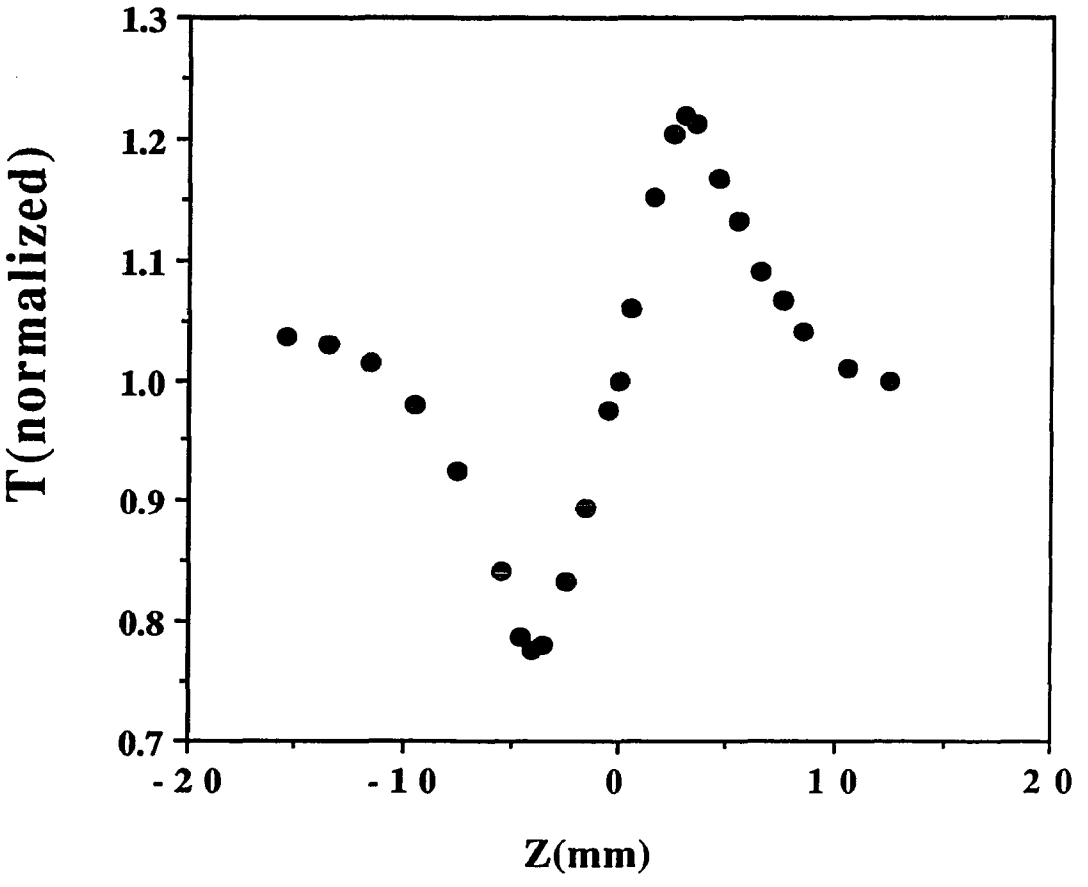

Fig.9.3.2 Normalized transmittance of the Z- scan measurements from a 1 mm polysilane solution with 0.5M concentration, the excitation is at λ=1064 nm, with 20μJ.

where L_{eff} is the effective sample length, and A is a constant which may depend on the aperture size. Thus, when CS_2 is used as a reference with the assumption that CS_2 and polysilane have the same L_{eff} values (which is reasonable since both CS_2 and polysilane are transparent in the wavelengths considered), the value of $\chi^{(3)}_{ps}$ is obtained from:

$$\chi^{(3)}_{ps} = \chi^{(3)}_{CS2} \frac{(\Delta T_{p-v}\, n_0)_{ps}}{(\Delta T_{p-v}\, n_0)_{CS2}}. \qquad (9.3.2)$$

When the data from Figures 9.3.1 and 9.3.2 are used, an extrapolation to the solid film yields $\chi^{(3)}_{532nm}$ = -7.0 X 10^{-12} esu, while $\chi^{(3)}_{1064nm}$ < +5.0 X 10^{-13} esu. After subtraction of the solvent contribution only an upper limit value for $\chi^{(3)}_{1064nm}$ could be obtained. The values of the linear indexes of refraction for CS_2 and THF were n_{0CS_2}=1.627, and n_{0PM}=n_{0THF}=1.407, respectively. The density of the polysilane sample d (d= 1.06 g/cm$^{3)}$ was obtained from our measurements using the *Specific Gravity Bottle* method.

From the measurements, $\chi^{(3)}_{532nm}$ is larger, -7.0 X10^{-12}esu and negative, while $\chi^{(3)}_{1064nm}$ is relatively small, +5.0 X 10^{-13} esu and positive. These values are comparable to those obtained in our previous DFWM measurements[3]. The Z- scan value at 532 nm is somewhat larger than the DFWM value ($\chi^{(3)}$ =1.2 x 10^{-12} esu) reflecting probably a larger TPA contribution. These values suggest that $\chi^{(3)}_{532nm}$ is enhanced by a resonance process although both 532 nm and 1064 nm are in the transparent region of single photon absorption spectrum.

Closer examination of the absorption spectrum shows that there are two main transitions peaking around 3.7eV and 4.6 eV in the linear absorption spectrum of poly(phenylmethyl)silane. They have been previously assigned[10] to σ - σ^* and π - π^* transitions, respectively. Recent measurements[11] of the quantum efficiency for carrier generation as a function of photon energy and of the electroabsorption spectrum in poly(phenylmethyl)silane have suggested that the band gap is at 4.6eV while 3.7eV is the peak of an exciton band. Furthermore, measurements[12] of fluorescent intensity as a function of incident light intensity at 532 nm in poly(phenylmethylsilane) films suggested that two photon transitions create excitons rather than free carriers. Strong two photon absorption at 532 nm has been observed previously in other polysilanes in birefringence measurements[5,6,7].

The two photon absorption process in the sample was further investigated by measuring the transmittance without the far field aperture. In this case, the transmittance is only a function of the nonlinear absorption. The normalized transmittance without an aperture is[13]:

$$T(z) = \frac{1}{1 + \frac{\beta I_0 L_{eff}}{1+z^2/z_0^2}}, \qquad (9.3.3)$$

where I_0 is the incident laser intensity at the focus point and β is the two photon absorption coefficient. The open aperture transmittance with I_0=74GW/cm^2 at 532 nm from a 1mm cell polysilane solution is shown in Fig. 9.3. 3 . The transmittance from the pure solvent (THF) does not show any TPA behavior.

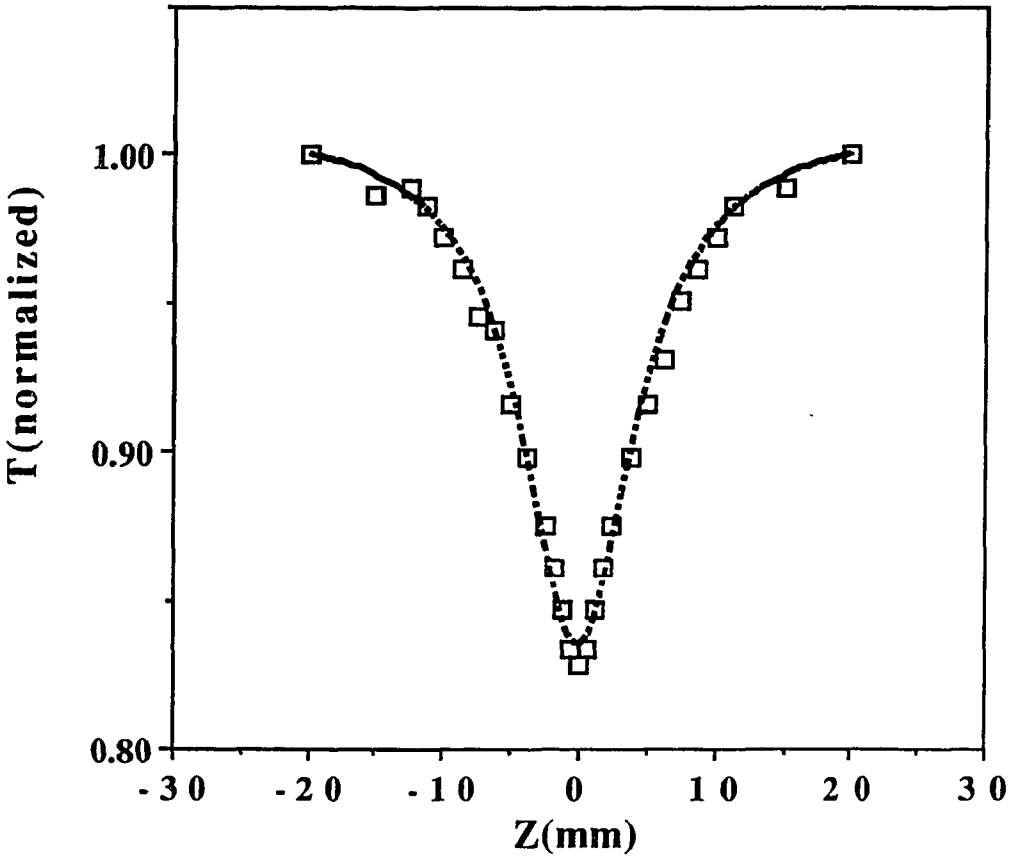

Fig.9.3.3 Normalized transmittance for polysilane with no aperture at 532 nm with I_0=74GW/cm^2.

The solid line is the theoretical results with β = 0.027cm/GW.

The solid line in Fig. 9.3.3 is the theoretical results using equation (9.3.3) with β=0.027cm/GW. An extrapolation to the solid film gives a TPA absorption coefficient β=0.468cm/GW for polysilane. This value is in good agreement with the values, <0.5cm/GW and

0.3cm/GW obtained from birefringence measurements[7] and from TPA fluorescence intensity measurements[12], respectively.

The TPA coefficient β is related to the imaginary part of $\chi^{(3)}$ by[13,14]:

$$\text{Im } \chi^{(3)} = \frac{n_0^2 c^2}{8\pi^2 \omega} \beta \quad . \tag{9.3.4}$$

The calculation gives Im $\chi^{(3)}$ = 7.4 X 10 $^{-13}$ esu. This value is about one order of magnitude smaller than the value of $\chi^{(3)}$ measured from the Z-scan experiment. The Z-scan value was obtained at relatively low pump beam intensity. These results suggest that the Z-scan value corresponds to the real part of $\chi^{(3)}$ with a negligible contribution from the imaginary part.

In general, $\chi^{(3)}$ can be written as the sum of a resonant part $\chi^{(3)}_R$ and a nonresonant part $\chi^{(3)}_{NR}$.[13,15,16] In a 4 - level approximation, with $\omega_1=\omega_2=\omega$ and $\omega_3=-\omega$, $\chi^{(3)}_R$ can be expressed as[17]:

$$\chi^{(3)}_R = \frac{e^4 N}{h^3} \sum_{gifj} \frac{\rho_{(g)} \Omega_{gi} \Omega_{if} \Omega_{fj} \Omega_{jg}}{(E_{ig} - \omega)(E_{fg} - \omega - \omega - i\Gamma)(E_{jg} - \omega)}$$

$$\propto \sum_{gifj} \frac{1}{(E_{ig} - \omega)(E_{fg} - \omega - \omega - i\Gamma)(E_{jg} - \omega)} \quad , \tag{9.3.5}$$

where $\rho_{(g)}$ is the density of the ground state g, i, f, j are the excited states, E_{ij} are the energy difference between states j and i (in h units), Ω_{ij} are the transition matrix elements, Γ is the band width of the excited state f, and ω is the photon energy (in h units). States i, j have the same parity as the ground state g, whereas f has the opposite parity. The exciton model[11,12] is adopted in the calculation. Parameters are chosen as follows: $E_{ig}=E_{jg}$=4.6eV, E_{fg}=3.7eV, and Γ = 100meV.

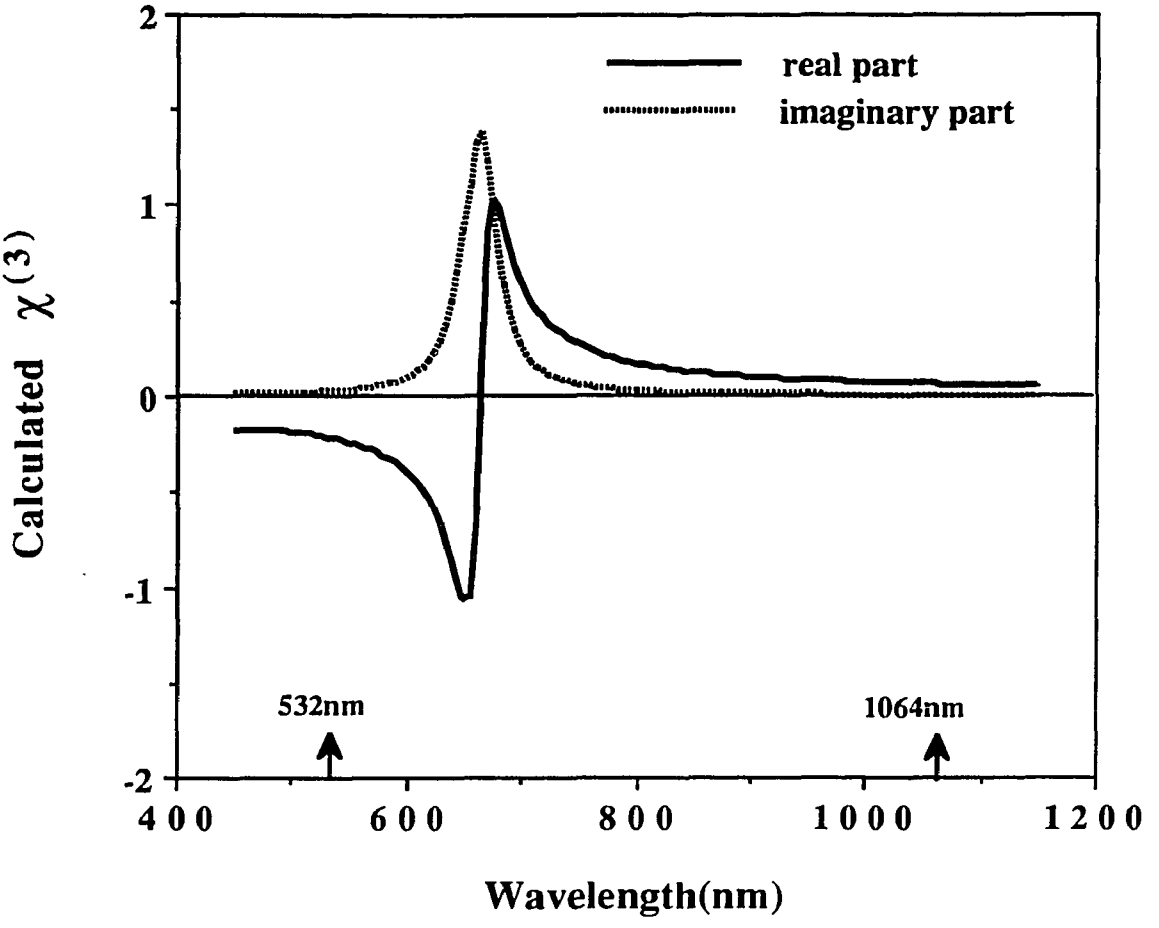

Fig. 9.3.4 Calculated real, and imaginary part of two photon absorption resonant $\chi^{(3)}$ $(-\omega,\omega,-\omega,\omega)$ as a function of the excitation photon frequency. The parameters are: $E_{ig}=E_{jg}=4.6eV$, $E_{fg}=3.7eV$ and $\Gamma = 100meV$.

The calculated relative values of both real and imaginary part of TPA resonant $\chi^{(3)}_R(-\omega; \omega,-\omega, \omega)$ from Eq.(9.3.5) are shown in Fig. 9.3.4 as a function of the incident photon frequency. The results in Fig. 9.3.4 show that the real part of $\chi^{(3)}$ at 532 nm is negative and is about an order of magnitude larger than the imaginary part. This calculation is in good agreement with our experimental observations. Most importantly, the model displayed in Fig.9.3.4 for $\chi^{(3)}$ predicts the change in the sign of $Re(\chi^{(3)})$ as the denominator $(E_{fg}-2\omega)$ changes sign. This model also predicts an enhancement of $\chi^{(3)}$ with about five times at 630nm relative to the value at 532nm.

The sign and magnitude at 1064 nm is positive and small as shown in Fig.9.3.4. The 1064 nm wavelength is away from any single or two photon resonance frequency. Therefore a smaller, faster and positive $\chi^{(3)}$ due to bound-electronic effects should be expected.

9.4 Conclusion

In conclusion, our Z-scan measurements have shown that $\chi^{(3)}$ reverses sign from negative to positive when the excitation wavelengths is changed from 532 nm to 1064 nm. The difference in sign arises from the difference in the physical processes responsible for the nonlinear response at the two wavelengths. The bond-electronical process is responsible for the small positive nonlinearity at 1064 nm, while the larger negative $\chi^{(3)}$ at 532nm is mostly due to TPA resonance. Furthermore, the imaginary part of TPA resonant $\chi^{(3)}$ at 532 nm has been found to be one order of magnitude smaller than the real part.

References

1. F. Kazjar, J. Messier, and C. Rossilio, J. Appl. Phys. **60**, 3040(1986).

2. J. C. Baumert, G. C. Bjorklund, D. H. Jundt, M. C. Jurich, H. Looser, R. D. Miller, J. Rabolt, R. Sooriyakumaran, J. D. Swalen, and R. J. Twieg, Appl. Phys. Lett. **53**, 1147(1988).

3. L. Yang, Q. Z. Wang, P. P. Ho, R. Dorsinville, R. R. Alfano, W. K. Zou, and N. L. Yang, Appl. Phys. Lett. **53**, 1245(1988).

4. D. J. McGraw, A. E. Siegman. G. M. Wallraff, and R. D. Miller, Appl. Phys. Lett. **54**, 1713(1989).

5. F. M. Schellenberg, B. L. Byer, R. D. Miller, and R. Sooriyakumaran, *XVI International Conference on Quantum Electronics Technical Digest*, (Japan Society of Applied Physics, Tokyo, Japan, 1988),pp. 702-703.

6. F. M. Schellenberg, B. L. Byer, and R. D. Miller, Opt. Lett. **15**, 242(1990).

7. F. M. Schellenberg, R. L. Byer, and R. D. Miller, Chem. Phys. Lett. **166**, 331(1990).

8. M. Sheik-bahae, A. A. Said, and E. W. Van Stryland, Opt. Lett. **14**, 955(1990).

9. M. Sheik-bahae, A. A. Said, and E. W. Van Stryland, IEEE J. Quan. Elec. **26**, 760(1990).

10. K. Takeda, H. Teramae and N. Matsumoto, J. Am. Chem. Soc. **108**, 8186(1986).

11. R. G. Kepler, and J. M. Zeigler, Mat. Res. Soc. Symp. Proc. Vol. 173, 453(1990).

12. R. G. Kepler, J. Zeigler, in Advances in Chemistry Series No. 224, *Silicon Based Polymer Science: A Comprehensive Resource* Ed. by J. M. Zeigler and F. W. Gordon. In this paper, the two photon absorption rate constant at 532nm $\kappa = 10^{-26} s/cm^3$ is obtained. When κ is converted to the cm/GW unit , it is equivalent to the two photon absorption coefficient β. This conversion gives 0.3cm/GW.

13.Y.R.Shen, *The Principles of Nonlinear Optics*(wiley, New York, 1984).

14.B. S. Wherrett, J. Opt. Soc. Am. B 1, 67(1984).

15. N. Bloembergen, *Nonlinear Optics* (Benjamin, New York, 1965)

16. C. Flyzanis, in *Quantum Electronics* Ed. by H. Rabin, C. T. Tang, Volume I, Part II (Academic Press Inc., New York, 1975).

17. H. Mahr, in *Quantum Electronics* Ed. by H. Rabin, C. T. Tang, Volume I, Part II (Academic Press Inc., New York, 1975)

Chapter X

Near Infrared Optical Nonlinear Response in Polysilane Polymers

10.1.Introduction

The third order nonlinear susceptibility $\chi^{(3)}$ in phenylmethyl polysilane was first measured by Kazjar *et al* using the third harmonic generation(THG) technique at two wavelengths(1064 and 1907nm)[1], new information has been obtained by number of other groups. Similar THG measurements by Baumert *et al* found that the value of $\chi^{(3)}$ vary substantially with thermally induced reversible changes in planar zigzag poly(di-n-hexylsilane) polymers[2]. The time response of $\chi^{(3)}$ at 532nm was determined to be < 3ps in our previous optical Kerr gate and degenerate four wave mixing(DFWM) measurements in phenylmethyl polysilanes[3]. McGraw *et al* performed a phase conjugation experiment using polarization discrimination method to resolve the nuclear and electronic contributions to $\chi^{(3)}$ at 532nm in octylmethylpolysilane[4]. Recently, Schellenberg *et al* [5,6,7] observed a strong two photon absorption in poly(di-n-hexylsilane) when the material is excited around 550-600nm and studied nonlinear effect induced by this nonlinear absorption. Most recently, the signs of $\chi^{(3)}$ in phenylmethyl polysilane has been determined to be negative at 532 nm and positive at 1064 nm respectively, by the single beam Z-scan

technique with picosecond pulses[8]. Various measurements have reached a good agreement about the magnitude of $\chi^{(3)}$, 10^{-12} - 10^{-10} esu in various polysilanes arising from two and three photon resonant transitions have been obtained. However, studies up to date have only concentrated on the enhanced nonlinearities around two or three photon resonant frequencies. And there was a discrepancy in the reported values of $\chi^{(3)}$ at 1907 nm in phenylmethyl polysilanes from THG measurements. In Ref. 2, $\chi^{(3)}$ as large as 10^{-12} esu has been obtained in 120 and 1200 nm films, while in Ref. 1, no signal was detectable from 150 nm films. In our signal beam Z - scan measurements at 1064 nm, only an upper limit of 5 X 10^{-13}esu has been obtained[8]. For optical device application, it is important to have a material with large n_2/α to minimize the optical energy dissipated by linear and nonlinear absorption. Often, only the nonlinearity off any resonance is of interest. In this chapter, we report on the study of the near infrared third order optical nonlinearity using degenerate four wave mixing(DFWM) with picosecond pulse at 1064 nm of various polysilanes having different sidegroups in solutions and films

.

Poly(phenylmethylsilane), poly(phenylmethyl-co-dimethyl-sialne) or co-polymer, poly(cyclohexylmethyl-silane) and poly(n-dodecylmethylsilane) have been chosen to be studied in this work. They can be divided into two classes: the first two polysilanes have sidegroups with π-electrons(aryl substituents), with the increasing intensity in the unit of copolymers. The last two only have σ-electrons.

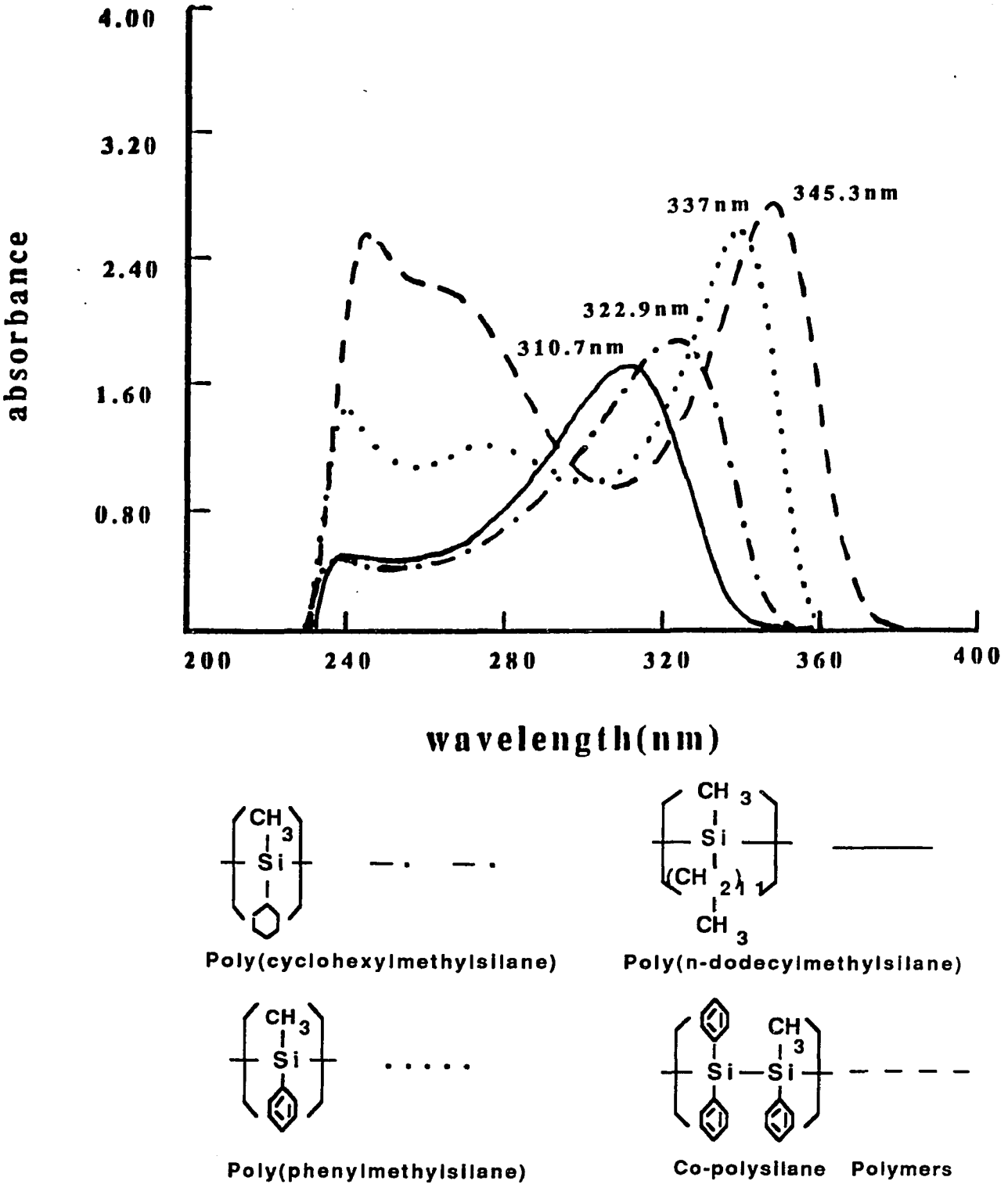

Fig.10.1.1 Single photon absorption spectra and molecular structures of polysilane solutions. The concentrations are 1.85 X 10^{-4}M.

Those polymers were synthesized by the method described in Ref. 9. The film casting was prepared on a large crystallization dish with controlled vapor pressure of organic solvent, tetrahydrofuran(THF). The film thicknesses were around 1μ. The linear absorption spectra from solutions with the same concentration of 1.85 X 10^{-4}M, along with their molecular structures are shown in Fig. 10.1.1. The maximum absorption wavelength is also indicated in Fig. 10.1.1. The solutions were contained in 1mm cells. Common to all polysilanes is that σ - σ* absorption edge is typically in the ultraviolet, thus those polymers are transparent from the visible to the infrared. The sidegroup affects the linear absorption peak in the UV region.

10.2 Results and Discussion

The laser source for this work was a mode-locked Quantel YAG laser provided the laser pulses with 25ps duration at 1064nm at a 10Hz repetition rate. The forward folded boxcar FWM geometry is used(which has been introduced in Chapter II). The signal was detected, recorded, and analyzed by a photomultiplier (PMT) and a boxcar averager interfaced with a microcomputer. Measurements from a 1mm cell containing CS_2 or THF solvents were also performed and used for standards and references.

The magnitude of $\chi^{(3)}$ was obtained by using the following equation when CS_2 is used as the reference(under same excitation condition)[3]:

$$\chi^{(3)}_S = \chi^{(3)}_{cs_2} \frac{n_{0s}^2 L_{effcs_2}}{n_{0cs_2}^2 L_{effs}} \left(\frac{I_s}{I_{cs_2}}\right)^{1/2} \quad , \qquad (10.2.1)$$

where S represents the sample, n_0 is the linear index of refraction, L_{eff} is the effective sample length, I is the signal intensity of the fourth beam, signal beam.

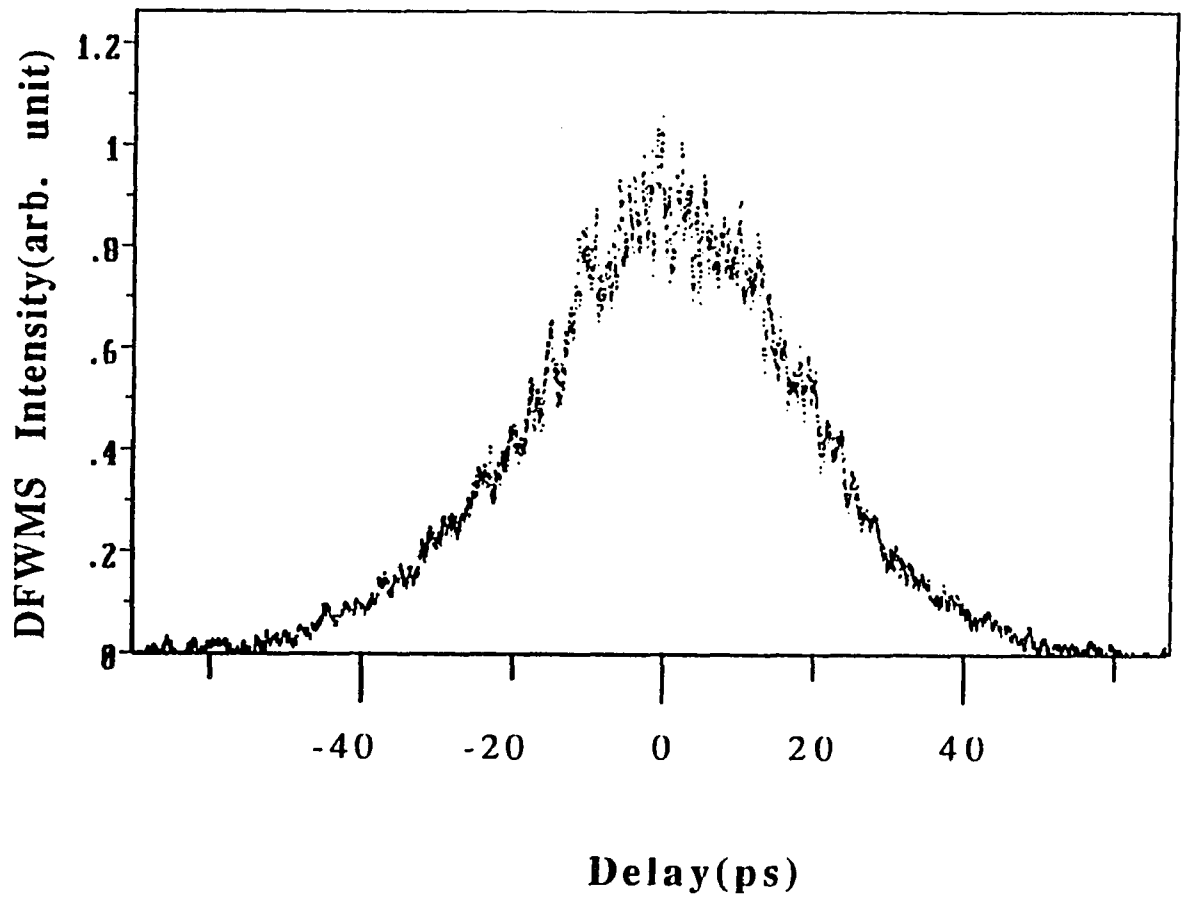

Fig. 10.2.1 DFWM signal intensity from poly(methylphenyl)silane solution as a function of the delay time between pump and probe beams. The excitation wavelength is at 1064 nm. The concentration is 0.5M.

Fig. 10.2.1 displays the DFWM signal intensity at 1064nm from phenylmethyl polysilane solution with 0.5M concentration as a function of the delay time between the pump and probe beams. The signal profile contains only a fast component, which is unresolved, limited by the laser pulse duration(<25ps). DFWM signal profiles from all four polysilane polymers have the same features.

The signals from the pure solvent THF were very close to the signals from the polysilane solutions in all experiments. This made it difficult to extrapolate the value of $\chi^{(3)}$ to the solid films. $\chi^{(3)}$ could be over estimated. After subtraction, only an upper limit could be obtained. In the calculation, a positive picosecond response $\chi^{(3)}_{CS_2} = 8.0 \times 10^{-13}$ esu[10] was chosen. The densities of polysilanes were obtained from our measurements using the *Specific Gravity Bottle* method. For poly(phenylmethyl)silane, copolymer, poly(cyclohexylmethyl)silane and poly(n-dodecylmethyl)silane, densities are 1.06 g/cm^3, 1.098 g/cm^3, 1.03 g/cm^3 and 0.84 g/cm^3 respectively. During the calculations, the following parameters: n_{0CS2}=1.627, and $n_{0PM} = n_{0THF}$ =1.407 have also been used.

The calculations of $\chi^{(3)}$ for poly(phenylmetyl)silane solution from Eq. (10.2.1) yielded <1.33 X 10 $^{-13}$esu.

$\chi^{(3)}$ ratios of other solutions relative to the poly(phenylmethyl)silane solution with same concentrations have been listed in Table 10.2.1.

Table 10.2.1 The ratio of $\chi^{(3)}$ relative to poly(phenylmethyl)silane

technique / solution(0.5M)	DFWM
Phenylmethyl	1.000 ± 0.1
cyclohexylmethyl	1.010 ± 0.1
dodecylmethyl	0.850 ± 0.1
Copolymer	1.029 ± 0.1
Films	not detectable

We also intended to measure $\chi^{(3)}_{1064nm}$ from thin films. There was no detectable signal in both measurements even when the intensity reached such high values(200GW/cm^2), that the films were damaged.

From our DFWM measurements, only a relatively small($\sim 10^{-13}$ esu) nonlinearity has been detected at 1064 nm from polysilane solutions, as shown in Table 10. 2. 1. A fast response of the signal, < 25ps has also been deduced in the DFWM measurements for all the polymers. However, there is a slight difference of the measured values for various polymers. Co-polymer has relatively larger value than the others. This difference might be a hint of a resonant process for copolymer. Although 1064 nm is away from single, or two photon resonant frequencies, there is a possibility of multiphoton absorption. Since the single photon absorption is peaking around 3.55eV(Co-polymer) to 3.99eV(poly-n-dodecylmethyl-silane), for the indirect transition with 1064 nm(1.165eV) one requires at least a three photon absorption process. Three photon absorption at

1064nm(1.165eV) is near the single photon absorption peak for co-polymer, but is at the absorption edge for poly(methylphenyl)silane, and is totally off the absorption band for the other polymers(see Fig.10.1.1). Thus, the nonlinearity at 1064nm for co-polymer may be in resonant with the three photon absorption process. Since the DFWM technique measures the nonlinearity at ω, the output signal dose not contain three photon resonance part at 3ω. The output signal dose include a resonant part from a six-photon process corresponding to the three photon absorption, the schematic diagram of this DFWM process is shown in Fig. 10.2.2, where a simple two level system is assumed. Under such an assumption, the nonlinearity that may also be involved for DFWM interaction is of the 5th order, that is χ^5. Such a fifth order polarization density will include all the combinations of the pump fields that satisfy both the phase matching and energy conservation. The total output signal would be a combination of both χ^3 and χ^5. The output DFWM signal for co-polymer is thus enhanced, and this may be the reason for the larger measured value of χ^3 for co-polymer. The details of this fifth order nonlinearity need further investigations.

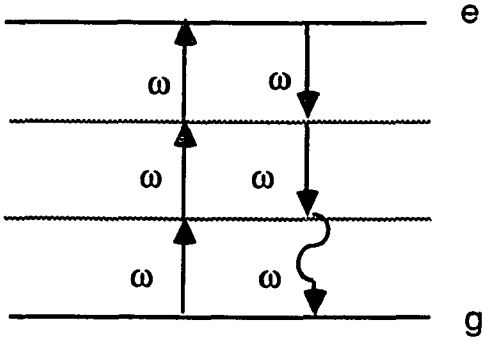

Fig.10.2.2 Schematic diagra showing a DFWM interaction with six-photon process.

Aother possible explanation for the difference in the measured values is also considered. Theoretical estimations and experimental investigations have firmly established that larger electron delocalization is a prerequisite for larger values of the nonlinear coefficients. The value of $\chi^{(3)}$ is proportional to the sixth power of the conjugation length for one dimensional systems, such as polysilanes. For polysilane polymers in solution or atactic materials in the solid state at ambient temperatures, previous electronic spectra studies[11] show that polysilane derivatives containing only alkyl substituents on the backbone absorb in the region from 300 - 325 nm with the larger substituents causing shifts to longer wavelengths. Those polymers with aryl substituents directly bonded to the backbone are spectrally red shifted to 335 - 350 nm. With the same sidegroups, the chain length increases as the absorption peaks shift to longer wavelength. However, recent studies[12] have indicated that the limiting spectral structures observed previously for simple atactic polysilanes both in solutions and in the solid state do not represent the intrinsic absorption of the polysilane chain, but instead result from the presence of conformational imperfections(deviations from coplanarity) in the backbone. Therefore, not much can be said about the differences in the chain lengths or conjugation lengths of the polysilanes been chosen here. Since the values of $\chi^{(3)}_{1064nm}$ for different substituents are very close to each other , the nonlinear response is probably due to the intrinsic nonlinearity of the polysilane polymers, and most likely arises from the contributions of the σ - electrons delocalized along the backbone.

Finally, polarization discrimination measurements were performed for polysilane solutions in DFWM measurements. Rotators and analyzers have been used in three incident beam paths. An analyzer was used in the front of the PMT to select different components of the signal beam. For $\chi^{(3)}_{ijkl}$, the indices i stands for the polarization direction for the signal beam($\mathbf{K}_4$), j, k stand for the pump beams($\mathbf{K}_1$, $\mathbf{K}_3$) and l stands for the probe beam($\mathbf{K}_2$). The following values were obtained:

$$\frac{\chi^{(3)}_{xyxy}}{\chi^{(3)}_{xxxx}}=0.39; \qquad \frac{\chi^{(3)}_{xxyy}}{\chi^{(3)}_{xxxx}}=0.33; \qquad \frac{\chi^{(3)}_{xyyx}}{\chi^{(3)}_{xxxx}}=0.37.$$

The ratios from other polysilanes are very close to the values from poly(phenylmethylsilane). The polarization discrimination results indicated that the response at 1064 nm is most likely electronic .

10.3 Conclusion

In conclusion, the near infrared(1064 nm) third order optical nonlinearity of polysilane polymers has been studied using the DFWM technique. Results have shown that $\chi^{(3)}_{1064nm}$ is, ~10^{-13}esu, and fast(<25ps). This value is about one order of magnitude smaller than that of CS_2. Thus polysilane solutions and thin films will not be so useful for applications. On the other hand, this value is about two order of magnitude larger than silicon glass fibers[12], thus it is possible to use polysilane polymers as a fiber nonlinear material.

Reference

1. F. Kazjar, J. Messier, and C. Rossilio, J. Appl. Phys. **60**, 3040(1986).

2. J. C. Baumert, G. C. Bjorklund, D. H. Jundt, M. C. Jurich, H. Looser, R. D. Miller, J. Rabolt, R. Sooriyakumaran, J. D. Swalen, and R. J. Twieg, Appl. Phys. Lett. **53**, 1147(1988).

3. L. Yang, Q. Z. Wang, P. P. Ho, R. Dorsinville, R. R. Alfano, W. K. Zou, and N. L. Yang, Appl. Phys. Lett. **53**, 1245(1988).

4. D. J. McGraw, A. E. Siegman. G. M. Wallraff, and R. D. Miller, Appl. Phys. Lett. **54**, 1713(1989).

5. F. M. Schellenberg, B. L. Byer, R. D. Miller, and R. Sooriyakumaran, *XVI International Conference on Quantum Electronics Technical Digest,* (Japan Society of Applied Physics, Tokyo, Japan, 1988),pp. 702-703.

6. F. M. Schellenberg, B. L. Byer, and R. D. Miller, Opt. Lett. **15**, 242(1990).

7. F. M. Schellenberg, R. L. Byer, and R. D. Miller, Chem. Phys. Lett. **166**, 331(1990).

8. Lina Yang, R. Dorsinville, R. R. Alfano, W. K. Zou and N. L. Yang, submitted to "Opt. Lett.".

9. Trefonas III, P. T., R. West, R. D. Miller, D. Hofer, J. Polym. Sci., Polym. Lett. Ed. **21**, 819(1983).

10. S. L. Shapiro, H. P. Broida, Phys. Rev., **154**, 129 (1967).

11.Trefonas III, P. T.; R. West, R. D. Miller, D. Hofer, J. Polym. Sci., Polym. Lett. Ed. **21**, 823(1983).

12. n_2=1.2 X 10^{-22} $(m/V)^2$ for SiO_2, R. Y. Chiao, E. Garmire and C. H. Townes, Phys. Rev. Lett. **13** , 479(1964).

Chapter XI
Summary

In this chapter, the major conclusions of this research work on both σ- and π- electronic systems have been summarized.

11.1 Summary

In summary, this thesis work is devoted to the basic understanding and characterization of the third order optical nonlinear properties of several polymers as they are the best candidates for the future optical device applications. Two distinct polymer systems have been studied.

The size, sign and the response time of the third order nonlinear susceptibility $\chi^{(3)}$ which have been measured in this thesis work, are summarized in Table 11.1.

In polythiophene, for the first time, interband π - π^* transition enhanced $\chi^{(3)}$ has been measured to be large, 10^{-9} esu; fast, <15ps; and real part of negative both at 532 and 1064 nm. The results are comparable to the best candidate in polymers, PDA-PTS, single crystals. Most importantly, $\chi^{(3)}$ has been measured directly inside the photoinduced polaronic bands in the materials, the results indicate that in those π-electron systems, $\chi^{(3)}$ can be enhanced either by electronic transitions or by photon induced real and virtual midgap states transitions.

Table 11.1 The third order nonlinear coefficient $\chi^{(3)}$

Polymer	size (10^{-9}esu) $\lvert\chi^{(3)}\rvert$	$\chi^{(3)}_{real}$	$\chi^{(3)}_{imag.}$	response (10^{-12}s)	λ(nm)	comments
PA	0.9			<20	532	SPT
PT	6.6± 1	-4.5		<20	532	SPT
	5.0± 1			<15	585	SPT
	3.0± 1			<15	590	SPT
	3.8± 1			<15	595	SPT
	3.2± 1			<15	600	SPT
	3.0± 1			<15	605	SPT
	0.7± 0.5			<15	630	SPT
	1.63± 1			<15	640	SPT
	1.49± 1			<15	650	SPT
	1.47± 1			<15	660	SPT
	0.03± 0.02			<20	1064	nonresonant
		-0.797			1064	TPA
PTT	5.9± 1	-2.24		<20	532	SPT
	4.4± 1			<15	585	SPT
	3.0± 1			<15	590	SPT
	3.6± 1			<15	595	SPT
	2.9± 1			<15	600	SPT
	3.0± 1			<15	605	SPT
	0.7± 0.5			<15	630	SPT
	0.03± 0.02			<20	1064	nonresonant
		-0.663			1064	TPA

PDTT	11.3± 2	-4.60		<20	532	SPT
	7.7± 1			<15	585	SPT
	5.8± 1			<15	590	SPT
	6.1± 1			<15	595	SPT
	4.5± 1			<15	600	SPT
	5.5± 1			<15	605	SPT
	1.3± 0.5			<15	630	SPT
	0.03± 0.02			<20	1064	nonresonant
		-0.9			1064	TPA
PS1	0.0016±0.0002			<20	532	TPA
	0.00133			<20	1064	**
		-0.007	0.00074		532	TPA
		+0.0005			1064	nonresonant
	0.002±0.0006			<3		OKG*
PS2	0.0013433			<20	1064	**
PS3	0.0011305			<20	1064	**
PS4	0.0013686			<20	1064	**

SPA-------for resonant with single photon transition(absorption)

TPA-------for resonant with two photon transition

PA---------Soluble Polyacetylane

PS---------polysilane polymers

PS1--------poly(methyphenyl)silane

PS2--------poly(cyclohexylmethyl)silane

PS3--------poly(dodecylmethyl)silane

PS4--------co-polymer

* In this OKG, 1064 nm was used as the pump, 532 nm was the probe;

**The possible mechanisms are: three photon process and the intrinsic nonlinearity entirely due to the bound - electronic effects.

$|\chi^{(3)}|$--------measured from DFWM

$\chi^{(3)}_{real}$ -----measured from Z - scan

$\chi^{(3)}_{imag.}$----measured from the single beam transmission

As a class of transparent materials, σ-conjugated polysilane polymers have shown to posses moderated $\chi^{(3)}(10^{-12}esu)$, the upper limit of the time response have been determined to be <3ps. The sign of $\chi^{(3)}$ has been determined to be negative at 532nm and positive at 1064nm. Results implies that two photon absorption plays an important role in the nonlinear optical response in the visible.

Besides the work listed above, there are two more important measurements done in well characterized π - electron systems. First, our studies in soluble polyacetylene have indicated that changes in morphology and chain order do not play a significant role in the nonlinear response. Second, experimental results in polydiacetylene, 4BCMU, have shown that the transient reversible light induced structure change in the material causes the dependence of nonlinearity response time on excitation intensity.

From our studies on both polythiophene and polysilane polymers, the conclusion can be drawn as that both of them are promising candidates in the future optical device applications.

Chapter XII
Future Work

Three experiments are listed below for both π- and σ-conjugated systems.

12.1 Time Resolved Photoinduced Absorption in Polythiophene Films

The intense study on Trans-$(CH)_x$ has led to a more complete understanding of the ground state and elementary excitations of conjugated polymer with degenerate ground state. Spinless charged solitons are found to be the dominant charge carriers. Measurements[2] of the dynamics of the photoinduced 0.45eV midgap absorption associated with photogenerated charged solitons in Trans-$(CH)_x$ confirmed that there are two types of solitons. First, there are directly photogenerated Su-Schrieffer soliton pairs which form following intrachain absorption and geminately recombine on a subpicosecond time scale. At later times($\geq$ 20ps), there are charged solitons formed by an interchain absorption mechanisms where polarons are formed and diffuse to convert the residual neutral solitons to charged solitons.

The dynamics of photoexcitations are not well understood in nondegenerate ground state systems, such as PT. There are two

midgap states(bonding-antibonding states a and b) formed when PT samples was pumped above gap. A schematic band diagram of the two midgap states along with the possible transitions for polarons and bipolarons, displayed in Fig.7.4.1(b)(page 84). Ultrafast pulsed-laser time-resolved interband bleaching experiments[1,2] which monitored the ground-state recovery have been performed to investigate the origin of the observed bipolarons. These results are difficult to interpret in terms of bipolarons generation and decay since they probed dynamics associated with other excitations. Thus photocarriers dynamics has not even been directly monitored on the short time scales, the nature and formation mechanism of these lattice deformation still remain unknown. Picosecond time resolved photoinduced absorption measurement in PT are necessary.

A synchronously pumped dye laser pulse(Spectra Physics, 0.5ps) at 2.1eV will be amplified at 10Hz repetition rate and divided into three parts. The first part will be used as the pump(excitation) source to insure the generation of polaronic bands in PT. The second part is focused into a D_2O(or H_2O) cell to generate a white light continuum(300 ~ 700nm). The third part and the white light continuum(idler) will be sent together into a $LiIO_3$ crystal as the pump and the idler beams for parametric mixing. The difference-frequency mixing of these two beams in the crystal will generate a tunable IR light source from 2 to 5μm [3]. The tunability will be achieved by changing the angle θ between the optical axis of the crystal and the beam axis, mainly by the phase matching condition of the parametric process, $\Delta \mathbf{K} = \mathbf{K}_s + \mathbf{K}_i - \mathbf{K}_p$. This tunable picosecond

infrared pulse will be used as the probe. The schematic diagram of this pump-probe setup is shown in Fig. 12.1.1

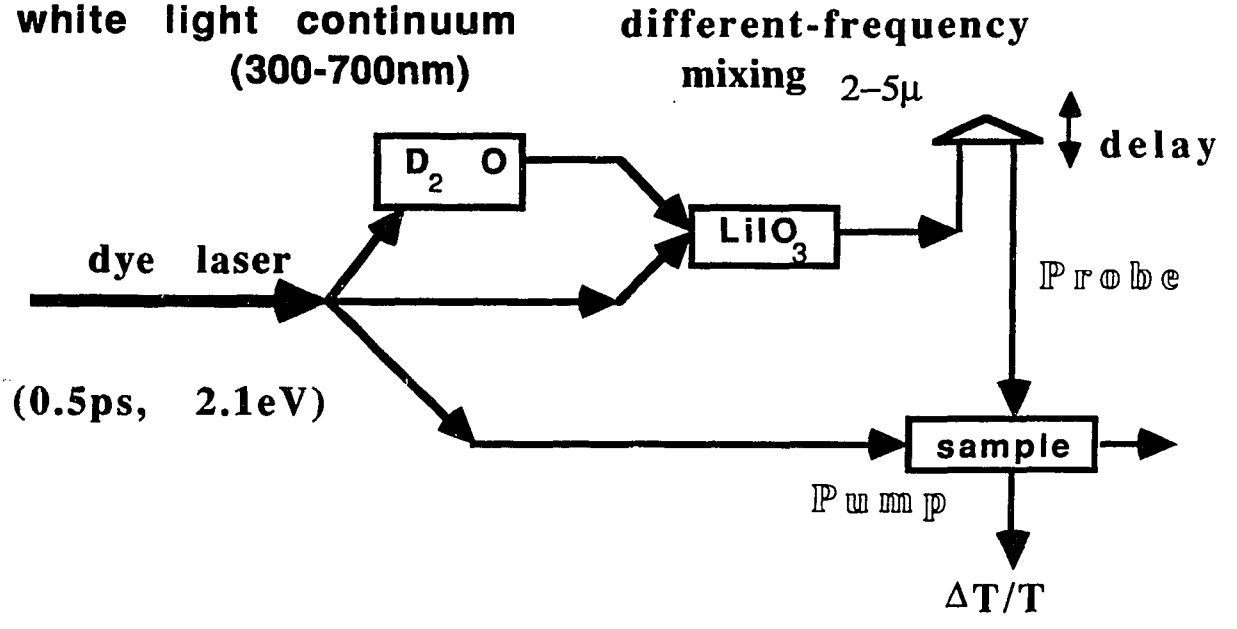

Fig.12.1.1 Schematic diagram of infrared pump-probe set up.

The following important pieces of information will be obtained: (a)For the information on the frequency domain, the time delay of the probe beam is fixed at zero relative to the pump(i.e. they are spatially and temporally overlapping), the frequency of the probe is changed. Photoinduced absorption $\Delta T/T$ will be obtained as a function of ω around 0.45eV(ω_a). The absolute value of $\Delta T/T$ will give the number of photoexcitations. If the pulse is fast enough, this picosecond photoinduced absorption spectra around band a should be shifted to the higher energy side relative to the steady state

photoinduced absorption spectra, since band a is split from the top conduction band and it takes time(although it is fast) to reach the steady state position;

(b)In order to perform the time measurements, the frequency of the probe is fixed, and the probe beam will be delayed relatively to the pump.

12.2 Two Photon Absorption Resonant $\chi^{(3)}$ Measurements in Polysilane

In chapter VIII, two photon absorption has been measured at 532 nm in poly(methylphenyl)silane polymers. A theoretical calculation of $\chi^{(3)}$ spectrum around two photon resonant transitions is also given. It is important to measure the two photon absorptions from 532 nm to 700 nm to cover the whole spectrum in order to provide the following informations:

(1) the basic two photon absorption spectrum to understand the basic optical properties of polysilane polymers;

(2) the predicted sign change of $\chi^{(3)}$ from $h\omega<1/2Eg$, to $h\omega>1/2Eg$, where $h\omega$ is the photon excitation energy and Eg is the two photon absorption gap of polysilanes.

In this work, a tunable dye laser, either PTL10 pumped by Nd:YAG laser or any other dye laser source which can provide the needed wavelength will be used.

12.3 Sign of $\chi^{(3)}$ Spectra in Resonant with the Single Photon Transition in Polythiophenes

The single beam Z - scan technique should be performed in the future to measure the sign of $\chi^{(3)}$ in polythiophene polymers about 450 to 600 nm. The goal of this work is to prove the theoretical estimations which predicts the sign change of $\chi^{(3)}$ from $h\omega<Eg$, to $h\omega>Eg$, as calculated in **6.4**, where $h\omega$ is the photon excitation energy and Eg is the single photon absorption gap of polysilanes.

In this work, a tunable dye laser, either PTL10 pumped by Nd:YAG laser or any other dye laser source which can provide the needed wavelength will be used.

Reference

1. Z. Vadeny, H. T. Grahn, A. J. Heeger, and F. Wudl, Synth. Metals. **28**, c299(1989).

2. G. S. Kanner, Z. Vardeny, and B. C. Hess, Phys. Rew. B **42**, 5403(1990).

3. L. Rothberg, T. M. Jedju, S. Etemad, G. L. Baker, Phys. Rew. Lett. **57**, 3229(1986).

Appendix

Derivations for the expression of $\chi^{(3)}$ in resonant with the single photon and the two photon transitions ---the application of double-Feynman diagram

The microscopic expressions of the nonlinear susceptibilities can be found from the Quantum mechanical calculations, such as the density matrix formalism and perturbation theory[1,2].

The density matrix operator ρ is introduced as:

$$\rho=\overline{|\phi><\phi|};$$

the electric polarization **P** is given as:

$$<\mathbf{P}> =\overline{<\phi|P|\phi>}= Tr(\rho\mathbf{P}),$$

where ϕ is the wavefunction of the material system interact with the electromagnetic field.

The motion equation for ρ is:

$$\frac{\partial\rho}{\partial t} =\frac{1}{i\hbar}[H, \rho] .$$

Where, the Hamiltonian H is composed of three parts:

$$H = H_0 + H_{int} + H_{random},$$

where H_0 is the Hamiltonian of the unperturbed material system, H_{int} is the interaction Hamiltonian describing the interaction of light with matter, and H_{random} is a Hamiltonian describing the random perturbation on the system by the thermal reservoir around the system.

To find nonlinear polarizations, and nonlinear susceptibilities of various orders, the perturbation expansion have to be used in the calculation:

$\rho = \rho^{(0)} + \rho^{(1)} + \rho^{(2)} + \rho^{(3)} + \ldots\ldots$,

$\langle P \rangle = \langle P^{(0)} \rangle + \langle P^{(1)} \rangle + \langle P^{(2)} \rangle + \langle P^{(3)} \rangle + \ldots\ldots$,

where $\rho^{(0)}$ is the density matrix operator for the system at thermal equilibrium; and $\langle P^{(0)} \rangle$ is chosen as 0 with the assumption that there is no permanent polarization in the medium. Inserting the serious expansion of ρ into the motion equation, collecting the terms of the same order with H_{int} treated as a first order perturbation, then $\rho^{(n)}$ can be calculated, so, $P^{(n)}$ and thus $\chi^{(n)}$ due to the electronic contributions can be obtained. Normally, the derivation for high orders are long and tedious. Fortunately, the calculation can be facilitated with the help of double-Feynman diagram, a technique devised by Yee and Gustafson[3].

The double-Feynman diagram consists two lines of propagation. One for the $|\phi\rangle$ side of ρ and the other for the $\langle\phi|$ side. The microscopic expression for a given diagram can be obtained by following the general rules defined for various multiplication factors[4]. In this Appendix, this diagram technique is used to obtain the expression of $\chi^{(3)}$ in resonant with the single and the two photon transitions.

(1)single photon resonant $\chi^{(3)}$

In the following single derivations, a simple two level system is assumed. The resonant excitations are assumed with the same frequency. The process is generally described by the four separate diagrams shown below.

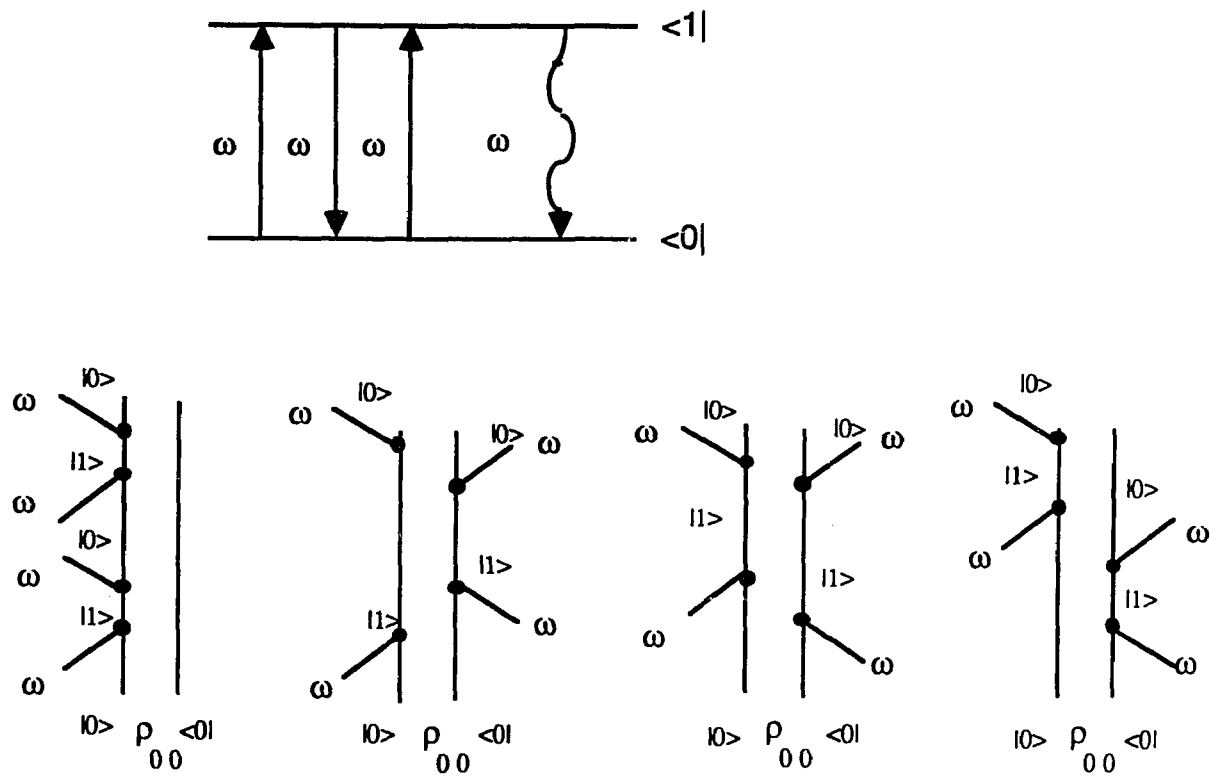

With the above diagrams, the expression of $\chi^{(3)}$ in resonant with the single photon transitions is:

$$\chi^{(3)}_{R(\omega = \omega - \omega + \omega)} = - \frac{Ne^4}{\hbar^3} \Omega_{01}\Omega_{10}\Omega_{01}\Omega_{10}\rho_{00}[A_a + A_b + A_c + A_d];$$

where Ω_{ij} are the transition matrix elements. A_i is the propagator corresponding to diagram (i).

For instance, the propagator in (b) A_b can be obtained in the following way:

(1)the propagation from the first vertex(on the left side) to the second vertex(on the right side) along the |1><0| double line is

completed by absorbing a photon ω at the first vertex, this process gives:

$$\frac{1.}{\omega-\omega_{10}+i\Gamma_{10}};$$

(2)the propagation from the second to the third vertex(both on the right side) by absorbing a photon ω at the second vertex, this process gives: $-\frac{1.}{\omega-\omega-\omega_{11}+i\Gamma_{11}} = iT_{11}$; the "- " is added since the second vertex is on the right side and $T_{10(1)} = 1/\Gamma_{00(11)}$ is the longitudinal relaxation time for state 0(or 1);

(3)the propagation from the third(right side) to the fourth(left side) vertex by emitting a photon at the third vertex, this process gives: $-\frac{1.}{\omega-\omega_{10}+i\Gamma_{10}}$, again the "-" sign is coming from the location of the right side of the third vertex;

thus the propagator of diagram (b) is the product of these three terms:

$$A_b = \frac{1.}{\omega-\omega_{10}+i\Gamma_{10}} \times (-\frac{1.}{\omega-\omega_{10}+i\Gamma_{10}}) \times iT_{11} = \frac{-iT_{11}}{(\omega-\omega_{10}+i\Gamma_{10})^2}.$$

From the same procedure, the propagator A_a can also be obtained:

$$A_a = \frac{-iT_{10}}{(\omega-\omega_{10}+i\Gamma_{10})^2};$$

The propagator in (c) A_c can be obtained in the following way:

(1)the propagation from the first vertex(on the right side) to the second vertex(on the left side) along the $|0><1|$ double line is completed by absorbing a photon ω at the first vertex, this process gives: $-\frac{1.}{-\omega-\omega_{01}+i\Gamma_{01}}$; the term is "-" since the first vertex is on the

right side. The "-" before ω is because the absorption happens on the right side. Notice that $-\omega_{01} = \omega_{10}$ and $\Gamma_{01} = \Gamma_{10}$, thus

$$-\frac{1.}{-\omega-\omega_{01}+i\Gamma_{01}} = \frac{1.}{\omega-\omega_{10}-i\Gamma_{10}};$$

(2)the propagation from the second vertex(on the left side) to the third vertex(on the left side) along the $|1><1|$ double line is completed by absorbing a photon at the left side second vertex, this process gives: $\frac{1.}{-\omega+\omega-\omega_{11}+i\Gamma_{11}} = -iT_{11}$;

(3)the propagation from the third vertex(on the right side) to the fourth vertex(on the left side) along the $|1><0|$ double line by emitting a photon at the third right hand side vertex, the propagator is: $-\frac{1.}{\omega-\omega_{10}+i\Gamma_{10}}$

the propagator of diagram (c) is the product of these three term:

$$A_c = \frac{1.}{\omega-\omega_{10}-i\Gamma_{10}} \times \left(-\frac{1.}{\omega-\omega_{10}+i\Gamma_{10}} \right) \times (-iT_{11}) = \frac{iT_{11}}{(\omega-\omega_{10})^2+i\Gamma_{10}^2};$$

Same way the propagator: $A_d = \frac{iT_{10}}{(\omega-\omega_{10})^2+i\Gamma_{10}^2}$.

Finally,

$$\chi^{(3)}_{R(\omega=\omega-\omega+\omega)} = -i\frac{Ne^4}{\hbar^3}\Omega_{01}\Omega_{10}\Omega_{01}\Omega_{10}\rho_{00}[A_a + A_b + A_c + A_d]$$

$$= -i\frac{Ne^4}{\hbar^3}\Omega_{01}\Omega_{10}\Omega_{01}\Omega_{10}\rho_{00}[T_{10} + T_{11}]$$

$$\left[\frac{1}{(\omega-\omega_{10}+i\Gamma_{10})^2} - \frac{1}{(\omega-\omega_{10})^2+i\Gamma_{10}^2}\right],$$

that is equation (6.4.1) in Chapter VI.

(2)two photon absorption resonant $\chi^{(3)}$

In the following derivations, a three level system is assumed. The resonant excitations are assumed with the same frequency ω, and $\omega_{10}=\omega_{21}=\omega$ has been assumed. The two photon absorption process is generally described by the diagram shown below.

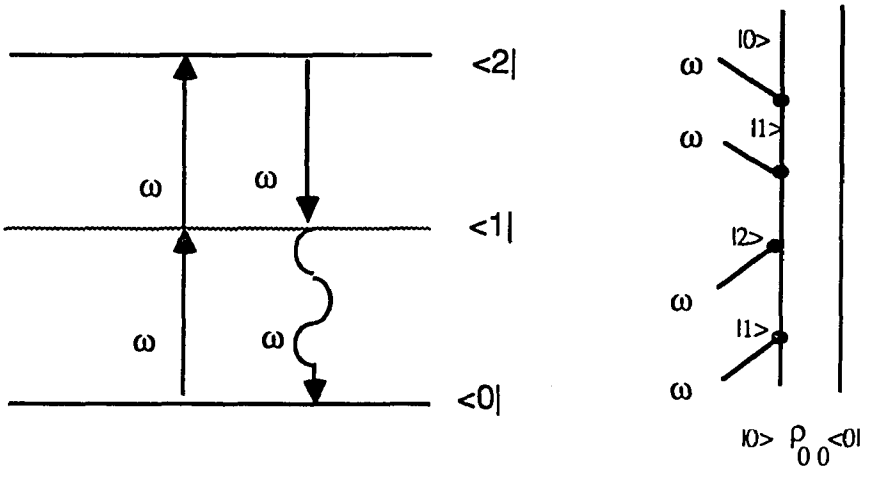

The propagator in this Feynman diagram can be obtained by the following way:

(1)the propagation from the first vertex(on the left side) to the second vertex(on the left side) along the |1><0| double line is completed by absorbing a photon ω at the first vertex, this process gives: $\dfrac{1.}{\omega-\omega_{10}+i\Gamma_{10}}$;

(2)the propagation from the second vertex(on the left) to the third vertex(on the left) along the |2><0| double line is completed by absorbing a photon ω at the second vertex, this process gives:

$$\frac{1.}{\omega+\omega-\omega_{20}+i\Gamma_{20}}=\frac{1.}{2\omega-\omega_{20}+i\Gamma_{20}};$$

(3)the propagation from the third vertex(on the left side) to the fourth vertex(on the left side) along the |1><0| double line is completed by emitting a photon ω at the third vertex, this process gives: $\dfrac{1.}{\omega+\omega-\omega_{10}+i\Gamma_{10}} = \dfrac{1.}{\omega-\omega_{10}+i\Gamma_{10}}$;

the propagator is the product of all three terms:

$$\frac{1.}{\omega-\omega_{10}+i\Gamma_{10}} \times \frac{1.}{2\omega-\omega_{20}+i\Gamma_{20}} \times \frac{1.}{\omega-\omega_{10}+i\Gamma_{10}} = \frac{1.}{(2\omega-\omega_{20}+i\Gamma_{20})(\omega-\omega_{10}+i\Gamma_{10})^2};$$

thus the expression for the two photon absorption resonant $\chi^{(3)}_R$ is:

$$\chi^{(3)}_{R(\omega=\omega-\omega+\omega)} = -\frac{Ne^4}{\hbar^3}\Omega_{01}\Omega_{12}\Omega_{21}\Omega_{10}\rho_{00}\frac{1.}{(2\omega-\omega_{20}+i\Gamma_{20})(\omega-\omega_{10}+i\Gamma_{10})^2}.$$

Refernce

1. J. A. Armstrong, N. Bloembergen, J. Ducuing, and P. S. Pershan, Phys. Rev. **127**, 1918(1962).

2. N. Bloembergen, and Y. R. Shen, Phys. Rev. **133**, A37(1964).

3. T. K. Yee and T. K. Gustafson, Phys. Rev. A **18**, 1597(1978).

4. Shen, Y. R. ***The principle of Nonlinear Optics***, Join Wiley &Sons, Inc. 1984, Chapter 2.

Bibliography

Armstrong, J. A., N. Bloembergen, J. Ducuing, and P. S. Pershan, Phys. Rev. **127**, 1918(1962).

Ball, R., W. P. Su and J. R. Shrieffer, J. Phys.(Paris) Colloq **44**, c3(1983).

Bartoli, F., M. Kruer, L. Esterowitz and R. Allen, J. App. Phys. **44**, 3713 (1973).

Baument, J. C., G. C. Bjorklund, D. H. Jundt, M. C. Jurich, H. Looser, R. D. Miller, J. Rabolt, R. Sooriyakumaran, J. D. Swalen, R. J. Twieg, Appl. Phys. Lett., **53**, 1147(1988).

Blanchet, G. B., C. R. Fincher, A. J. Heeger, Phys. Rev. Lett., **51**, 2132(1983).

Bloembergen. N., ***Nonlinear Optics***, Benjamin, New York, 1965.

Bloembergen, N., and Y. R. Shen, Phys. Rev. **133**, A37(1964).

Carter, G. M., M. K. Thakur, Y. J. Chen, and J. V. Hryniewicz, Appl. Phys. Lett. **47**, 457(1985).

Carter, G. M., J. V. Hrynuewicz, M. K. Thakur, Y. J. Chen and S. E. Meyler, Appl. Phys. Lett. 49 998(1986).

Carter, G. M., J. Opt. Soc. Am. B **6**, 1018(1987).

Carter, G. M., Y. J. Chen, M. F. Rubner, D. J. Sandman, M. K. Thakur, S. K. Tripathy, ***Nonlinear Optical Properties of Organic Molecules and Crystals***, vol. 2, Ed. by D. S. Chemla and J. Zyss(academic Press, New York, 1987).

Chiao, R. Y., E. Garmire and C. H. Townes, Phys. Rev. Lett. **13** , 479(1964).

Collins, Edward A., Jan Bares, and Fred W. Billmeyer,Jr., **Experiments in Polymer Science,** by: Edward A. Collins, Jan Bares and Fred W. Billmeyer,Jr. (New York John Wiley & Sons, Inc., 1973).

Cotts, P. M., R. D. Miller, P. T. Trefonas III, R. West and G. N. Ficks, Macromolecules, **20**, 1046(1987).

Danieli, R., C. Taliani, R. Zamboni, G. Giro, M. Biserni, M. Mastragostino and A. Testoni, Synth. Met., **14**, 325 (1986).

Dewar, Michael J. S., J. Am. Chem. Soc. **106**, 669(1984).

Dorsinville, R., R. Tubino, S. Krimchansky, R. R. Alfano, J. L. Birman, A. Bolognesi, S. Destri, M. Castellani, W. Porzio, Phys. Rev. B, **32**, 3377 (1985).

Dorsinville, R., Lina Yang, R. R. Alfano, R. Tubino, S. Destri, Solid State Commun. **68**, 875(1988).

Dorsinville, R., Lina Yang, R. R. Alfano, R. Zamboni and C. Taliani, Opt.Lett. **14**, 1321(1989).

Eichler, H. J., G. Salje and H. Stahl, J. Appl. Phys. **44**, 5383(1973).

Eichler, H. J., P. Gunter, and D. W. Pohl, ***Laser Induced Dynamic Gratings***, (Springer-Verlag, Berlin Heidelberg, 1986).

Eichler, H.J., P. Gunter, D.W. Pohl, "Laser Induced Dynamic Gratings," Springer-Verlag (1986). B. Ya. Zeldovich, N.F. Pilipetsky, V.V. Shkunov, " Principles of Phase Conjugation," Springer-Verlag (1985).

Etemad, S. , G. L. Baker, D. Jaye, F. Kayzar, J. Messier, Proc. SPIE, **682**, 44(1986).

Fann, W. S., S. Benson, J. M. J. Madey, S. Etemad, G. L. Baker and F. Kajzer, Phys. Rev. Lett., **62**, 1492(1989).

Fisher, Robert A. ***Optical Phase Conjugation***, Academic Press, 1983.

Flyzanis, C., in *Quantum Electronics* Ed. by H. Rabin, C. T. Tang, Volume I, Part II (Academic Press Inc., New York, 1975).

Green, B. I., J. Orenstein, R. R. Millard and L. R. Williams "Nonlinear Optical Response of One-Dimensional Excitons in Polydiacetylene" in Ultrafast Phenomena V , Ed. by G. Fleming and A. Siegment, 472-474, (Springer-Verlag, New York, 1986).

Hanamura E., and N. Nagaosa, Solid State Commun. **62**,5(1987).

Harbeke, G., E. Meier, W. Egli, H. Kiess and E. Tosatti, Solid State Commu. **55**, 419(1985).

Ho, P. P., R. Dorsinville, N. L. Yang, G. Odian, G. Eichmamn and R. R. Alfano, "Molecular and Polymeric Optoelectronic Materials", G. Khanarian,ed.,Proc. Soc. Photo-Opt. Instrum. Eng. 682, 36(1986).

Ho, P. P., N. L. Yang, T. Jimbo, Q. Z. Wang and R. R. Alfano, J. Opt. Soc. Am. B **34**, 1025(1987).

Kajzar F., and J. Messier. Thin Solid Films, **132**, 10 (1986).

Kajzar, F., J. Messier and C. Rosilio, J. Appl. Phys. **60** 3040(1986).

Kajzar, F., S. Etemad, G. L. Baker and J. Messier, Solid State Commun.**63**, 1113(1987).

Kanetake, T. , Y. Tokura and T. Koda, Solid State Commun. **56**, 803(1985).

Kaneto, K., F. Uesugi and K. Yoshino, J. Phys. Soc. Jpn. **56**, 3703(1987).

Kaneto, K., F. Uesugi and K. Yoshino, J. Phys. Soc. Jpn. **57**, 1859(1988).

Kepler, R. G., J. Zeigler, in Advances in Chemistry Series No. 224, *Silicon Based Polymer Science: A Comprehensive Resource* Ed. by J. M. Zeigler and F. W. Gordon.

Kepler, R. G., and J. M. Zeigler, Mat. Res. Soc. Symp. Proc. Vol. 173, 453(1990).

Laser Hand Book, vol.4 Ed. by M. L. Stitch and M. Bass, (Elsevier Science Publishers, B. V.,1985), Chap. 4, p333.

Mackie, D. M., R. J. Cohen and A. J. Glick, Phys. Rev. B **39**, 3442(1989).

Mahr, H.,in *Quantum Electronics* Ed. by H. Rabin, C. T. Tang, Volume I, Part II (Academic Press Inc., New York, 1975)

Maloney, C., W. Blau, K. H. Drexhage, Optics Letters, **11**, 434 (1986)

Marco, P. D., M. Mastragostino,and C. Taliani, Molec. Cryst. and Liq. Cryst., **118**, 241 (1985).

McGraw, D. J., A. E. Siegman. G. M. Wallraff, and R. D. Miller, Appl. Phys. Lett. **54**, 1713(1989).

McGraw, D. J., C. E. Barker, R. Trebino, A. E. Siegman, M. Thakur, G. M. Wallraff and R. D. Miller, a report in **The Third International Laser Society Conference**, American Physical Society, Atlantic City, Vol.32 No.8, p.162 (1987).

Miller, D. A. B., C. T. Seaton, M. E. Price, S. D. Smith, Phys. Rev. Lett. **47**, 197(1981).

Miller, D. A. B., D. S. Chemla, D. J. Eilenberger, P. W. Smith, A. G. Gossard, W. Wiegmann, Appl. Phys. Lett. **42**, 925(1983).

Miller, J. Rabolt, R. Sooriyakumaran, J. D. Swalen, and R. J. Twieg, Appl. Phys. Lett. **53**, 1147(1988).

Narayana Rao, D., Pratibha Chopra, Suniti K.Ghoshal, Jacek Swiatkienwicz, Paras N. Prasad, J. Chem. Phys. **84** 7049(1986).

Nonlinear Optical Properties of Organic Molecules and Crystals, vol. 2, Ed. by D. S. Chemla and J. Zyss(academic Press, New York, 1987).

Nonlinear Optical Properties of Organic Polymeric Materials, Ed. by D. J. Williams, American Chemical Society Symposium, Series 233(Amer. Chem. Soc., Washington D. C. 1983).

Orenstein, J., Z. Vardeny, G. L. Baker, G. Eagle and S. Etemad, Phys. Rev., **B30**, 786 (1984)

Patel, G. N., R. R. Chance and J. D. Witt, J. Chem. Phys. **79** 4387(1979).

Phillips, S. D., G. Yu and A. J. Heeger, Synth. Metals, **28**, D669(1989).

Quantum Electronics, Ed. by Herbert Rabin, C. L. Tang, Vol.1, Nonlinear Optics Part A.

Rothberg, L., T. M. Jedju, S. Etemad and G. L. Baker, Phys. Rev. Lett. 57, 3229(1986), Phys. Rev. B **36,** 7524(1987).

Rothberg, L., T. M. Jedju, S. Etemad, G. L. Baker, IEEE Journal of Quantum Electronics, **24,** 311 (1988)

Schellenberg, F. M. , B. L. Byer, and R. D. Miller, Opt. Lett. **15,** 242(1990).

Schellenberg, F. M., B. L. Byer, R. D. Miller, and R. Sooriyakumaran, *XVI International Conference on Quantum Electronics Technical Digest,* (Japan Society of Applied Physics, Tokyo, Japan, 1988),pp. 702-703.

Schellenberg, F. M., R. L. Byer, and R. D. Miller, Chem. Phys. Lett. **166,** 331(1990).

Shank, C., R. Yen, R. L. Fork, J. Orenstein and G. L. Baker, Phys. Rev. Lett. **49,** 1666(1982), Phys. Rev. B **28,** 6095(1983).

Shank, C., R. Yen, J. Orenstein, G. L. Baker, Phys. Rev., **B28,** 6095 (1983)

Shapiro, S. L. , H. P. Broida, Phys. Rev., **154,** 129 (1967).

Sheik-bahae, M. , A. A. Said, and E. W. Van Stryland, IEEE J. Quan. Elec. **26,** 760(1990).

Sheik-bahae, M., A. A. Said, and E. W. Van Stryland, Opt. Lett. **14,** 955(1990).

Shen, Y. R. ***The principle of Nonlinear Optics***, Join Wiley &Sons, Inc. 1984.

Shirley, J. A. , R. J. Hall, and A. C. Eckbreth, Opt. Lett. **5,** 380(1980).

Sinclair, M., D. Moses, K. Akagi, and A. J. Heeger, Phys. Rev. B **38,** 10724(1988).

Singh, B. P., M. Samoc, H. S. Nalwa and P. N. Prasad, submitted for publication.

Smith, P. W. , A. Ashkin and W. J. Tomlinson, Opt. Lett. **6**, 284(1981).

Su W. P. , and J. R. Shrieffer, Proc. Natl. Acad. USA **77**, 5626(1980).

Su, W. P. , J. R. Shrieffer, Proceedings of the National Academy of Science, USA, **77**, 5626 (1980)

Takeda, K., H. Teramae and N. Matsumoto, J. Am. Chem. Soc. **108**, 8186(1986).

Taliani, C., R. Danieli, R. Zamboni, P. Ostoja and W. Porzio, Synth. Metals. **18**, 177(1987).

Taliani, C., R. Zamboni, R. Danieli, P. Ostoja, W. Porzio, R. Lazzaroni and J. L. Bredas, Physica Scripta **40**, 781(1989).

Thomazeau, I. , J. Etchepare, G. Grillon, A. Migus, Opt. Lett. **10**, 223(1985).

Tokura, Y. , K. Ishikawa, T. Kanetake and T. Koda, Phys. Rev. B **36** 2913(1987).

Torruellas, W. E. , D. Neher, R. Zanoni, G. I. Stegeman, F. Kajzar and M. Leclerc, *"Dispersion measurements of the third order nonlinear susceptibility of polythiophene thin films"*, to be published in Chem. Phys. Lett.

Trefonas III, P. I. Djurovich, X. H. Zhang, R. West, R. D. Miller and D. Hofer, J. Polym. Sci. Polym. Lett. Ed. **21** 819(1983).

Tubino, R. , R. Dorsinville, W. Lam, R. R. Alfano, J. B. Birman, A. Bolognesi, S. Destri, M. Castellani, W. Porzio, Phys. Rev. B, **30**, 6601 (1984).

Ultrashort Laser Pulses, Ed. by W. Kaiser,(Springer-Verlag, Berlin Heidelberg, 1988), Chap.3, p60.

Vardeny, Z. , E. Ehrenfreund, O. Brafman, M. Nowak, H. Schaffer, A. J. Heeger and F. Wudl, Phys. Rev. Lett. **56**, 671(1986).

Vardeny, Z. , H. T. Grahn, A. J. Heeger and F. Wudl, Synth. Metals.**28**, C299(1989).

Walser, A., A. Seas, R. Dorsinville, R. R. Alfano, R. Tubino, Solid State Commun., **67** 333(1988)

Wherrett, B. S. , A. L. Smirl, T. F. Borggess, IEEE J. of Quant. Elec., QE-**19**, 680 (1983).

Wherrett, B. S. , J. Opt. Soc. Am. B 1, 67(1984).

Wong, K. S. , W. Hayes, T. Hattori, R. A. Taylor, J. F. Ryan, K. Kaneto, Y. Yoshino and D. Bloor. J. Phys. C: Solid State Physics, **18**, L843 (1985).

Worland, R. , S. D. Phillips, W. C. Walker and A. J. Heeger, Synth. Metals **28**, D663(1989).

Yang, Lina, R. Dorsinville, Q. Z. Wang, W. K. Zou, P. P. Ho, N. L. Yang, R. R. Alfano, R. Zamboni, R. Danieli, G. Ruani and C. Taliani, J. Opt.Soc. Am. B **6**, 753(1989).

Yang, Lina, Q. Z. Wang, P. P. Ho, R. Dorsinville, R. R. Alfano, W. K. Zou, and N. L. Yang, Appl. Phys. Lett. **53**, 1245(1988).

Yang, Lina, R. Dorsinville, R. R. Alfano, W. K. Zou and N. L. Yang, submitted to "Opt. Lett.".

Yang, Lina , R. Dorsinville, Q. Z. Wang, W. K. Zou, P. P. Ho, N. L. Yang, R.

Yariv, A., Quantum Electronics, 2nd ed. (Wiely, New York, 1975).

Yee, T. K., and T. K. Gustafson, Phys. Rev. A **18**, 1597(1978).

Zamboni, R., C. Taliani, G. Ruani, A. J. Pal and F. Kajzar,submitted for publication.

Zeldovich, B. Ya, N. F. Pilipetsky, V. V. Shkunov, "Principles of Phase Conjugation," Springer-Verlag, 1985.